Three-dimensional modeling of interlaminar normal stresses in curved laminate components

Modélisation tridimensionnelle des contraintes normales interlaminaires dans des composants de matériaux composites courbés

A Thesis Submitted

to the Division of Graduate Studies of the Royal Military College of Canada

by

Anthony Robert Nagle, B.Eng,

Captain

In Partial Fulfillment of the Requirements for the Degree of

Master of Applied Science in Mechanical Engineering

May 2019

I would like to dedicate this work to my wife Gillian and my two daughters Sienna Rose and Lily for their invaluable support, encouragement and motivation.

Acknowledgements

First and foremost, I would like to thank my wife Gillian for pushing me to go back to school and pursue my MASc. Without her motivation, there is no way I could have gotten to this point. I would also like to thank my supervisor Dr. Diane Wowk for amazing guidance and support at every step of the journey. Maj David Holsworth was an excellent sounding board and a constant source of great advice throughout my entire post-graduate academic journey. Additionally, Capt Kevin Charlebois' translation expertise was greatly appreciated. Finally, I would like to thank all of the graduate students which I spent time with in the Mechanical and Aerospace Engineering Department for their availability when needed. I was able to bounce most of my best and worst ideas off them first and get an immediate review.

Abstract

Curved composite components are being used more frequently in engineering applications due to their desirable and customizable mechanical properties coupled with their low density. However, the stress analyses that have been published thus far are mostly for two-dimensional finite element models and for a cross-ply and unidirectional laminates. These do not accurately model how the interlaminar stresses induced by the lay-up of the laminate couple with the radial stresses induced by the geometry of the curved component. A three-dimensional finite element model of a curved composite component was created and compared to published experimental data to verify its accuracy. The model was then used to model six symmetric lay-ups: unidirectional, $[0/10]_s$, $[0/20]_s$, $[0/45]_s$, $[0/70]_s$, and $[0/90]_s$ subjected to similar loading as the published experiment. The interlaminar normal stresses were modeled across the width of the curved composite component at selected regions of the circumference. Interlaminar normal stress was determined to have the largest effect in delamination initiation of a curved composite component. The radius of the curve was varied and the maximum radial stress was found to increase as the radius of the curve decreased. The effect that the lay-up had on the interlaminar normal stress distribution was investigated and it was found to influence both the interlaminar stresses induced at the free edge of the laminate and the torsion induced as a result of the constraints of the coupon and the proneness of the laminate to twisting. It was concluded that three-dimensional modeling is required to accurately determine where delamination will initiate on a curved composite component with angled plies, as a two-dimensional model could underpredict the interlaminar normal stress by up to 37%.

Résumé

Les pièces fabriquées de matériaux de composites courbées sont utilisées de plus en plus fréquemment dans les applications d'ingénierie en raison de leurs propriétés mécaniques attrayantes et facilement adaptable, et cela couplé avec leurs densités peu-élevé. Cependant, les analyses de contraintes publiées jusqu'à présent ont été effectué principalement à l'aide de modèles d'éléments finis bidimensionnels se concentrant sur des stratifiés croisés et unidirectionnels. Celles-ci ne modélisent pas de façon précise la manière dont les contraintes normales interlaminaires induites par la superposition des couches du stratifié sont couplées aux contraintes radiales induites par la géométrie du composant courbé. Un modèle tridimensionnel d'éléments finis d'un composant composite courbé a été créé et comparé aux données expérimentales publiées pour en vérifier l'exactitude. Le modèle a ensuite été utilisé pour modéliser six stratifiés symétriques: unidirectionnelle, $[0/10]_s$, $[0/20]_s$, $[0/45]_s$, $[0/70]_s$ et $[0/90]_s$. Ceux-ci ont été soumis à un chargement similaire à celui de l'expérience publiée. Les contraintes normales interlaminaires ont été modélisées sur toute la largeur du composant à des endroits présélectionné dans la circonférence de la courbe. Il a été déterminé que la contrainte normale interlaminaire avait le plus grand effet sur l'initiation de la délamination d'un composant de composite courbée. Le rayon de la courbe a été modifié et il a été constaté que la contrainte radiale maximale augmentait à mesure que le rayon de la courbe diminuait. L'effet de la superposition sur la distribution normale des contraintes interlaminaires a aussi été étudié. Il a été constaté que la superposition influençait à la fois les contraintes interlaminaires induites au bord libre du stratifié et qu'elle influençait la torsion induite par les contraintes du coupon, incitant ainsi le stratifié à tordre. Il a été conclu qu'une modélisation tridimensionnelle est nécessaire pour déterminer avec précision la contraint maximale à laquelle de la délamination aura lieu sur un composant fabriquée de composites courbées. Il est estimé qu'un modèle bidimensionnel pourrait sous-prédire la contrainte normale interlaminaire jusqu'à 37%.

Table of Contents

List of Figures

List of Tables

List of Symbols and Abbreviations

γ_{12}	In-Plane Shear Strain (dimensionless)
ε_{11}	Axial Strain (dimensionless)
ε_{22}	Transverse Strain (dimensionless)
η	Angle Around a Curve (˚)
ν	Poisson's Ratio (Dimensionless)
σ_{11}	Axial Stress (or Circumferential Stress around a Curve) (MPa)
σ_{22}	Transverse Stress (MPa)
σ_{33}	Interlaminar Normal Stress (MPa) – ILNS
τ_{12}	In-Plane Shear Stress (MPa)
τ_{13}	Interlaminar Shear Stress on the 13 Plane (MPa)
τ_{23}	Interlaminar Shear Stress on the 23 Plane (MPa)
[A]	Extensional Stiffness Matrix for CLT (N/mm)
ACP	ANSYS Composite Prep/Post – Module Used for Modeling Composites
2b	Width of a Laminate (mm)
[B]	Coupling Stiffness Matrix for CLT (N)
CLT	Classical Laminate Theory
[D]	Bending Stiffness Matrix for CLT (N*mm)
E	Young's Modulus or Modulus of Rigidity (GPa)
FEA	Finite Element Analysis
FRP	Fibre Reinforced Polymer
G	Shear Modulus (GPa)
M	Moment per Unit Length ($\frac{N*mm}{mm}$)

N	Force per Unit Length ($\frac{N}{mm}$)
P	Force Applied (N)
Q	Transverse Shear Strength of the Ply (MPa)
R	Through Thickness Shear Strength (MPa)
S	In-Plane Shear Strength of the Ply (MPa)
t	Thickness of the Laminate (mm)
U	Displacement Applied (mm)
t/2	Half of the Thickness of the Laminate (mm)
w	Width (mm)
X_C	Longitudinal Compressive Strength (MPa)
X_T	Longitudinal Tensile Strength (MPa)
Y_C	Transverse Compressive Strength (MPa)
Y_T	Transverse Tensile Strength (MPa)
y/b	Percentage of the Half Width of a Laminate
Z	Through Thickness Tensile Strength (MPa)

This Page is Left Intentionally Blank

1.0 Introduction

1.1 Background

Composite materials are composed of two or more constituent materials. Engineers can combine the two constituent materials to create a hybrid material, which can be more able to accomplish a task, that the individual constituent materials could not perform on their own. A common type of composite material is fibre reinforced polymer (FRP), where one of the materials has high strength, stiffness, and low density (the fibre), while the second material has high shear properties and low density and can be used to combine the fibres and distribute their high strength and stiffness throughout the entire material (the matrix) [1]. Typical FRP composites include using Carbon Fibre, Fibreglass, or Aramid (Kevlar) as the fibre and epoxy resin, polyester resin, or vinylester resin as the matrix.

Composite materials, specifically FRP, are being increasingly used for engineering purposes due to their favourable mechanical characteristics such as their high strength-to-weight ratio. One such example is the composition of the Boeing 787 Dreamliner which is composed of 50% composite materials by weight and 80% composite materials by volume [2]. Additionally, composite materials can have their mechanical properties tailored for specific uses through design. As composite laminates are composed of a series of laminae each with their own specific properties, specific stacking sequences can be used to obtain the desired mechanical properties by application [3].

FRP composites are frequently used in aerospace applications where weight savings is a driving factor in the design. Current applications of composite materials in aircraft design include full skins, structural members, nosecones, and landing gear doors [1]. There are several drawbacks when using composite materials in design, largely due to their failure mechanisms. One such example is joining composite materials. When joining composite materials using mechanical fasteners, a stress concentration is introduced as is the case when mechanically fastening any material. However, the individual lamina plies are exposed and a stress concentration could lead to delamination of the individual plies from one another which is not an issue in an isotropic material such as steel. When adhesive bonding is used for joining composites, possibility exists for imperfections in the layer of adhesive and spontaneous failure leading to catastrophic results can be realized. This is non-ideal in designing critical components in engineering such as primary structure in aircraft where the damage must be detected and addressed prior to failure.

One configuration in which composite materials are being increasingly used, is in the shape of an L-shaped curve. L-shaped curved composite components can be used to reinforce ribs in hollow structures such as turbine blades and aircraft wings while introducing weight savings [4]. A schematic of a typical curved composite component can be seen in Figure 1.

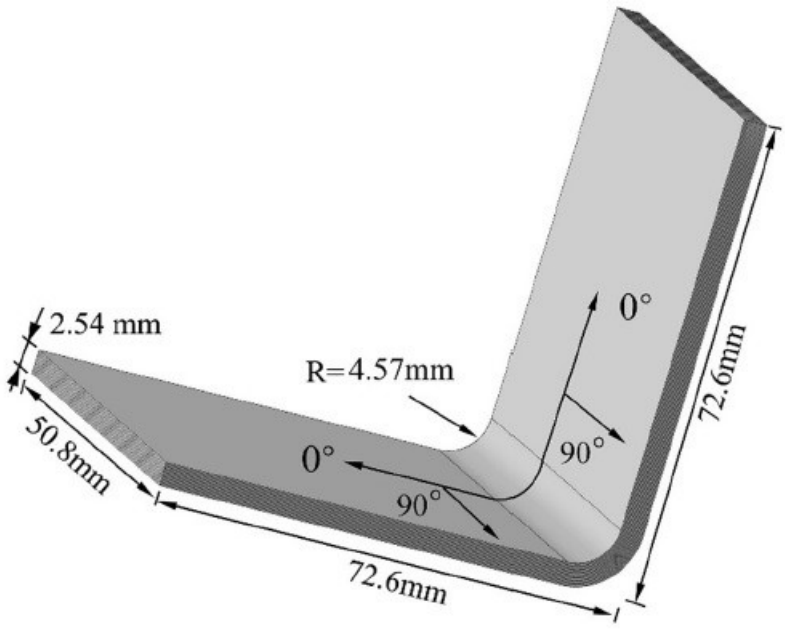

Figure 1: Schematic of a typical curved composite component [5].

Curved components, whether composite or isotropic are subject to unique stresses when subjected to an "opening load." Refer to Figure 2 to see circumferential stresses which act tangentially to the circumference of the curve and radial stresses which act perpendicular to the circumference of the curve which occur in curved components. Circumferential stress is substantially greater than the radial stress for curves with solid cross sections [6]. For failure analyses in isotropic components, the radial stress can be disregarded due to its magnitude when compared to its material allowable. However, in composite curved components where there is a lower material allowable in the out of plane direction, the radial stress can become critical especially when coupled with out of plane stresses (interlaminar stresses) which are typical at the free edge of composite laminates.

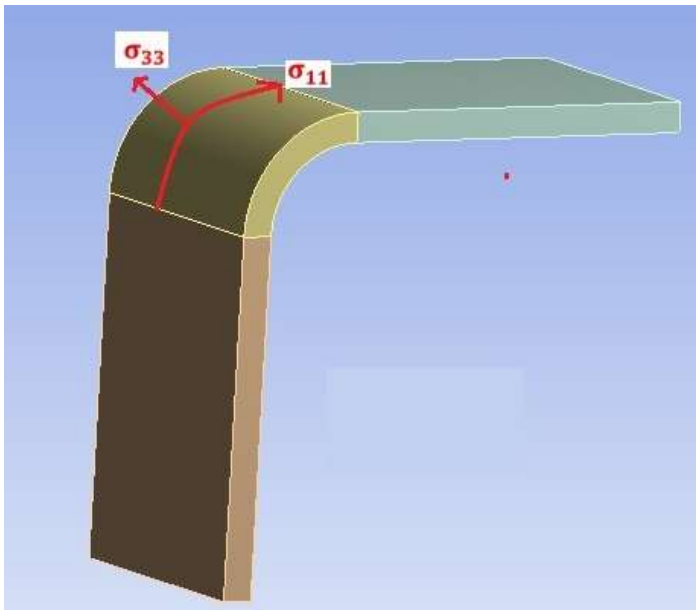

Figure 2: Curved component subjected to unique loading consisting of circumferential stress (σ_{11}) around the curve and radial stress (σ_{33}) out-of-plane to the curve.

Various researchers have constructed finite element models to model curved composite laminates and to determine what the critical failure load is and where the critical failure location is. The laminates modeled have all been unidirectional or cross-ply. In addition, the majority of these models are performed in two dimensions, which assumes that the stresses are constant across the width of the laminate. However, when looking at straight laminates subject to in-plane loading the stresses are not constant across the width due to the increase at the free edges [7]. The two-dimensional models of the curved coupon are disregarding any potential free edge effects that could occur as a result of material mismatch at the interface between two plies. In addition, by only modeling unidirectional and cross-ply laminates, one is also disregarding potentially larger effects that could exist at the free edge.

1.2 Objectives

The purpose of this research was to determine how a curved geometry affects the interlaminar stress distribution and delamination initiation of a curved coupon. There were four aspects considered when achieving the purpose:

- Which interlaminar stress drives the delamination of curved coupons?
- What effect does the geometry of the curve have on the radial stress distribution around the circumference of the curved coupon?
- How do the free edge effects induced because of interlaminar stresses interact with the radial stress induced due to geometry?
- What effect does constraining the curved coupon component have on the radial stress distribution?

1.3 Motivation

The studies performed on delamination initiation of curved composite components that have been published thus far have been performed using two-dimensional finite element analysis (FEA) and a limited number of lay-ups. By performing the FEA on two-dimensional models, the researchers are disregarding the potential of the interlaminar stresses varying across the width of the curved laminate. This is of importance in composite materials where potential free edge effects exist at the free edge of the laminate where the interlaminar stresses increase locally when compared with the mid-plane. In addition, the researchers looked at unidirectional and cross-ply laminates where the free edge effects are not as drastic as other lay-ups. By disregarding lay-ups with angled plies, greater free edge effects are not considered and the site of delamination initiation could be improperly predicted.

This research modeled a curved composite component as a three-dimensional finite element model and allowed the interlaminar stresses to be analysed across the entire width of the curved composite component. Additionally, this thesis modeled varying lay-ups allowing the free edge effects to differ between the individual lamina. Practical applications of curved composite components will have differing lay-ups and will also be subjected to loading which induces interlaminar stresses at the free edge of the components.

1.4 Outline

The thesis is comprised of six sections. Section 1.0 – Introduction contains a brief introduction to the topic of stress analysis of curved composite components, the purpose of this thesis, and the motivation for the research. Section 2.0 – Literature Review gives background information and contains a review of the research that has already been conducted on the topic and currently exists in literature. Section 3.0 – Materials and Methodology contains the set-up of the model used for performing the analysis and extracting the results. Section 4.0 – Observations and Results contains the results from the models for each of the studies performed. It also contains a brief discussion on what each of the studies prove and how they relate to the overall purpose. Section 5.0 – Discussion contains an in depth discussion on four points which relate to the topic to engineering design. Section 6.0 – Conclusions and Recommendations contains five specific conclusions that have been reached as a result of this research as well as recommendations for furthering this research.

2.0 Literature Review

2.1 Stresses in Composites

2.1.1 Isotropic vs Orthotropic Materials

Isotropic materials are defined as having the same material properties regardless of orientation. Hooke's Law for an isotropic material can be seen in Equation (1) [8].

$$\begin{bmatrix} \varepsilon_{11} \\ \varepsilon_{22} \\ \varepsilon_{33} \\ 2\varepsilon_{23} \\ 2\varepsilon_{13} \\ 2\varepsilon_{12} \end{bmatrix} = \begin{bmatrix} \varepsilon_{11} \\ \varepsilon_{22} \\ \varepsilon_{33} \\ \gamma_{23} \\ \gamma_{13} \\ \gamma_{12} \end{bmatrix} = \frac{1}{E} \begin{bmatrix} 1 & -\nu & -\nu & 0 & 0 & 0 \\ -\nu & 1 & -\nu & 0 & 0 & 0 \\ -\nu & -\nu & 1 & 0 & 0 & 0 \\ 0 & 0 & 0 & 2+2\nu & 0 & 0 \\ 0 & 0 & 0 & 0 & 2+2\nu & 0 \\ 0 & 0 & 0 & 0 & 0 & 2+2\nu \end{bmatrix} \begin{bmatrix} \sigma_{11} \\ \sigma_{22} \\ \sigma_{33} \\ \sigma_{23} \\ \sigma_{13} \\ \sigma_{12} \end{bmatrix} \quad (1)$$

Alternatively, anisotropy describes materials which have their material properties change dependent on the material's orientation. There could possibly be an infinite amount of material properties depending the material's orientation when it is subjected to stress [8]. Three dimensional orthotropy is a special type of anisotropy where the material has three orthogonal planes of symmetry. There are three distinct directions by which the material orientations change as opposed to an infinite amount in general anisotropy. Hooke's Law for an orthogonal material can be seen in Equation (2) .

$$\begin{bmatrix} \varepsilon_{xx} \\ \varepsilon_{yy} \\ \varepsilon_{zz} \\ 2\varepsilon_{yz} \\ 2\varepsilon_{zx} \\ 2\varepsilon_{xy} \end{bmatrix} = \begin{bmatrix} \frac{1}{E_x} & -\frac{\nu_{yx}}{E_y} & -\frac{\nu_{zx}}{E_z} & 0 & 0 & 0 \\ -\frac{\nu_{xy}}{E_x} & \frac{1}{E_y} & -\frac{\nu_{zy}}{E_z} & 0 & 0 & 0 \\ -\frac{\nu_{xz}}{E_x} & -\frac{\nu_{yz}}{E_y} & \frac{1}{E_z} & 0 & 0 & 0 \\ 0 & 0 & 0 & \frac{1}{G_{yz}} & 0 & 0 \\ 0 & 0 & 0 & 0 & \frac{1}{G_{zx}} & 0 \\ 0 & 0 & 0 & 0 & 0 & \frac{1}{G_{xy}} \end{bmatrix} \begin{bmatrix} \sigma_{xx} \\ \sigma_{yy} \\ \sigma_{zz} \\ \sigma_{yz} \\ \sigma_{zx} \\ \sigma_{xy} \end{bmatrix} \quad (2)$$

When comparing Equation (1) to Equation (2) there are two main differences which can be explained by the difference between isotropic materials and orthotropic materials. The modulus of elasticity (E) for the isotropic material is the same in all directions, whereas it changes depending on the orientation of the material in the orthotropic material. The second difference is the Poisson's ratio (ν), and as a result the shear modulus (G), changing value depending on the orientation of the material for the orthotropic material. Note that the shear modulus remains the same in isotropic materials.

An individual lamina in a composite material is defined as an orthotropic material in that it has differing properties in all three directions due to its composition of fibres and a matrix. Referring to Figure 3 [9] one can see the individual fibres as well as the matrix material. If one were to apply a tensile load along the fibre direction (defined as 1-direction in Figure 3), the strength would be significantly greater as opposed to pulling transverse to the fibre direction (defined as 2-direction).

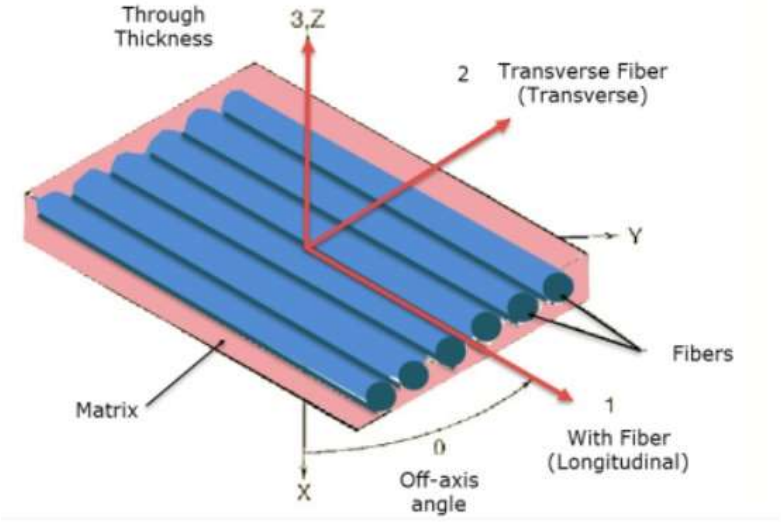

Figure 3: Macroscopic view of an individual lamina [9].

2.1.2 Classical Laminate Theory

2.1.2.1 Coordinate System

Refer to Figure 4 for a visual representation of the two coordinate systems that are followed during laminate analysis. The global coordinate system can be seen on Figure 4 as represented by x, y, and z. The global coordinate system is the same through the thickness of an entire laminate. The local coordinate system can be seen in Figure 4 as represented by the 1, 2, and 3 directions. It is independent to each ply and its orientation is described in relation to the global coordinate system as described above. The 1-direction is said to be along the direction of the fibre, the 2-direction is perpendicular to the fibre, but still in the plane of the ply. The 3-direction is perpendicular to both the 1 & 2 directions, but out of plane of the ply. Note the 3-direction will be the same as the z-direction for straight laminates.

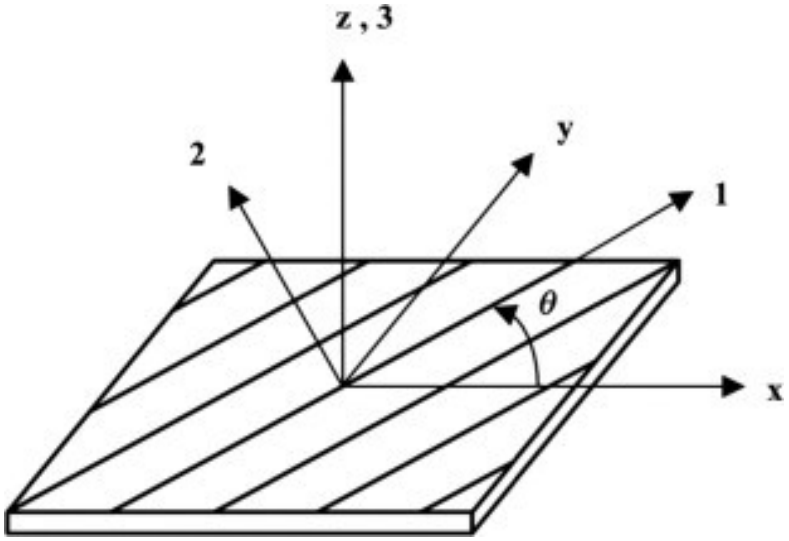

Figure 4: Diagram of the global and local coordinate systems for a lamina [10].

2.1.2.2 Classical Laminate Theory – An Overview

Classical Laminate Theory (CLT) is a theory that can be used to formulate a method by which a laminate can be analysed by noting that it is composed of a certain number (n) of laminae. Each lamina is analysed by considering its individual material properties and orientation to determine its stiffness relative to the global coordinate system. By considering the individual stiffness of each ply; extensional, coupling, and bending stiffness matrices can be

determined and combined into one 6x6 matrix which defines the stress/strain behaviour of the laminate [7].

If the loading is known, the in-plane strains and curvatures can be determined for the entire laminate. As per Figure 5, loading can be normal, in shear, or via moment. Each ply can then be analysed to determine the stresses and strains experienced at a given point through the thickness of the laminate. Due to the difference in properties between plies, the stress will appear to jump from one value immediately to the next. An example of this can be seen in Figure 6. Note that the change in strain is linear through the laminate due to compatibility between the plies. However, the difference in the stiffness between plies makes for discontinuities in the stress distribution throughout the laminate.

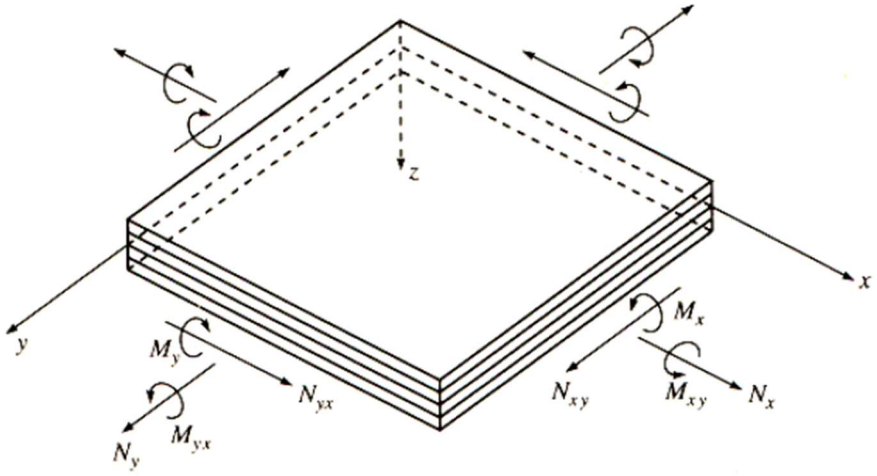

Figure 5: Example loading on a laminate and nomenclature used in Classical Laminate Theory [11].

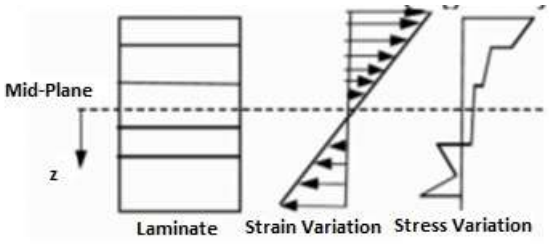

Figure 6: Example stress and strain variations through the thickness of a laminate [12].

According to Herakovich [7], several main assumptions that are part of the Classical Laminate Theory include:

1) The bond between the laminae is perfect. No defects exist.

2) Each lamina is modeled as a homogeneous material with constant material properties through the entire thickness.

3) Individual layer properties can be either isotropic, orthotropic, or transversely isotropic.

4) Plane stress exists in each layer of the laminate.

2.1.2.3 Calculating the Global Stiffness Matrix Using CLT

The global stiffness matrix of a laminate is composed of three matrices titled the [A], [B], and [D] matrices. These matrices are calculated using the individual stiffness matrices from each ply which compose the laminate. Each matrix numerically represents various physical properties of the laminate. The [A] matrix is the extensional stiffness matrix relating the in-plane strains (ε^0) to the in-plane loading (N). The [B] matrix is the bending-extension coupling matrix relating the in-plane strains to the bending curvature (κ) or the bending moment (M) to the in-plane strains. The [D] matrix is the bending stiffness matrix relating the bending curvature to the bending moment. The mid-plane strains and curvatures can be calculated for the laminate if the loads per unit length are known. The numerical representation of CLT is seen in Equation (3).

$$\begin{Bmatrix} \varepsilon_x^0 \\ \varepsilon_y^0 \\ \gamma_{xy}^0 \\ \kappa_x \\ \kappa_y \\ \kappa_{xy} \end{Bmatrix} = \begin{bmatrix} A_{11} & A_{12} & A_{16} & B_{11} & B_{12} & B_{16} \\ A_{12} & A_{22} & A_{26} & B_{12} & B_{22} & B_{26} \\ A_{16} & A_{26} & A_{66} & B_{16} & B_{26} & B_{66} \\ B_{11} & B_{12} & B_{16} & D_{11} & D_{12} & D_{16} \\ B_{12} & B_{22} & B_{26} & D_{12} & D_{22} & D_{26} \\ B_{16} & B_{26} & B_{66} & D_{16} & D_{26} & D_{66} \end{bmatrix}^{-1} \begin{Bmatrix} N_x \\ N_y \\ N_{xy} \\ M_x \\ M_y \\ M_{xy} \end{Bmatrix} \quad (3)$$

In laminates there are additional coupling terms between the in-plane bending and the out of plane twisting. In CLT they are represented in the D matrix as the terms D_{16} and D_{26}. These terms refer to the coupling between the in-plane bending applied to the laminate and the out-of-plane twisting [7].

2.1.3 Types of Laminates

Laminates can be classified by lay-up and their behaviour can be predicted based on their classification. Several types of laminates exist including: symmetric laminates, cross-ply

laminates, angle-ply laminates, anti-symmetric laminates, specially orthotropic laminates, and quasi-isotropic laminates [7]. Symmetric laminates and cross-ply laminates will be discussed throughout this thesis and are described further below.

2.1.3.1 Symmetric Laminates

A symmetric lay-up has the same plies and thicknesses above and below the laminate's mid-plane. The B matrix of a symmetric matrix consists of entirely 0 values. As stated previously, this means that a symmetric matrix has its in-plane response decoupled from its bending response [7]. An example image of a symmetric laminate can be seen in Figure 7. Note the symmetry above and below the laminate's mid-plane.

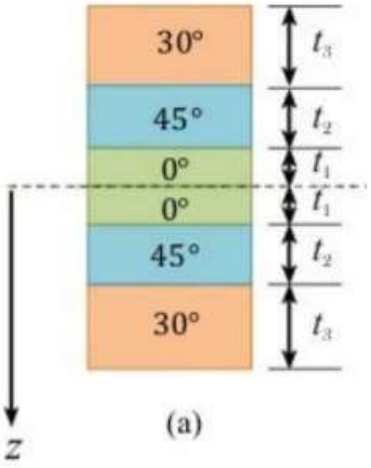

Figure 7: Example lay-up for a symmetric laminate [13].

2.1.3.2 Cross-Ply Laminates

A cross-ply laminate consists of only 0˚ and 90˚ oriented laminae. For a cross-ply laminate the A_{16} =A_{26}=B_{16}=B_{26}=D_{16}=D_{26} = 0. When A_{16}=A_{26}=0, it means that the cross-ply laminate is also considered specially orthotropic. This refers to a laminate that do not exhibit coupling between in-plane extensional and shear responses. When D_{16}=D_{26}=0, this refers to the coupling between the bending and torsion. This means that there is no inherent twisting in a cross-ply laminate as a result of a bending moment applied. An example of a cross-ply laminate can be seen in Figure 8.

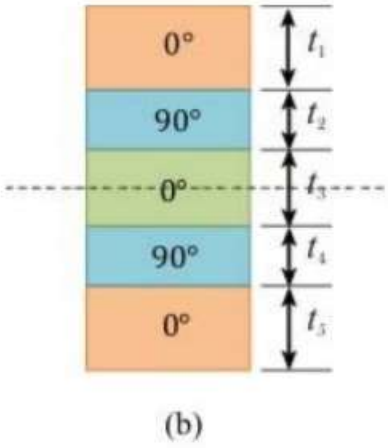

Figure 8: Example lay-up for a cross-ply laminate [13].

2.1.4 Interlaminar Stresses

Classical Laminate Theory is not valid for analysing interlaminar stresses as the state of stress at the boundary layer region is not in a state of plane stress. In order to use CLT, the laminate must be in a state of plane stress [7]. Interlaminar stresses can lead to premature failure in designs if unaccounted for. Delamination type failure can occur at loads significantly lower than the in-plane failure that the laminate was designed to endure.

As per Herakovich [7], interlaminar stresses in composite materials are defined as the out-of-plane stresses (σ_{33}, τ_{13}, and τ_{23}) within a laminate. These values are typically zero through the width in a finite width laminate subjected to in-plane loading. However, when analysing the interlaminar stresses at the free edge of the laminate, these stresses are found to be non-zero and can approach high values relative to the mid-plane of the laminate. Refer to Figure 9 (taken from reference [14]) to see an example of in-plane loading causing out-of-plane stresses. Note that for this case the x, y, and z directions can be approximated as the 1,2, and 3 directions (ie. σ_z, τ_{xz}, and τ_{yz} represent σ_{33}, τ_{13}, and τ_{23} respectively).

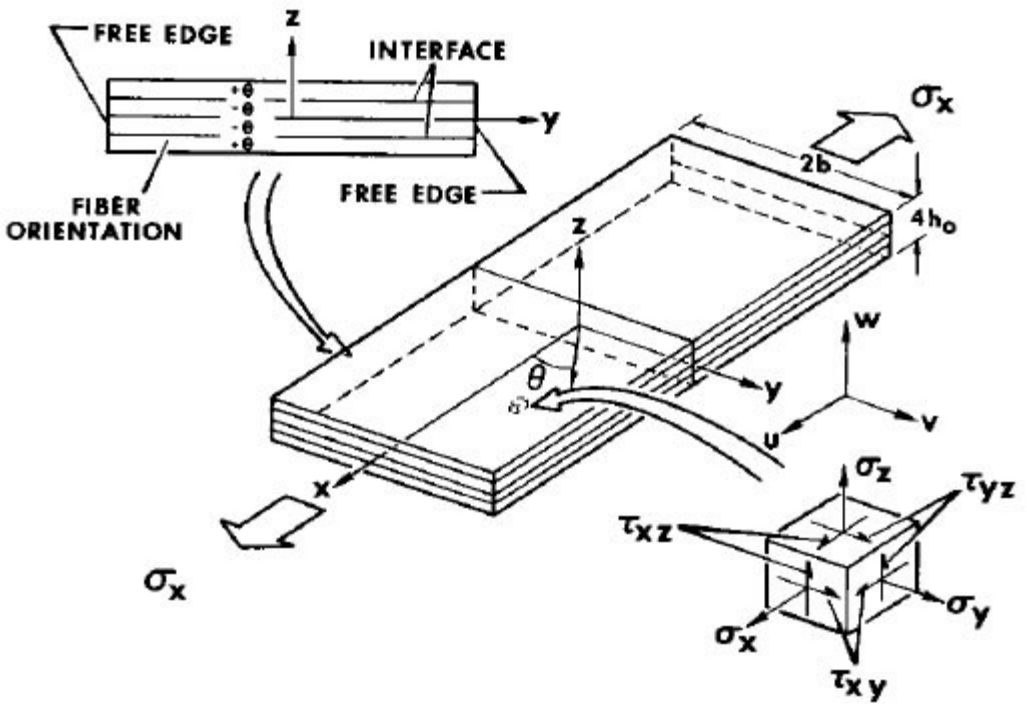

Figure 9: Interlaminar stress at the free edge of a finite width laminate [14].

The free edge effect is noticed within a boundary from the free edge of the laminate. The boundary region is approximately a distance of t/2 from the free edge, where t is the thickness of the laminate.

The mismatch of the material properties at the interface between two plies is what causes the interlaminar stresses at the free edges of the laminate. An approximate analytical solution was presented by Kassapoglou and Lagace [15] based on the complementary energy formulation. This approximate solution assumes the admissible stress states which satisfy equilibrium, the boundary conditions are assumed to be stress free, and traction continuity is assumed at the interfaces between each ply. Rose and Herakovich added to the Kassapoglou and Lagace model by adding terms to the admissible stress state to include the mismatching of material properties [16], [17], [18]. Rose and Herakovich state that the statically admissible stress state is a function of global equilibrium, coefficient of mutual influence mismatch, and the Poisson's ratio mismatch.

An example distribution of the interlaminar normal stress and interlaminar shear stress in the 1-3 direction can be seen in Figure 10 (taken from Ref [19].) The interlaminar normal stress navigates into the compression zone prior to approaching the large tensile value right at the free edge. The interlaminar shear stress has a more gradual increase, but ultimately reaches a larger value.

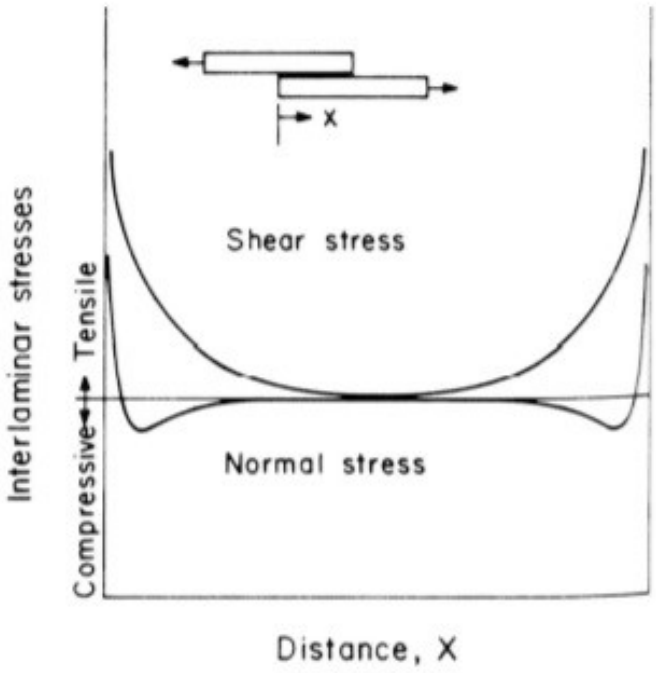

Figure 10: Example of interlaminar stress distributions across the width of a straight composite laminate [19].

2.1.5 Failure in Composite Laminates

There are several failure modes that exist in composite laminates that are unique when compared to that of an isotropic material such as steel, which are illustrated in Figure 11. Fibre fracture occurs when the load in the fibre (1) direction of a composite exceeds the allowable load leading to fracture of the fibres. Interfacial debonding occurs when the fibre separates from the matrix due to excess loading in the transverse (2) direction. Matrix cracking occurs when the strength of the matrix is exceeded. The matrix between the fibres can crack and cause failure on the lamina level. Delamination occurs when lamina plies separate from one another due to loading in the out-of-plane (3) direction and is described further below.

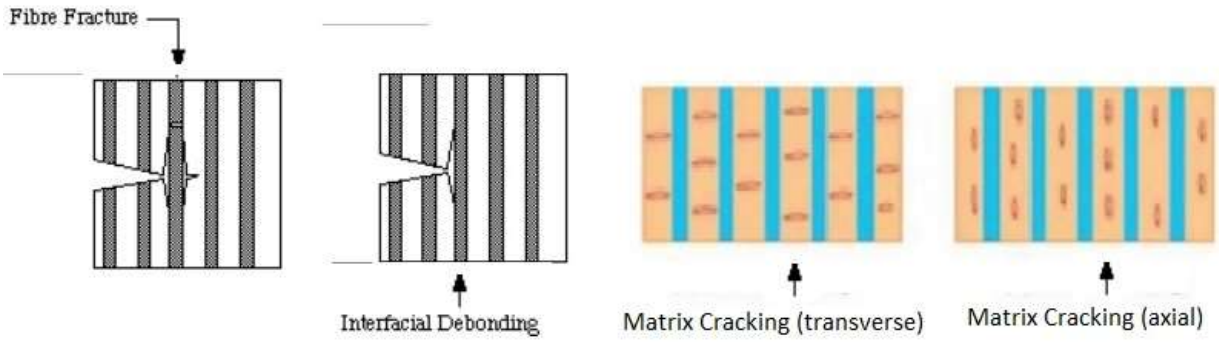

Figure 11: Examples of failure modes for composite materials at the lamina level [20], [21].

2.1.5.1 Delamination

While the other three failure modes of composite materials are initiated on the lamina level, delamination occurs on the laminate level. It occurs when lamina plies separate from one another. Two main causes of delamination are imperfections which exist in the resin between the lamina plies and the interlaminar stresses that exist between the laminae. Refer to Figure 12 for a diagram of the initiation of a delamination between two lamina plies.

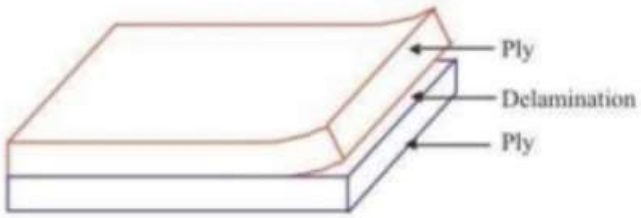

Figure 12: Diagram of delamination failure mode in a composite laminate [21].

As stated previously, the interlaminar stresses are highest at the free edge for straight laminates subjected to in-plane loads. As such one would expect to see delaminations initiate at the free edge of the laminate.

2.1.5.2 Delamination Onset in Laminates and Failure Theories

Parts of the laminate can fail at varying times due to the failure modes being caused by different failure loads. As each lamina fails, the load is redistributed to the intact parts of the laminar which results in a progressive failure analysis as described by Puck [22]. This is often referred to as a "ply-by-ply analysis."

Yarrington *et al.* [23] summarize various analytical methods by which delamination initiation can be predicted in composite adherends in adhesively bonded joints. Several of the more common failure criteria are presented below.

The simplest failure criterion is proposed by Adams and Wake [24] and assumes that delamination initiates when the normal interlaminar stress (σ_{33}) exceeds that of the laminate's through-thickness tensile strength (Z), which can be seen in Equation (4) :

$$\frac{\sigma_{33}}{Z} \geq 1 \qquad (4)$$

The delamination initiation criterion proposed by Adams and Wake disregards the effect of interlaminar shear stresses on delamination. The interlaminar shear stress can play a role in the initiation of delamination and Hoyt *et al.* [25] take this into consideration in Equation (5). Hoyt *et al.* state that delamination initiation also considers the squared ratio of the interlaminar shear stress (τ_{13}) to the through thickness shear strength (R). This criterion was evaluated by Long experimentally [26] to be true in the delamination initiation within the prepreg layer of the composite adherends of adhesively bonded ARALL-1 double and single lap joints.

$$\frac{\sigma_{33}}{Z} + \left(\frac{\tau_{13}}{R}\right)^2 \geq 1 \qquad (5)$$

Generally for Equation (5), σ_{33} will contribute more to delamination initiation than τ_{13} as the value for Z is less than that of R in most materials [23].

Tong made a prediction that prior to delamination initiation, fibre breakage may play a role and as such tested six different failure criteria [27]. Ultimately Tong deduced that taking into account the fibre breakage and interlaminar stresses yield Equation (6). X_T and X_C are the respective longitudinal tensile and compressive strengths of material. Y_T and Y_C are the respective transverse tensile and compressive strengths of the material. Q is the transverse shear strength of the ply, and S is the in-plane shear strength of the ply.

$$\left(\frac{\sigma_{11}^2 - \sigma_{11}\sigma_{33}}{X_T X_C}\right) + \left(\frac{\sigma_{22}^2 - \sigma_{22}\sigma_{33}}{Y_T Y_C}\right) + \left(\frac{\sigma_{33}}{Z}\right)^2 + \left(\frac{\tau_{23}}{Q}\right)^2 + \left(\frac{\tau_{13}}{R}\right)^2 + \left(\frac{\tau_{12}}{S}\right)^2 \geq 1 \quad (6)$$

Camanho and Matthews [28] proposed two quadratic equations for initiation of delamination depending on whether the interlaminar normal stress was in tension (Equation (7)) or compression (Equation (8)). Note that when the interlaminar normal stress is in compression, only the shear stresses are considered.

$$\left(\frac{\sigma_{33}}{Z}\right)^2 + \left(\frac{\tau_{23}}{Q}\right)^2 + \left(\frac{\tau_{13}}{R}\right)^2 \geq 1 \quad (7)$$

$$\left(\frac{\tau_{23}}{Q}\right)^2 + \left(\frac{\tau_{13}}{R}\right)^2 \geq 1 \quad (8)$$

2.2 Stress Analysis of Curved Components

Curved beams are subjected to circumferential (σ_{11}), radial (σ_{33}), and out-of-plane shear stresses (τ_{13}) when experiencing bending loads. σ_{11} acts as a normal stress tangential to the curve at any given point. σ_{33} acts perpendicular to the curve at any given point (Figure 13) and is often significantly smaller than that of the circumferential stress [6]. The out-of-plane shear stress can be seen in Figure 14.

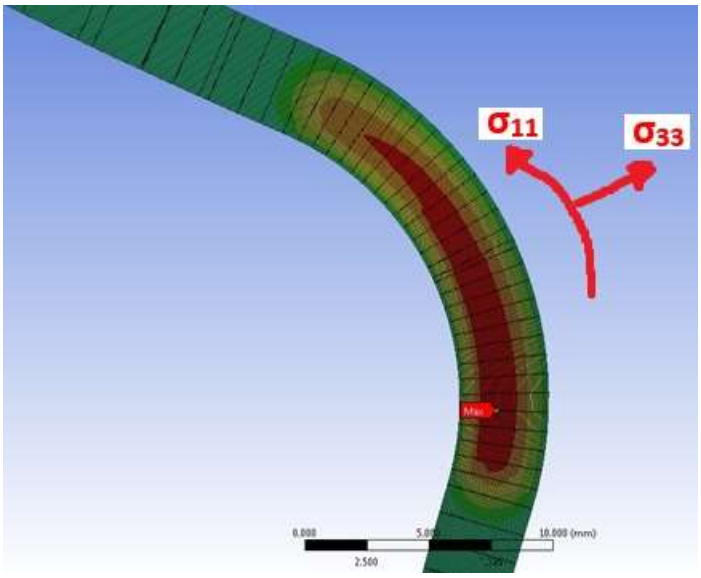

Figure 13: Circumferential and radial stresses represented around the curve of a curved beam [29].

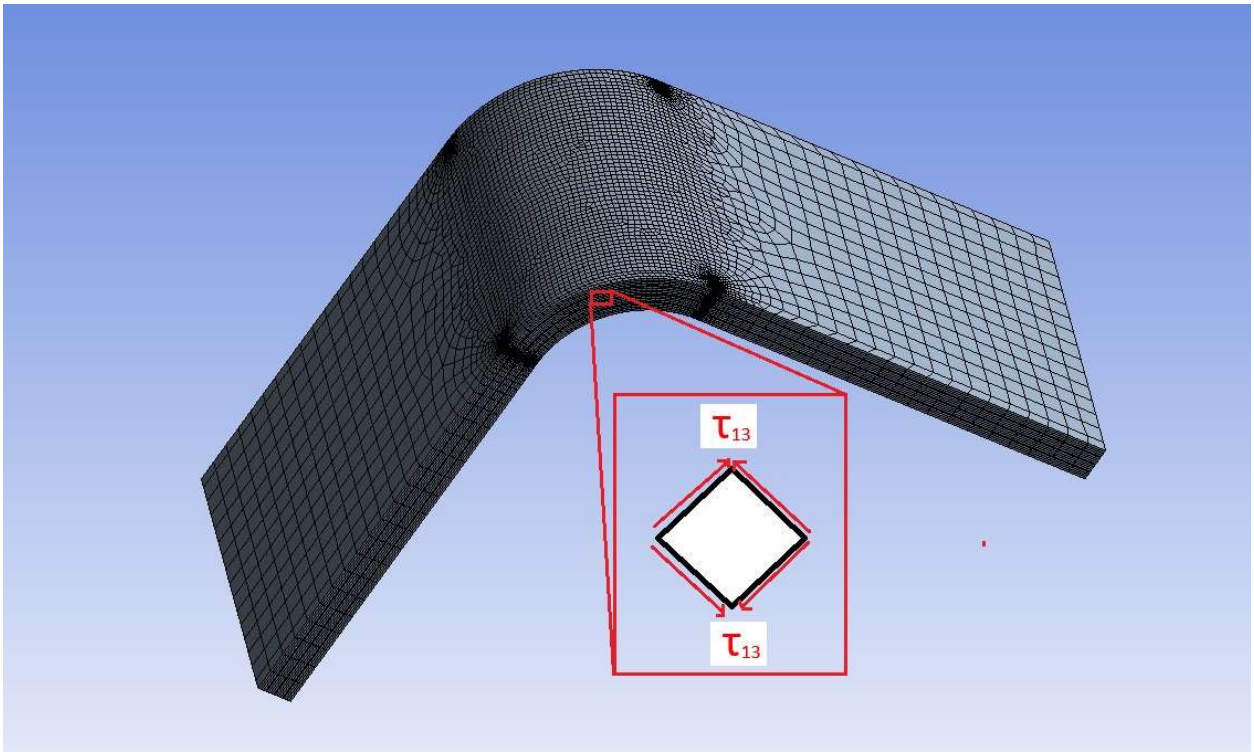

Figure 14: Out-of-plane shear stress in the 1-3 plane represented around the curve of a curved beam.

2.2.1 Radial Stresses in a Curved Beam

Radial stresses in curved beam analysis are often disregarded during stress analysis. This is due to the fact that radial stress is often small when compared to the value of the circumferential stress [6]. When analysing isotropic materials, the focus is on the circumferential stress as it will lead to failure since the properties of the material are the same in all directions. However, it has been found for layered orthotropic materials that the critical stress can be the radial stress [30]. The radial stress can initiate delamination of the layered plies because even though the radial stress may be relatively small, the strength is significantly weaker in the interface between plies in the radial direction.

Several exact solutions and studies have performed studying the 2-D distribution of radial stress across the thickness of a curved beam at the mid-plane width. Timoshenko and Goodier [31] used an elasticity approach to develop an exact solution for the radial stress at any given point around the curve for a homogeneous isotropic material. Kedward developed a solution using mechanics of materials that can determine the maximum radial stress given the applied moment at the end of the beam. These different approaches to solving a similar problem yield similar results in a semi-circular curved beam problem (represented in Figure 15). In Figure 15,

P represents the load applied at each end of the beam, t represents the thickness of the beam, r represents the inner radius of the beam and A-A, B-B, and C-C are respective 2-D cross-sections taken through the thickness at angles (η) of 0˚, 45˚, and 67.5˚. The t/r ratio of the beam is 0.1 for this test-case.

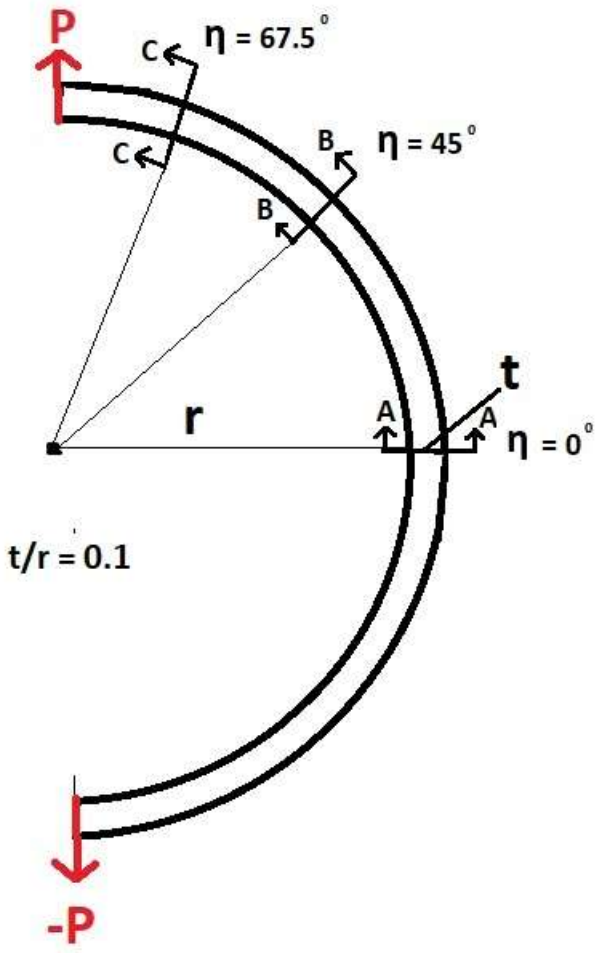

Figure 15: Representation of loading and nomenclature in a semi-circular curved beam.

Referring to Figure 16 one can see various radial stress distributions through the thickness of a curved beam at the aforementioned cross-sections. Notice that the maximum normalised radial stress, $\left(\frac{\sigma_{normal} t\, w}{P}\right)$ where t and w are the thickness and width of the beam, respectively, and σ_{normal} is the nomenclature used for σ_{33} stress, through the thickness occurs around the mid-point regardless of location along the circumference where the solution is looked at. The maximum radial stress occurs at the mid-point of the curve. Additionally, the second plot in Figure 16 shows the Timoshenko and Kedward solutions predict the same maximum location of radial stress. An additional conclusion made by Velazquez is that the t/r ratio does not play a factor in the radial stress distribution [29].

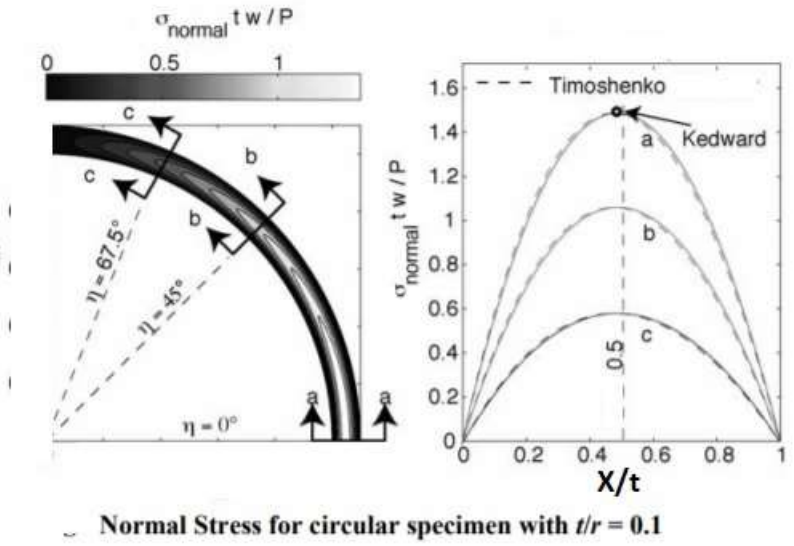

Figure 16: Radial stress distribution through the thickness of a curved beam [29].

Cheung and Sorenson conducted a study on radial stresses and their effects in Glulam Beams (Orthotropic Material) [30]. Their results can be seen in Figure 17. Note that the distributions appear similar to those in Figure 16. The maximum radial stress occurs almost at mid-thickness regardless of the cross-section looked at, the value on top and bottom surface of the curve is 0 psi, and the location of maximum stress occurs at the centre where η = 0˚.

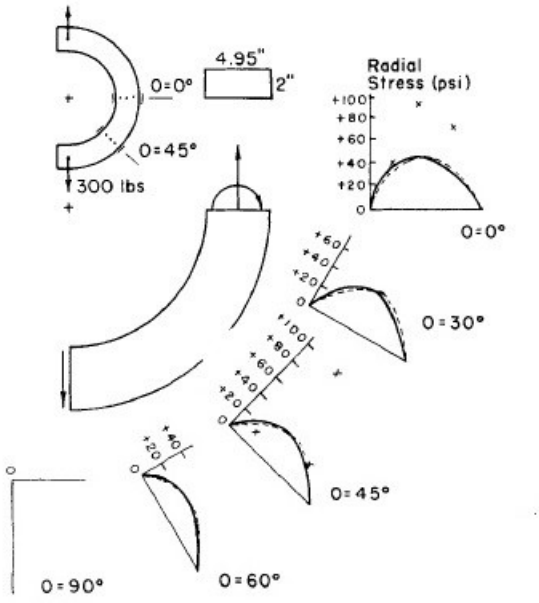

Figure 17: Radial stress distribution through the thickness of glulam beam [30].

All analyses found in literature were for 2-D models and would only be valid in isotropic materials, not taking into account free edge stresses that would be present in composite laminate. The loading case used also influences the result. There is nothing in literature that refers to radial stresses across the width of a composite laminate with angled plies, while also taking into consideration loading induced from applied constraints. When an analytical solution is not available, FEA or experimental analysis can be performed. However, for the case of measuring interlaminar stresses across various cross sections of curved laminates, experimental analysis would prove to be difficult if not impossible. It becomes significantly more difficult when taking into consideration free edge effects of interlaminar stresses at the free edge of the laminate.

2.3 Finite Element Analysis of Composite Materials

Two common methods of performing stress analysis on most material are analytical analysis and numerical analysis, such as finite element analysis. The same is true with respect to composite materials. Analytical analysis for composite materials can be done utilizing classical laminate theory for the assumptions mentioned above, and other more complex numerical methods exist for when the above assumptions do not exist (ie. for interlaminar stresses).

Various levels of macroscopic finite element analysis can be performed for composite materials. The most basic level is using homogenous orthotropic properties to represent the overall laminate as was done by Tauhiduzzaman and Carlsson [32] to model the influence of constraints on the in-plane extensional properties of honeycomb core. This method can give a basic stress analysis but will not give accurate results through the thickness of the laminate and will ignore the different ply angles that make up the lay-up of the laminate. Basic stress analysis through the thickness of the laminate cannot be performed (such as CLT verification), nor can analysis of interlaminar stresses.

The second level of finite element analysis that can be performed on composite materials is by having each individual ply joined directly to each other by node sharing or bonded contact. This method can be referred to as the perfect interface model. Pipes and Pagano began their work on interlaminar stress analysis using this method [33], [34]. Each ply's individual mechanical and physical properties (ie. orientation, thickness) is represented. The in-plane stresses can be accurately determined using this method in most cases. However, where issues arise is between the plies at free edges. When perfect interfaces are used, there is a stress singularity in the interlaminar stresses at the free edge of the laminate due to the difference in properties between the two plies. Stress convergence will be impossible at the perfect interface regardless of mesh refinement as a result of this singularity [35]. Several researchers have used the perfect interface model to predict interlaminar stresses using various methods. Wang and Crossman probed the results at a prescribed distance from the stress singularity in an effort to find the interlaminar stress result where the mesh was converged [36]. Kim and Soni [37], and Brewer and Lagace

[38] used the average of the interlaminar stresses within a given distance from the free edge at the interface where the singularity no longer exists.

The third macroscopic finite element method that has been used to analyse stresses in a composite laminate is resin interface modeling. Isakson and Levy [39] and Murthy and Chamis [40] describe the method as placing a thin layer of isotropic resin between each ply of the laminate. This has the effect of moving the stress singularity from the interface between the two lamina plies to the interface between the resin and the lamina ply. The interlaminar stresses can be extracted through the resin interface layer where the stress singularity no longer exists at the free edge. Haboussi *et al.* [41], [42] created a more complex model for the resin interface where the properties are based on the fibre distribution on either side of the resin layer. Kim *et al.* [43] simulated a resin layer using constant or linear varying compliance matrices. All studies mentioned above illustrate that the relative magnitude of the interlaminar stresses can be accurately determined via placing a resin interface between the layers.

Some drawbacks of this method include the great computing effort that is required due to the incredibly small elements needed to model the resin interface. This effort may not be required in some cases, such as when the edge effect is minimal or not present at all. Therefore, a perfect interface study should be conducted in most cases prior to completing a resin interface model. If the interlaminar stress results at the free edge of the laminate cannot converge with mesh refinement, then a resin interface model should be used. This will likely occur in all but unidirectional composite laminates as unidirectional laminates do not demonstrate the same free edge effects due to their constant material properties through the thickness.

2.3.1 Two-Dimensional Models of Curved Composite Components

There are minimal published studies that consider failure of curved laminate components using two-dimensional finite element models. The studies that do exist typically predict that the failure is due to delamination and go on to predict the likely location for delamination initiation.

Wimmer *et al.* used the two-dimensional modeling methodology to predict delamination of a 15 ply cross-ply laminate [44]. The location of delamination initiation was predicted in terms of ply interface and the location around the curve to be between the fifth and sixth plies and an angle of 50˚-60˚ around the curve from the applied load. A diagram of Wimmer's model and experiment including loading and boundary conditions can be seen in Figure 18.

.

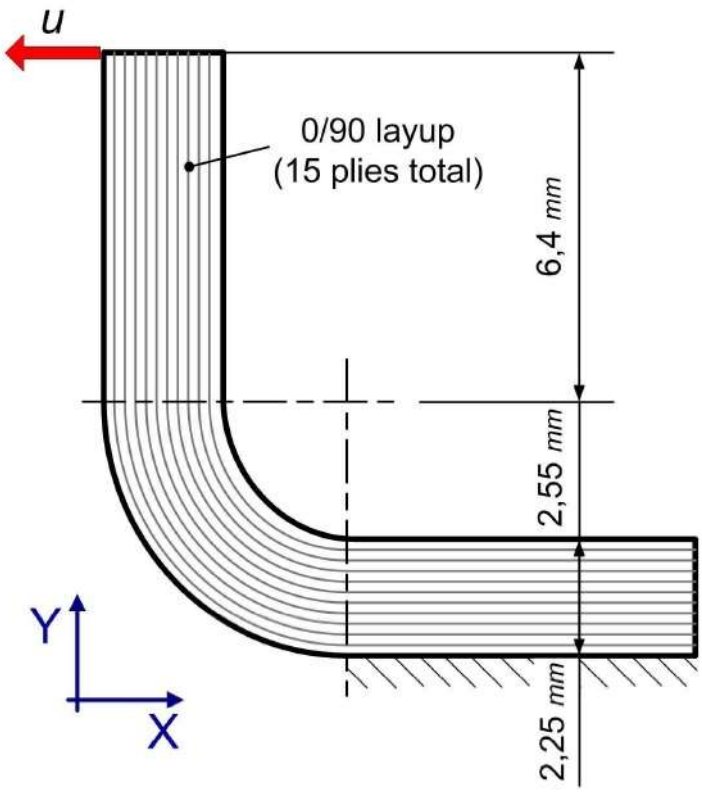

Figure 18: Two-dimensional model of a curved cross-ply laminate created by Wimmer et al. for failure analysis [44].

Cao *et al.* also used a two-dimensional model of a cross-ply laminate with lay-up of $[0_3/90/0_3/90/0/90]_s$ [5] subjected to similar loading as Wimmer *et al*. He determined that delamination initiates at approximately 35% of the thickness of the laminate from the inner surface. Additionally, the location around the circumference of the curve is at 25˚ above the bottom of the curve (refer to Figure 19). These results were confirmed via the experiment performed by Sun and Kelly in reference [45].

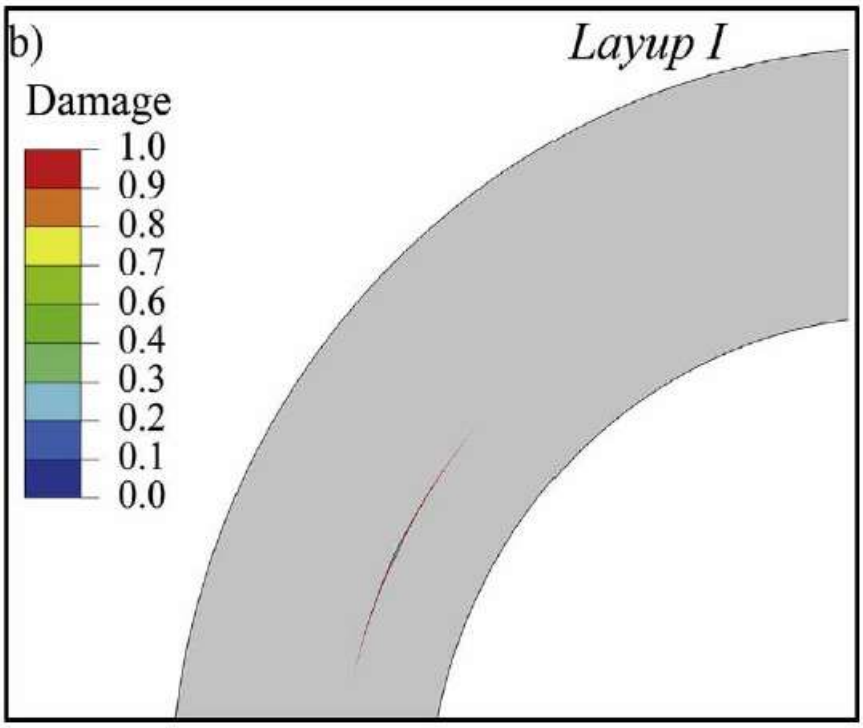

Figure 19: Delamination of a curved cross-ply laminate as predicted by Cao et al. [5].

Gozluku *et al.* used a 2-D FEA model to predict the failure initiation of a cross-ply curved coupon of lay-up $[0/90]_{6s}$ [46]. He verified his model experimentally and determined that the failure mode would be delamination. The delamination was expected to initiate at the fifth resin interface at an angle of 29˚ from the vertical arm to the curve transition. Geleta also used a 2-D FEA to predict delamination initiation in a 24-ply unidirectional laminate [4]. His model was also verified experimentally. He determined that the delamination would initiate at an angle of 22.5◦ from the vertical arm to the curve transition.

The 2-D models were used for the four models above as Wisnom [47] states that plane strain can be assumed when the width to thickness ratio is greater than 10. However, this does not allow for the modeling of the interlaminar stresses across the width of the laminate. Therefore, if there were any interlaminar stress variations in the models above, they would not be captured in this model. Such variations could include free edge effects which are common in laminate composite components. Another variation could be induced torsion as a result of the laminate's proneness to twisting and the boundary conditions applied to the problem. In unidirectional and cross-ply laminates, it is not expected that twisting would occur.

The models above also only look at cross-ply and unidirectional laminates. These are a small subset of the laminates which are used in practical applications. If angled plies were used, the free edge effects which are not captured in the above models would be expected to increase and cause the higher interlaminar stresses to occur at the free edge of the component. In addition,

as angled plies are added, the composite will want to twist and lead to stress variations across the width of the laminate.

2.3.2 Three-Dimensional Stress Analysis

Even fewer researchers have used three-dimensional analysis to predict delamination initiation for curved laminates. Martin in 1991 performed a study in which he used FEA to determine where delamination would initiate in a curved cross-ply laminate component of lay-up $[0_4/90_3/0_5]_s$ as well as how it would propagate [48].

A graph of the interlaminar normal and shear stresses plotted across the width of the coupon (Figure 20) clearly showed localized increases in stress near the free edges. These free edge effects were not shown in his closed form solution. As such, he concluded that free edge effects must be considered when looking at delamination initiation in curved laminates. This requires a three-dimensional model.

After the extensive literature review, no research was found which looked at interlaminar normal stresses across the width of curved laminates between angled plies. The minimal research performed across the width of three-dimensional curved laminates was limited to cross-ply and unidirectional laminates. The free edge effects in laminates with angled plies are expected to be different as the effect changes based on the lay-up. Additionally, unidirectional and cross-ply laminates are not inherent to bending-twisting coupling, so the effect that twisting has on curved composites was analysed in this thesis.

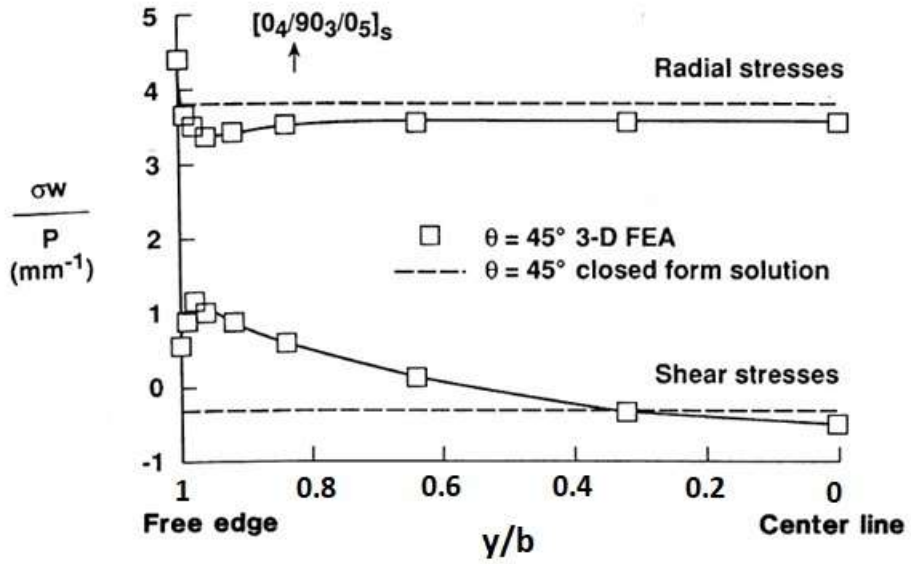

Figure 20: Free edge effects in an L-shaped component along the 0/90 interface [48].

3.0 Materials and Methodology

This section will outline the primary model (baseline model) used for the analyses. Small changes to the primary model were made depending on the study being performed, and each respective sub-section in Section 4.0 - Results and Observations will make note of any modifications made to the model description presented in this section.

3.1 Overall Approach

Three-dimensional finite element analyses were conducted using the software ANSYS Mechanical 18.2 to determine the magnitude and distribution of interlaminar stresses in a curved composite component. An orthotropic resin interface model was used to predict the magnitude and distribution of interlaminar stresses (σ_{33} and τ_{13}) between plies of interest. Resin interface modeling involves placing a thin layer of resin between each ply in the model to represent the

physical layer that coats fibers within a prepreg. The thickness of the resin in this model was assumed to be 10% of the thickness of each ply as 10% is a typical and realistic value as is shown by Kim *et al.* [43] and is further demonstrated by the cross-sectional image taken by Biernacki [49] seen in Figure 21. However, this value will vary in physical models and 10% is Including a resin layer eliminates the stress singularity that exists at the free edge when plies are stacked on top of one another due to the abrupt change in mechanical properties [35] and allows for finite values of interlaminar stresses to be determined.

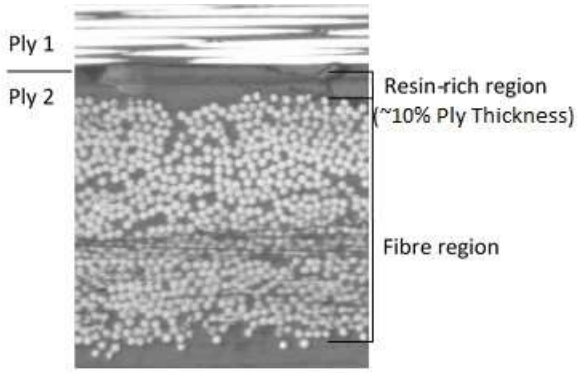

Figure 21: Cross-section image of laminate illustrating that the resin layer is approximately 10% of the ply thickness [49]

Elements were concentrated at both free edges of the curved laminate in selected areas of interest to capture the localized stress gradients. The interlaminar stresses were extracted from within the resin layer across the width of the laminate at multiple locations around the curve of the component.

Several assumptions that were made in this model include:

- A linear analysis was performed as the interlaminar stress results around the curve are not significantly affected by the large deflection occurring at the loaded edge of the curved coupon.
- There are no defects from the manufacturing process (ie. Constant thickness around the curve, all resin has cured uniformly throughout the laminate, no voids).
- There are assumed to be no residual stresses from the curing process. In reality, it is expected that the curved laminate will have a “spring-in” effect as a result of the manufacturing process. This can lead to residual out-of-plane stresses.
- The failure of the component was assumed to be because of delamination due to interlaminar stresses. Failures in the laminae themselves (ie. fibre breakage, matrix cracking) were not considered.
- The magnitude of the applied loads was arbitrary and because this was a linear analysis, the stress scales linearly with the applied load. Even though the predicted stresses are above the failure criteria, failure does not occur as no failure model was implemented in the FEA analysis.

- Delamination failure due to the interlaminar normal stress was assumed to be in tension. Delamination due to compression was ignored for this test case as other failure criteria must be used.
- The boundary conditions are ideal, therefore the portion of the laminate that was clamped was fully constrained in the applicable directions.

3.2 Geometry

The geometry of the curved component is shown in Figure 22 along with the local and global coordinate systems. For the local coordinate system, the 1-Direction is along the length of the arm and around the circumference of the curve, whereas the 3-Direction is always perpendicular to the arms and normal to the curve. It should be noted that for the purposes of this thesis, the 1 and 3 directions are the same throughout the laminate and do not change with each ply regardless of fibre orientation. They are aligned with the 1 and 3 material directions for a 0˚ lamina only. The X and Z coordinates are displayed in Figure 22 as the global coordinates and do not change regardless of the location of the curve. The local coordinate system will be used throughout this thesis and is important for identifying the circumferential (σ_{11}) and radial stresses (σ_{33}).

The horizontal and vertical arms have a length of 40 mm and the inner radius of the curve modeled is 10mm which is 25% of the arm length. The laminate has a total thickness of 3.36mm and a width of 30mm as summarized in Table 1. The thickness of each ply is 0.84 mm, which represents one quarter of the total thickness of the 4-ply laminate.

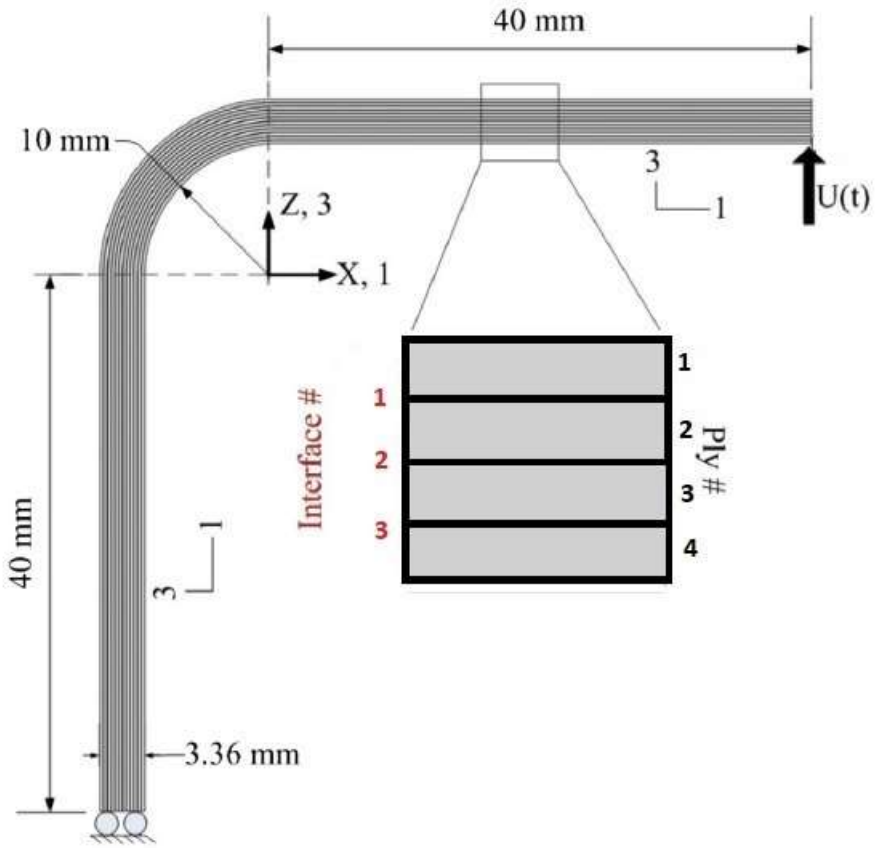

Figure 22: Geometry of the curved component used for the current study [46].

Table 1: Geometry of the curved component used for the current study.

Dimension	Value (mm)
Horizontal Arm Length	40
Vertical Arm Length	40
Inner Radius	10
Outer Radius	13.36
Width (Y direction)	30
Thickness	3.36

3.3 Material Properties

Six different lay-ups were considered in this thesis with the following 4-ply lay-ups being used for the majority of the studies:

The first two lay-ups have been considered in literature:

i) $[0/0]_s$ is a unidirectional laminate.

ii) $[0/90]_s$ is a cross-ply laminate

The following four symmetric lay-ups are composed of angle plies and have not been widely considered in literature:

iii) $[0/10]_s$

iv) $[0/20]_s$

v) $[0/45]_s$

vi) $[0/70]_s$

All laminates modeled in this thesis have a top and bottom ply at a 0˚ orientation. This was done for this study in order to isolate the effects of the radial stress induced by the geometry of the curved component. Having a 0˚ outer ply allowed the circumferential stress to remain relatively constant and independent of the orientation of the inner plies. This enabled the radial and interlaminar stresses to be compared between different lay-ups while keeping the overall circumferential stress equal. Additionally, laminates (iii) – (vi) were analysed to provide a range of ply angles between 0˚ and 90˚. Four plies were used to keep the number of elements in the model at a minimum for computational efficiency.

The FEA software defines the ply orientations by assigning a local element coordinate system to each ply. The material properties are defined with respect to the local element coordinate system and are in effect being oriented in space to represent the fibre direction.

The material that was used in the finite element models was based on a AS4/3501-6 graphite epoxy material with properties taken from Bhat and Lagace [50]. An orthotropic material model was used to represent the laminae and the mechanical properties can be seen in Table 2.

Table 2: Mechanical properties of AS4/3501-6 Graphite Epoxy [50].

Property	Value
E_{11}	142 GPa
E_{22}, E_{33}	9.81 GPa
ν_{12}, ν_{13}	0.3
ν_{23}	0.54
G_{12}, G_{13}	6 GPa
G_{23}	3.78 GPa

An isotropic material model was used to represent the resin between the plies of the laminate and the mechanical properties can be seen in Table 3. The value of E and ν for the resin

was assumed to be the same as the 3-direction properties of the laminate, which is an idealization. In reality, despite the properties being taken perpendicular to the fibre direction, the fibres would still play a role in the property determination especially in compression. Additionally, the resin properties would likely differ in tension and compression, and this is ignored for the purposes of this research as failure is assumed to be in tension which the properties are valid in. Shear and tension allowables were obtained from Cytec [51] and are required to predict delamination in between plies.

Table 3: Mechanical properties of resin modeled in the laminate.

Property	**Value**
E	9.81 GPa
N	0.3
Interlaminar Shear Allowable	94 MPa [51]
Interlaminar Tension Allowable	47 MPa [51]

3.4 Element Type and Mesh

In composite laminates there are free edge effects and potentially high interlaminar stress gradients within a distance of t/2 from the free edge. These must be captured accurately as they may be the maximum interlaminar stresses across the width of the component and as such be the main contributors to delamination. In order to capture these stress gradients accurately, a fine mesh of 3-D elements is required at the free edge (within a distance of t/2 from the free edge). It is important to note that 2-D simulations using layered elements are unable to capture these free edge effects. Convergence studies were performed in order to determine the minimum number of elements required within a distance of t/2 from the free edge so that predicted stress is within 2% of further mesh refinements. It was determined that 50 elements were required in order to converge the magnitude of the interlaminar stresses as seen in Figure 23 .

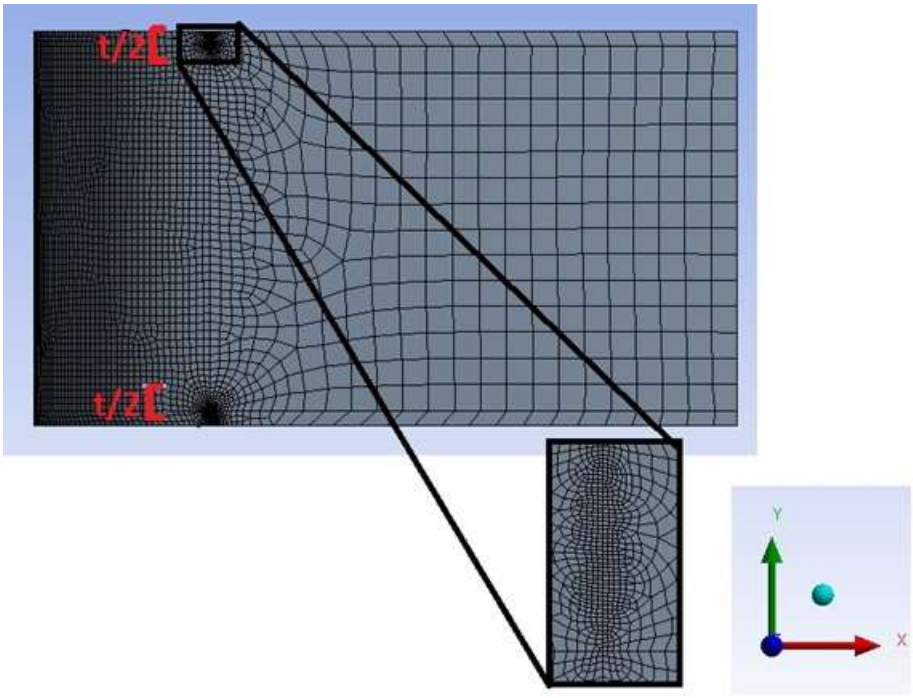

Figure 23: Fifty elements placed at a distance of t/2 from the free edge of the curved coupon.

Higher order hexahedral elements were used for meshing the curved laminate. Refined meshing was used at the free edge in four locations for the curved laminate; both free edges at the ends of the curve identified as zone 1 in Figure 24. A finer mesh was placed at the top and bottom of the curve as this is where the results were extracted. The location of the maximum interlaminar stresses could change with different lay-ups so these two locations were chosen for consistency and to avoid having to mesh the entire edge with small elements. Apart from the free edges, the remainder of the mesh remained relatively coarse in order to allow for a more computationally efficient model. The overall mesh for the curved component can be seen in Figure 24 for a laminate with 4 plies.

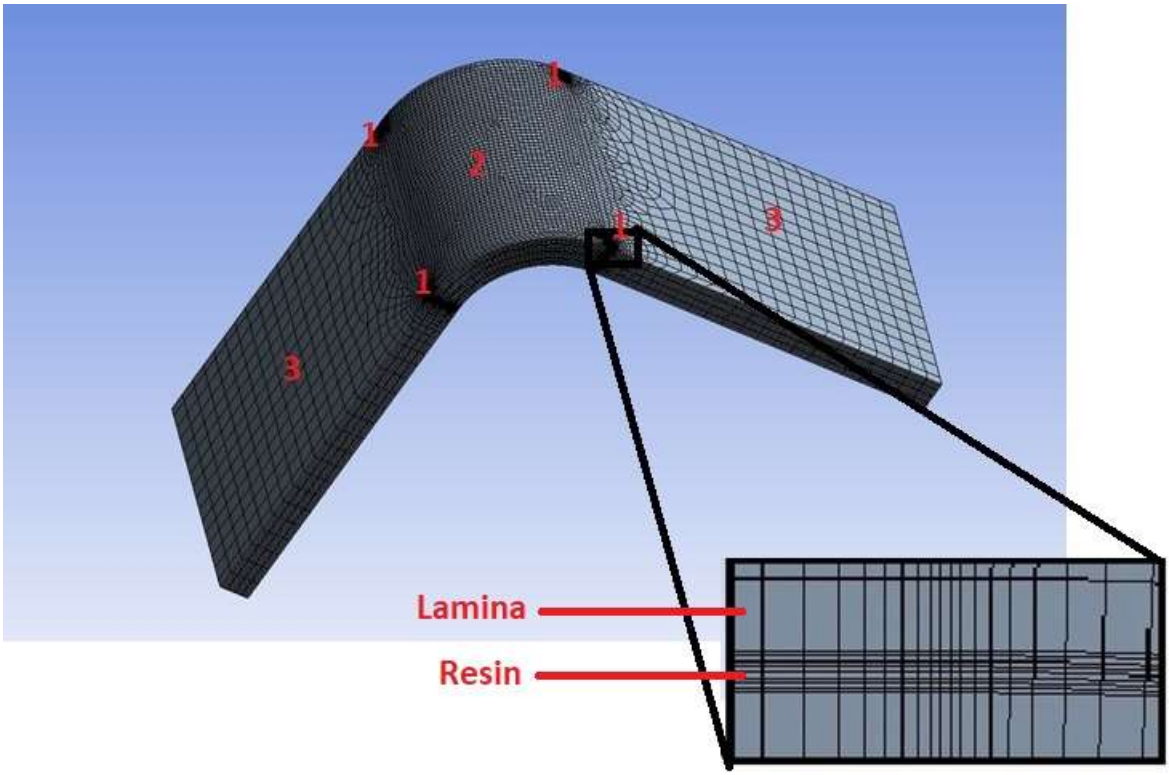

Figure 24: Overall mesh of the curved component showing three regions of meshing refinement. The inset shows a close up of a resin layer.

Within the ACP module in ANSYS the thickness of each ply and its orientation is specified. A shell mesh is created, and then extruded with a specified number of four elements through the thickness of each lamina and eight elements through each resin layer. The ACP model extrudes the shell towards the inside of the curve. Refer to Table 4 to see a description of the meshing parameters for the curved model.

Table 4: Meshing parameters by zone for the FEA model performed in this thesis.

Zone Number	Zone	Mesh Description
1	4 Free Edges	Edge Sizing of 50 Divisions at each free edge (t/2). Higher order hexahedrals.
2	Face of Curve	Face Sizing of 0.5 mm. Higher order hexahedrals.
3	Remainder	Face Sizing of 4 mm. Higher order hexahedrals.

As stated previously, for each lay-up the component was created with four elements through each lamina ply and eight elements through the resin layer. The laminate consists of four plies and has a total thickness of 3.36 mm. The laminae are expected to take up 90% of the volume resulting in a thickness of 0.756 mm per ply. The resin between the plies is expected to take up 10% of the volume resulting in a thickness of 0.112 mm per resin interface layer. An image of the meshing through the thickness of the laminate can be seen in Figure 25. The four elements through each lamina ply can be seen in the first image, while the zoomed in image shows the eight elements through the resin interface.

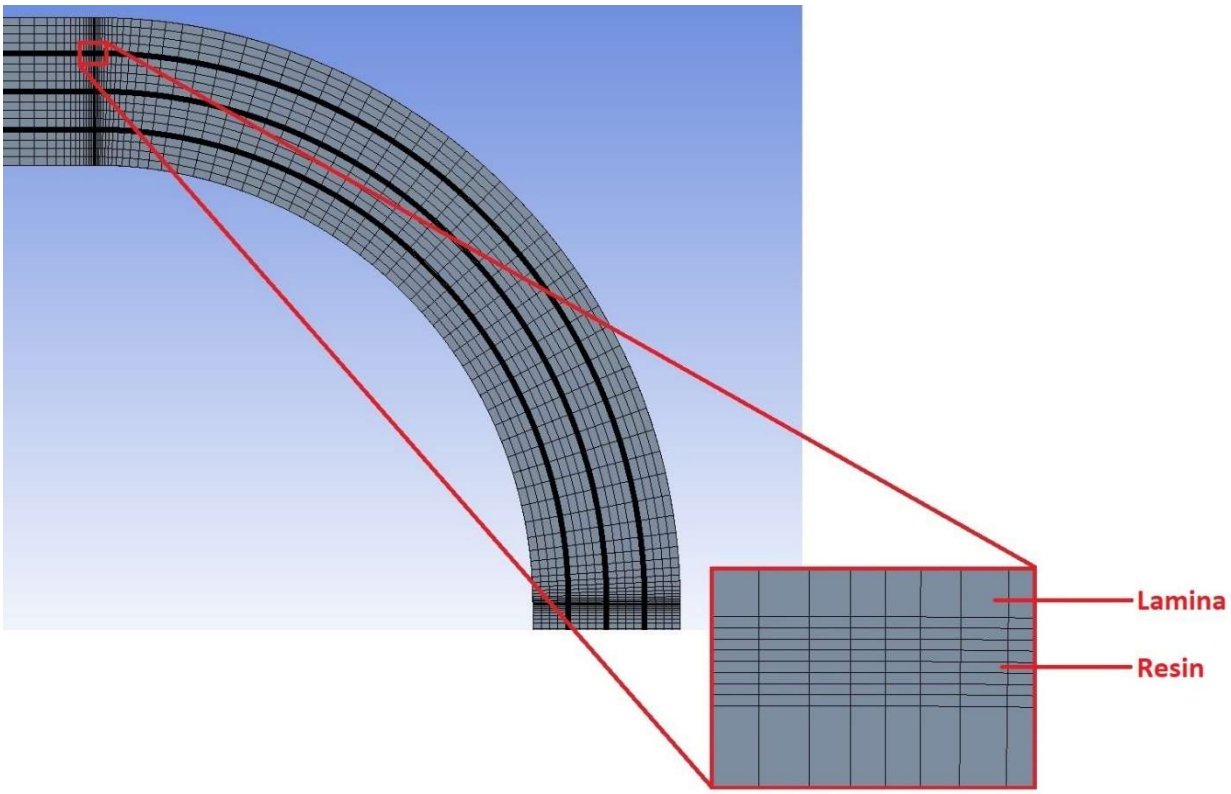

Figure 25: Meshing through the thickness of the curved laminate with a zoom-in of the resin layer modeled between the top and bottom lamina plies.

The aspect ratio of the elements where the results were taken is 2.4. This is an acceptable aspect ratio, as it is under the value of 3.0 [52]. The ideal aspect ratio of an element with quadrilateral faces is 1.0, and if exceeded should be minimized in order in maintain accuracy in the solution [53] . The aspect ratio was limited to 2.4 only in the region where the results were extracted. In the bulk of the component, the same level of accuracy is not required and aspect ratios up of up to 200 were used to maintain computational efficiency.

3.5 Loading and Boundary Conditions

The loading and boundary conditions applied to the curved component were derived by Gozluku *et al.* [46] as a simplified representation of the loading expected to be realized by a wing spar box in an aircraft wing. Refer to Figure 26 to see how the axial load (P), the transverse load (V), and the moment (M) are expected to be transferred from the wing spar box to the wing skin. The model constructed for this thesis only looks at the shear as it still allows the free edge effects of the interlaminar stresses to be modeled while simplifying the loading case.

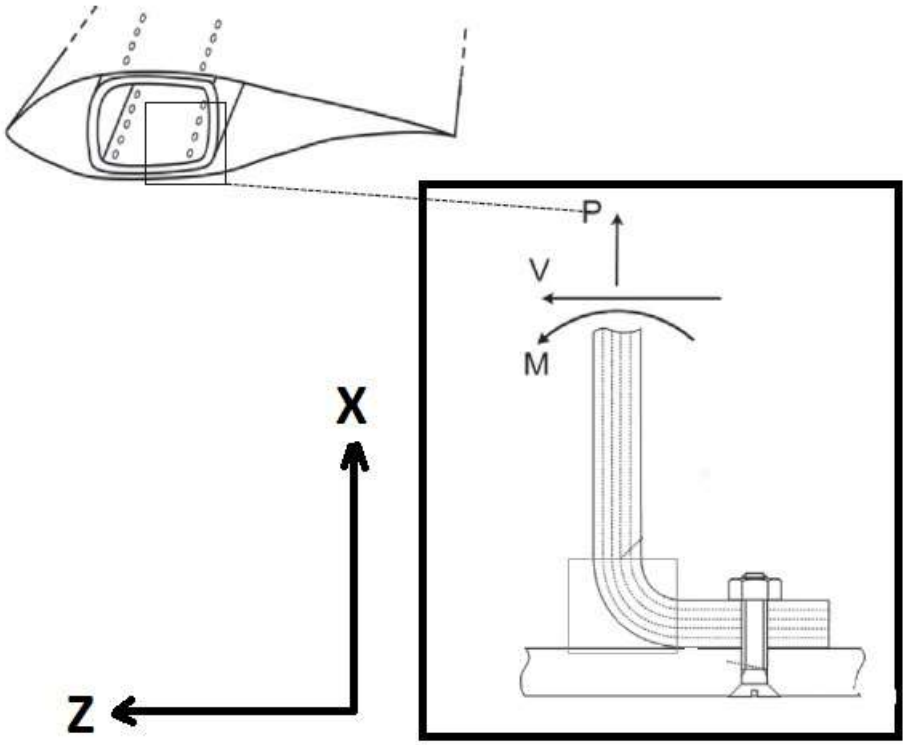

Figure 26: Wing spar box representation of a curved composite component [46].

In the model the free end of the component was displaced 25 mm in the positive Z-direction while the bottom face of the vertical arm is constrained in the Z-direction, but free to move in all other directions. The X and Y directions were constrained using a built-in feature for preventing rigid body motion of the component, while still allowing it to deform locally in the X and Y directions. The physical representation of the loading and boundary conditions can be seen in Figure 27.

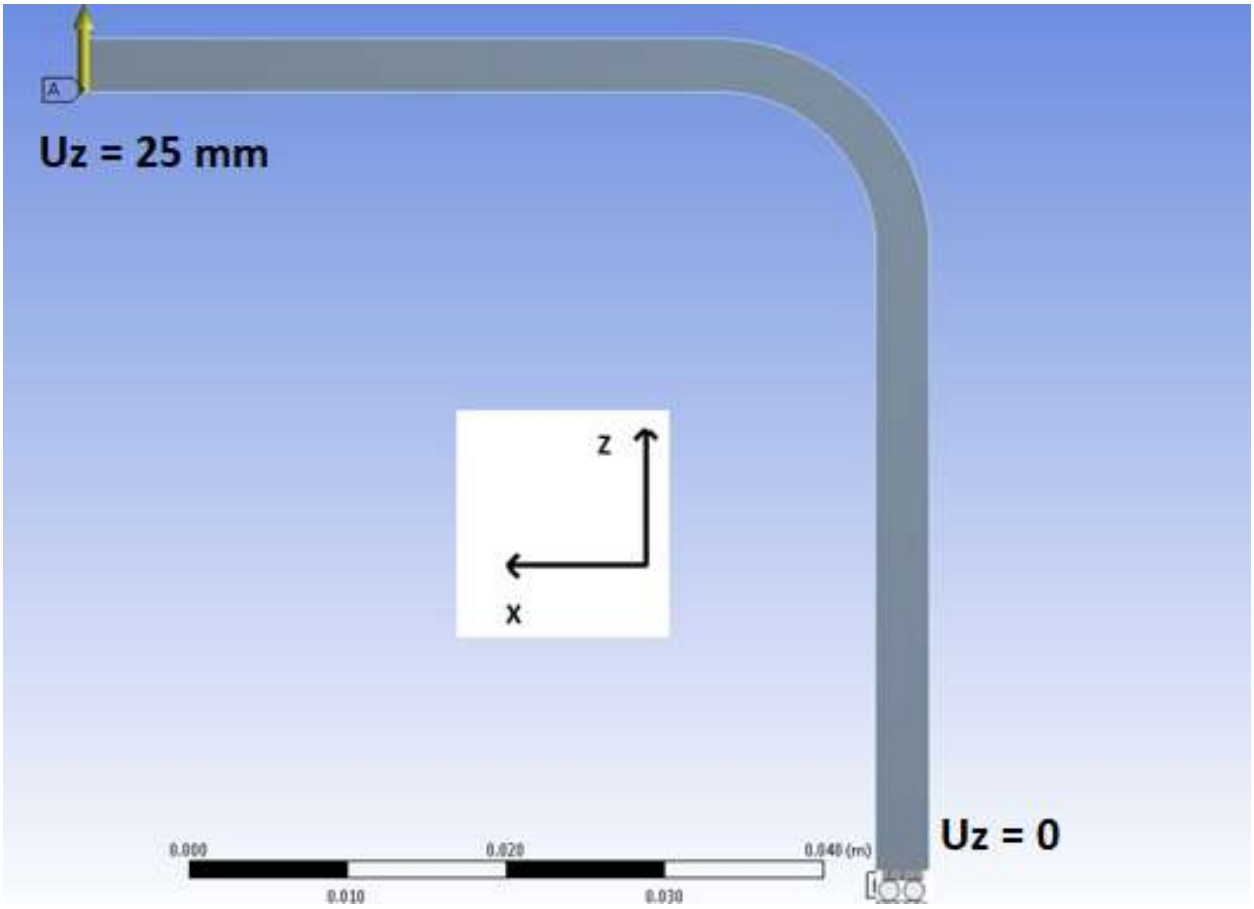

Figure 27: Loading and boundary conditions applied to the FEA model performed.

3.6 Solution and Post-Processing

Despite there being a large deflection of 25 mm taking place at the unclamped end of the curved coupon, it was determined that the predictions of the overall deflected shape and the overall interlaminar stress distribution remained the same between a linear and non-linear analysis. The interlaminar normal stresses around the curve of the coupon only varied by 2 MPa between the two analysis methods. A linear model was chosen because of the linear relationships between loading and stress as well as computational efficiency. The linear relationship allowed the displacement to be scaled in order to obtain the same circumferential stress between models. Computational efficiency is gained by using a linear model as the linear model takes < 5 minutes to run, while a non-linear model with the same meshing parameters takes > 60 minutes. The models were run on an Intel (R) Xeon (R) CPU E7-4870 v2 @ 2.30 GHz 2.29 GHz (2 Processors) with 32 GB of RAM.

The results were extracted along the transition between the curve and the straight portion of the curved laminate at the centre of the resin layer at both the bottom and top of the curve as shown in Figure 28 and Figure 29. Since the location of maximum stress could change with the different lay-ups, a consistent location was chosen for comparison.

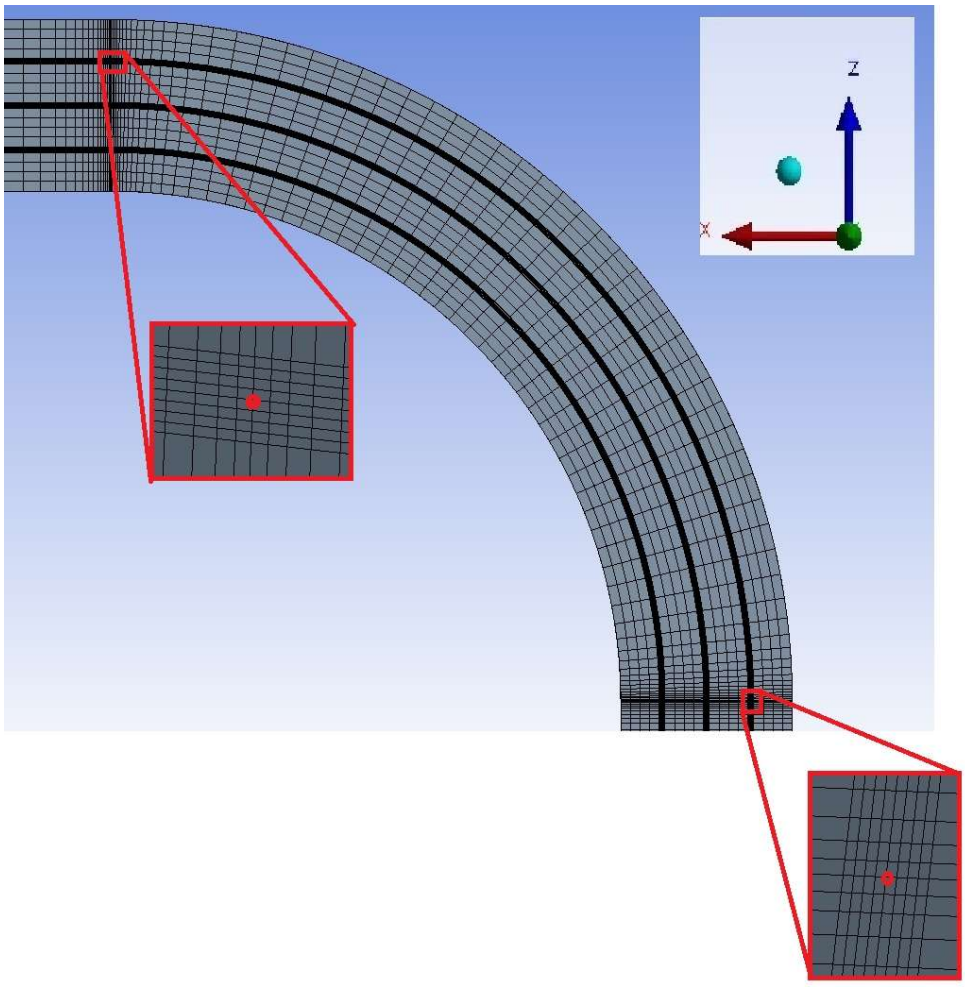

Figure 28: Extraction paths at the top and bottom of the curve taken through the centre of the resin layer at the resin interface between the top and bottom lamina.

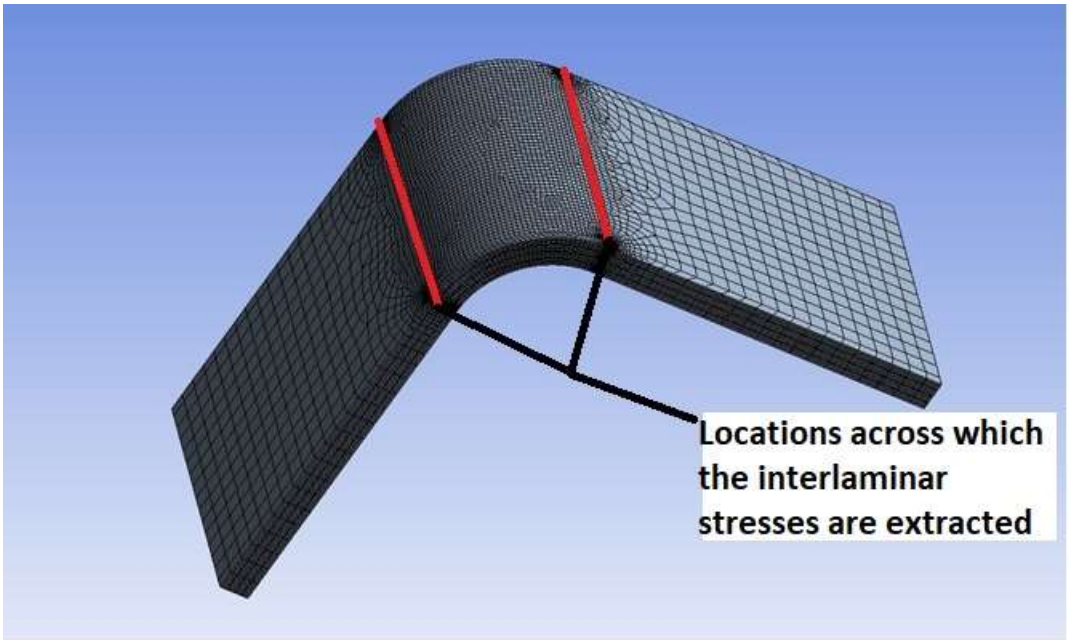

Figure 29: Extraction paths at the top and bottom of the curve across the width.

4.0 Results and Observations

The results of this thesis can be categorized into five main areas. Firstly, the cross-ply model that was used to make the predictions for this thesis was verified through comparison with predicted stresses and published experimental results from Gozluku *et al.* [46]. Once verified, the model was used to predict which interlaminar stress (σ_{33} or τ_{13}) is the main contributor to delamination in a curved laminate. This was done by modeling the interlaminar stresses across the width of the curved composite components of five distinct lay-ups and using the Hoyt failure criterion from Equation (5) to predict delamination initiation. The Hoyt criterion was then separated into σ_{33} and τ_{13} contributions and the main contributor to delamination initiation in a curve was determined. Thirdly, a model was run to determine the effect that changing the radius of the curved component has on the radial stress. The radius of the curved component was varied from 2.5 mm to 15 mm and the effect on the maximum radial stress in the component was noted. Next, the location of maximum interlaminar normal stress across the width of a laminate was determined by varying the lay-up. There was a comparison between straight and curved laminate components to explain the compounded effects of interlaminar normal stress at the free edge and radial stress across the width of the laminate. Finally, the effects of induced torsion in a laminate due to constraints and loading which exist due to practical applications, were investigated with respect to the interlaminar normal stress distribution and maximum value.

4.1 Verification of the Modeling Procedure

The modeling procedure used in this thesis was verified through comparison with published finite element predictions, published experimental results and comparison studies. Verification involved two steps: comparison of maximum midplane stresses with published 2-D FE and experimental results and a comparison between stress predictions for perfect and resin interface models.

4.1.1 Gozluku *et al*'s Finite Element Model and Experimental Results

Gozluku *et al.* published one of the few studies which has investigated interlaminar stresses in curved composite components [46]. They performed a 2-D FEA using a linear perfect interface model to predict where delamination initiated and how it propagated in a cross-ply laminate. They performed a physical experiment to verify the predictions of the FEA model. Their FEA prediction of delamination initiation was the same as the delamination initiation realized in the physical experiment. As a result of the accuracy of the model, it was chosen to be re-created using a 3-D model within this thesis. By showing that the mid-plane of the 3-D model matches Gozluku *et al*'s 2-D FEA model, it can be said that the 3-D model also matches the results of the physical experiment. Once the 3-D stress was verified, the interlaminar stress distribution across the width of the curved laminate could be taken, which has not previously been possible using 2-D models.

4.1.1.1 Experimental Set-Up and Results from Gozluku *et al.* [46]

As per reference [46], Gozluku *et al.* performed an experiment on delamination initiation of a cross-ply curved component with the physical dimensions seen in Figure 30. The laminate was composed of 12 layers of Hex-Ply AS4/8552-5HS plain weave fabric plies with a lay-up of $[0/90]_{6s}$. Their experiment involved clamping the vertical arm in a clamp free to slide along the x-axis and displacing the bottom edge of the horizontal arm in the positive z-direction until delamination initiated. The experimental set-up can be seen in Figure 31.

At a displacement of 19mm on the unclamped end of the coupon, delamination was seen to initiate at 42% thickness from the inner surface of the laminate, which was the fifth resin interface from the inner surface. The delamination initiated at approximately 33˚ from the vertical arm to the curve transition. A photograph of the delamination initiation and propagation can be seen in Figure 32. The location of initiation is represented by the "x," while the left most

and right most points of the delamination propagation are represented by the “L” and “R” respectively.

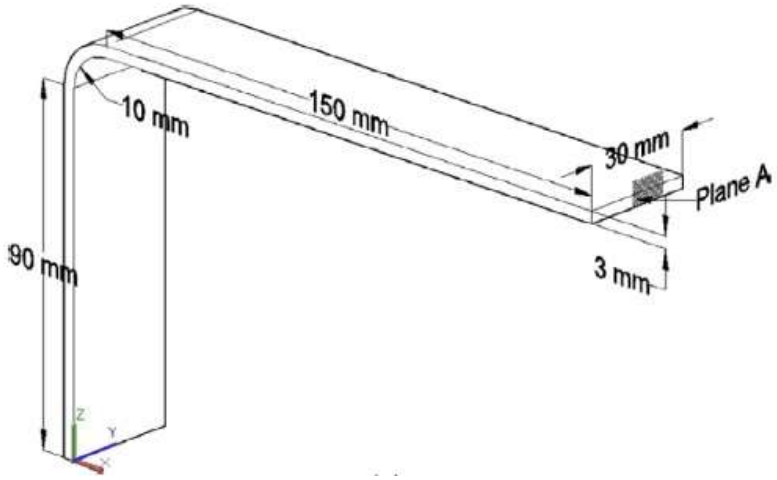

Figure 30: Physical dimensions of the curved laminate used in Gozluku et al’s experiment [46].

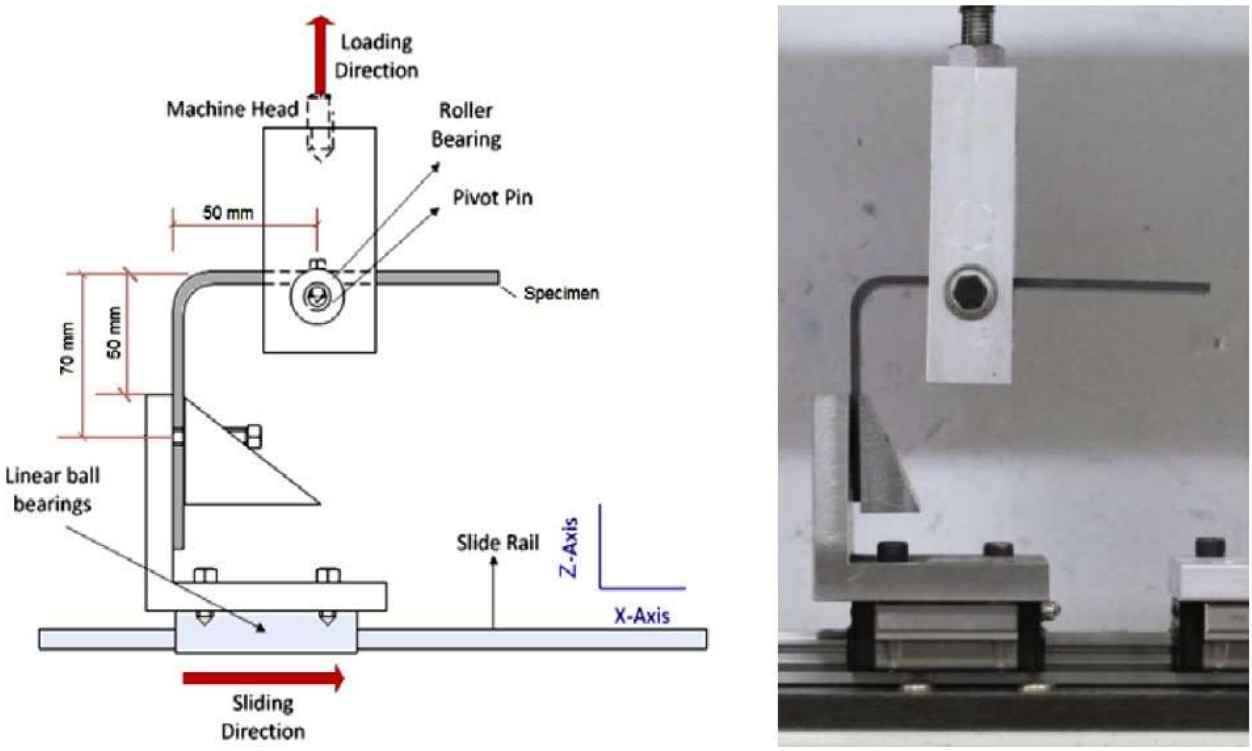

Figure 31: Experimental apparatus used in the experiment performed by Gozluku et al. [46].

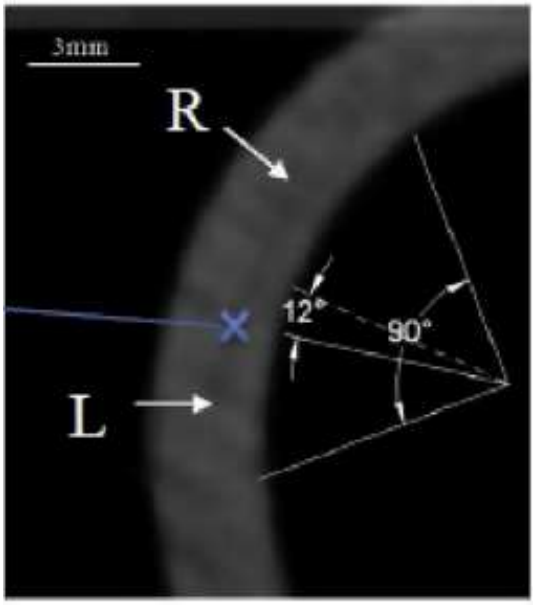

Figure 32: Photograph representation of Gozluku et al's experimental results where "x' marks delamination initiation site, "L" and "R" represent the left and right most points of delamination propagation [46].

4.1.1.2 Finite Element Analysis from Gozluku *et al.* [46]

Gozluku *et al.* created a 2-D, linear, perfect interface FEA model to re-create the interlaminar stresses experienced by the curved component during the experiment. The physical geometry of the curved coupon was simplified to be a 50mm by 50mm angle as that is where the clamp and loading were applied as per Figure 31. A vertical displacement of 25 mm was applied at the unclamped end of the angle component. Failure was noted to occur in the model at 19.4 mm displacement, which is nearly identical to the experimental result of 19 mm. The bottom portion of the vertical arm was constrained in the z- axis to only allow it to roll along the x-axis.

Interlaminar stress predictions for σ_{33} and τ_{13} can be seen in Figure 33 where the regions of highest stress are indicated in red. The delamination initiation point was determined to be at the fifth resin interface from the inner surface at an angle of 29˚ from the vertical arm to the curve transition as identified in Figure 34. This corresponds to the same interface and a 4˚ difference in location around the curve as the experimental results. The location of maximum σ_{33} coincides with the location of delamination initiation. This is expected as σ_{33} is often the key indicator of delamination as per several of the failure theories identified in the literature review in Section 2.1.5.2.

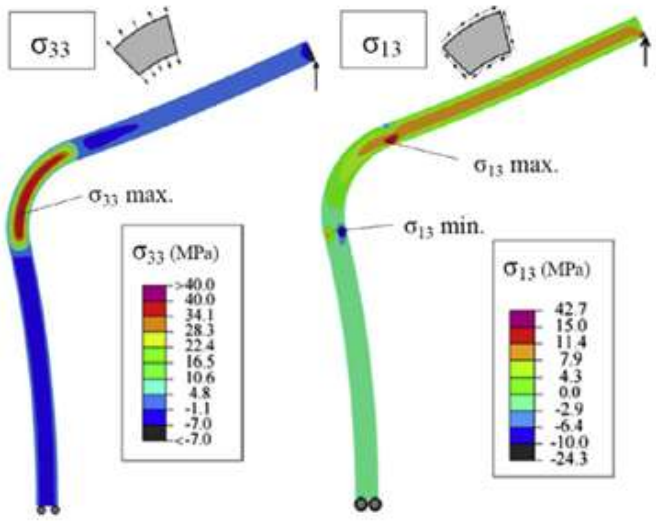

Figure 33: Gozluku et al. FEA results for interlaminar normal and interlaminar shear stress in the 1-3 plane [46].

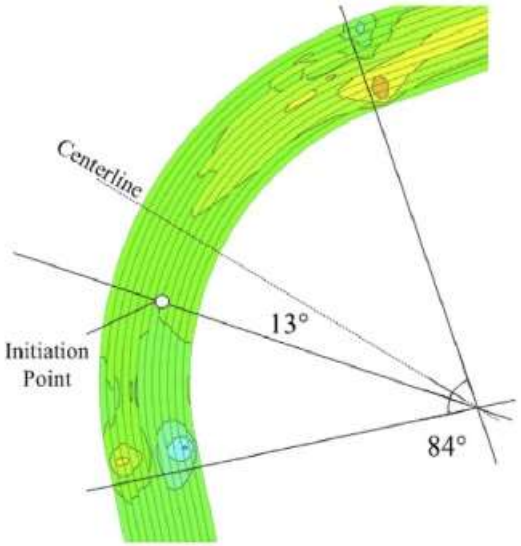

Figure 34: Gozluku et al. FEA result for delamination initiation point in the curved laminate component [46].

4.1.1.3 Verification of Modeling Approach

Gozluku *et al*'s finite element model used to predict delamination initiation was a two-dimensional, perfect interface, linear representation. This represents a state of plane strain and is unable to capture any variance in stress distribution across the width of the laminate. Two dimensional models are often employed for computational efficiency and time effectiveness [54], however, they are unable to predict the free edge stresses between laminae plies due to material mismatches. Although Gozluku *et al*'s 2-D model was able to predict the same location for delamination as the experiment, the free edge stresses may not be critical in the specific cross-ply laminate he used. A 3-D model was considered for this research because the free edge stresses may be critical in other cross-ply laminates and laminates with angle plies as shown by Martin [48] and the interlaminar stress distributions across the width will be required.

In the current research, a 3-D approach was used in an effort to model stress distributions across the width of the laminate. In order to verify the 3-D model, the geometry, material properties loading and boundary conditions were chosen to be the same as Gozluku *et al*'s model. Details of the geometry, loading, and boundary conditions were presented in Section 3.0. The material properties were taken from Gozluku *et al.* [46] as Hex-Ply AS4/8552-5HS and can be seen in Table 5. The 3-D model was compared to Gozluku *et al*'s results in terms of magnitude and overall distribution of stresses therefore a coarse mesh was sufficient. A perfect interface was assumed between each laminae ply with no resin modeled in between. Each ply was meshed with four elements through the thickness and the overall mesh can be seen in Figure 35. A linear solution was used for reasons mentioned in Section 3.0 despite the large deflection of 25 mm. The maximum values of σ_{33} and τ_{13} as well as their distribution at the laminate's mid-plane were extracted.

Table 5: Material properties for Hex-Ply AS4/8552-5HS used in FEA model [46].

Property	Value
Lamina - E_{11}	55.7 GPa
Lamina - E_{22}, E_{33}	8.5 GPa
Lamina - ν_{12}, ν_{23}	0.3
Lamina – ν_{13}	0.045
Lamina - G_{12}, G_{23}	4.9 GPa
Lamina – G_{13}	3.1 GPa
Matrix – E	8.5 GPa

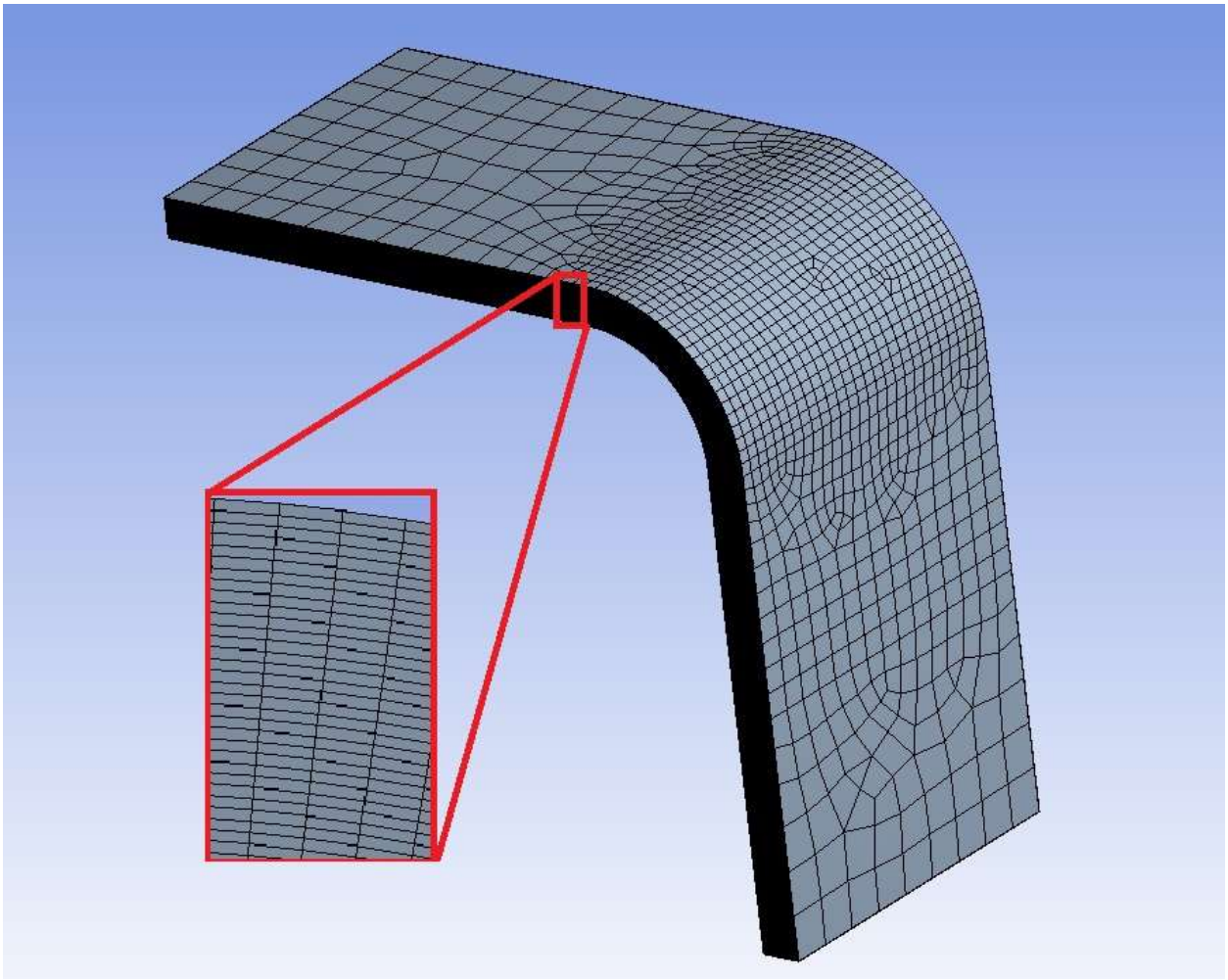

Figure 35: Mesh of 3-D perfect interface FEA model of the curved laminate component with zoom-in of mesh through the thickness.

The mid-plane results of the σ_{33} distribution for the 3-D model can be seen in Figure 36. It can be seen that the maximum σ_{33} occurs at the fifth interface at approximately 25˚ from the vertical arm to curve transition. This is within 8˚ of the experimental result of where delamination initiated. In addition, by comparing the 3-D model to Gozluku *et al*'s model (Figure 33), it becomes evident that the σ_{33} distribution is similar. The maximum σ_{33} value occurs within 4˚ of one another. The mid-plane results are expected to be representative of the 2-D model as both are in a state of plane strain.

The mid-plane results of the τ_{13} distribution for the 3-D model can be seen in Figure 37. It can be seen that the maximum magnitude values of τ_{13} occur at the transition between the horizontal arm and the curve as well as the transition between the vertical arm and the curve. This is the same as was seen in Gozluku *et al*'s FEA model in Figure 33.

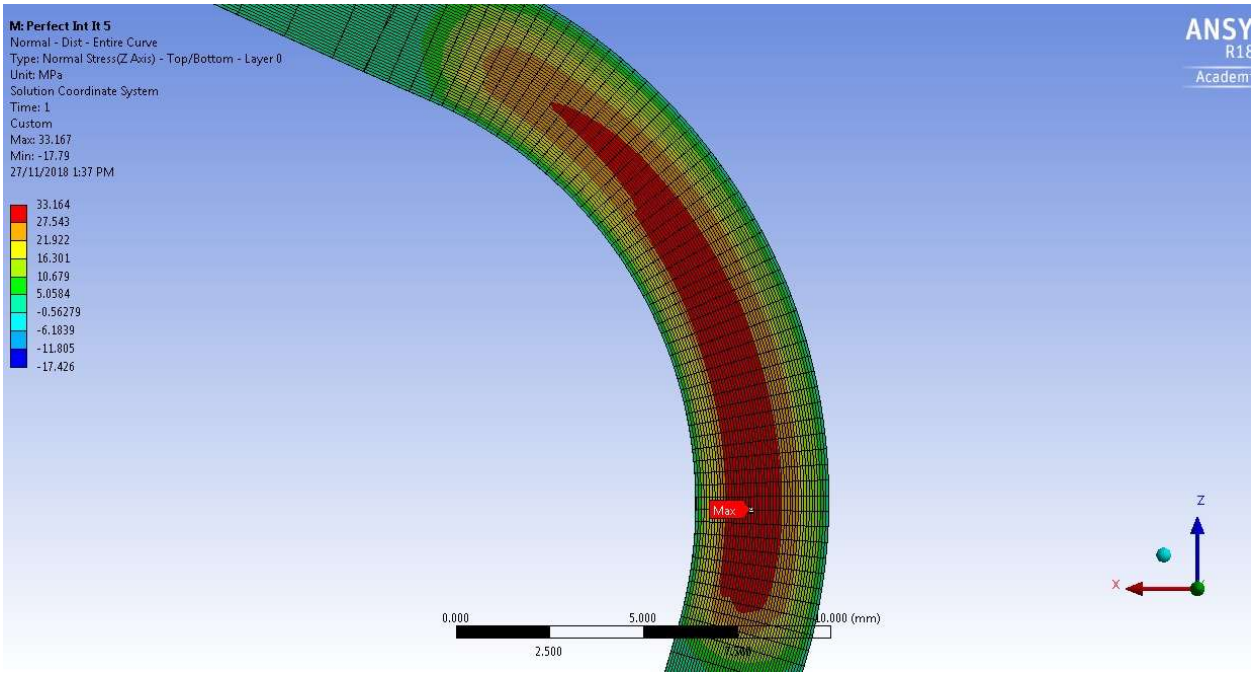

Figure 36: FEA Results - σ_{33} distribution at the mid-plane of the curved laminate component re-creating Gozluku et al's experiment.

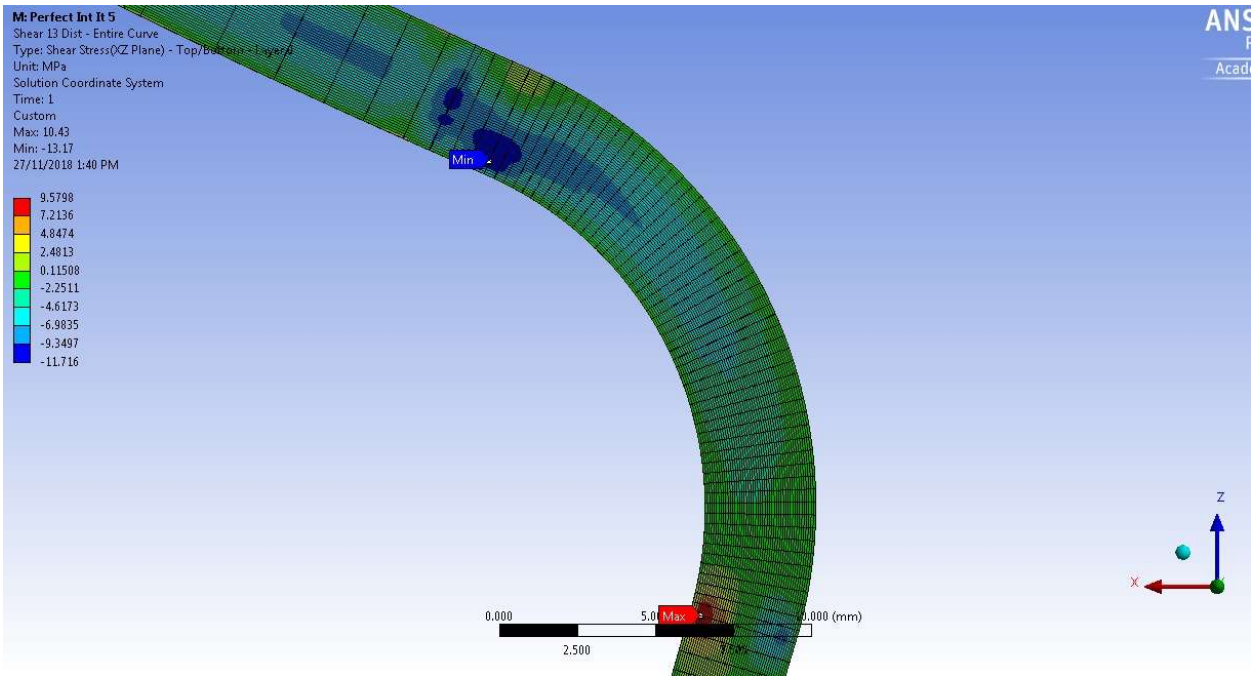

Figure 37: FEA Results - τ13 distribution at the mid-plane of the curved laminate component re-creating Gozluku et al's experiment.

Refer to Table 6 in order to see the magnitudes of the maximum σ_{33} and τ_{13} values for the 3-D model and Gozluku *et al*'s model. The magnitude of the maximum σ_{33} in the 3-D model is within the range seen in Gozluku *et al*'s model as there is a high stress gradient. Referring to Figure 33 it is evident that the contour colour purple cannot be seen in the image despite it representing the maximum value. As such, the range is what is represented by the contour colour red which can be seen in the image. Some difference is expected when comparing the predictions of the two models as the mesh is not the same, in terms of sizing and element type

When comparing the τ_{13} magnitudes, there is a high stress gradient in the Gozluku *et al.* model where the maximum value of the interlaminar shear stresses vary greatly in one miniscule region (refer to Figure 33). As a result of this, the predictions of the 3-D model appear to be closer to the lower bound of Gozluku *et al*'s prediction. Both magnitudes at the top and bottom of the curve transition are within 25% of the lower bound of Gozluku *et al*'s predictions.

Table 6: Comparing Gozluku et al's 2-D Model to the 3-D model where the interlaminar stress results are taken at the mid-plane.

Model	Max σ_{33} (MPa)	Top of Curve $\lvert\tau_{13}\rvert$ (MPa)	Bottom of Curve $\lvert\tau_{13}\rvert$ (MPa)
Gozluku *et al.* Model (2-D)	34.1 - 40	15 – 42.7	10 - 24
Three-Dimensional Model	33.2	11.7	9.6

4.1.1.4 Conclusion – Verification of Modeling Approach

The 3-D model is able to predict the overall distribution of the interlaminar stresses at the mid-plane of a curved laminate. This was shown by comparing the 3-D model to a published experiment and showing that the 3-D model accurately predicted the results. In addition the 3-D model, when compared to a published FEA model, validated by experiment, illustrated similar interlaminar stress distributions and magnitudes. As the results were matched at the mid-plane of the three-dimensional model, the results can now be looked at across the width of the laminate in order to see how the interlaminar stresses vary across the width of the laminate. This was not previously possible with the 2-D model.

4.1.2 Comparison Between Resin and Perfect Interface Models

The resin interface and the perfect interface models were compared to determine capabilities of each for predicting interlaminar stress distributions. While the perfect interface

model provides a computationally efficient method for determining the overall distribution of stresses and the magnitude in the bulk of the laminate, it is not able to predict finite values (converged) of the interlaminar stresses at the free edge. This is due to the stress singularity that is inherent when two dissimilar materials meet at a free surface. In laminates with angled plies, it can be reasonably expected that there will be free edge effects at the free edges of the laminate. As stated in Section 2.3, a resin interface has been shown in the past to have the ability to predict the magnitude of the interlaminar stresses at the free edges of laminates. Predictions of σ_{33} distribution across the width of the laminate using the perfect interface model verified in Section 4.1.1 were compared to the resin interface model outlined in Section 3.0. The physical geometry, material properties, loading and boundary conditions remained the same for both the perfect and resin interface models of this $[0/90]_{6s}$ laminate. The resin interface model contained 11 resin layers with eight elements through the thickness and four elements through each lamina ply. There were 75 elements within a t/2 region from the free edge while the perfect interface mesh remained coarse. The interlaminar stresses were extracted across the width of the laminate in the outer resin interface where the vertical arm transitioned to the curve.

Figure 38 shows a comparison between the radial stress distribution across the width of the laminate for the perfect and resin interface approaches. The radial stress is 5 MPa +/- 0.9 MPa between y/b = -0.99 and y/b = 0.99 for both approaches. Within the range of y/b =-0.99 to y/b=-1.0 and y/b = 0.99 to y/b =1.0, however, the free edge effect is identified by the sharp increase in magnitude using resin interface modeling. This shows that resin interface modeling is required to model curved laminates if the maximum interlaminar stress of the entire laminate is required. This is especially important when predicting delamination initiation.

The sharpness in the free edge effect where it begins at y/b = 0.99 is common of cross-ply laminates and has been confirmed by Sarvestani [55]. Herakovich [56] predicted the interlaminar normal stress to increase by a factor of 300% between the regions of y/b=0.99 and the free edge for a cross-ply laminate using FEA.

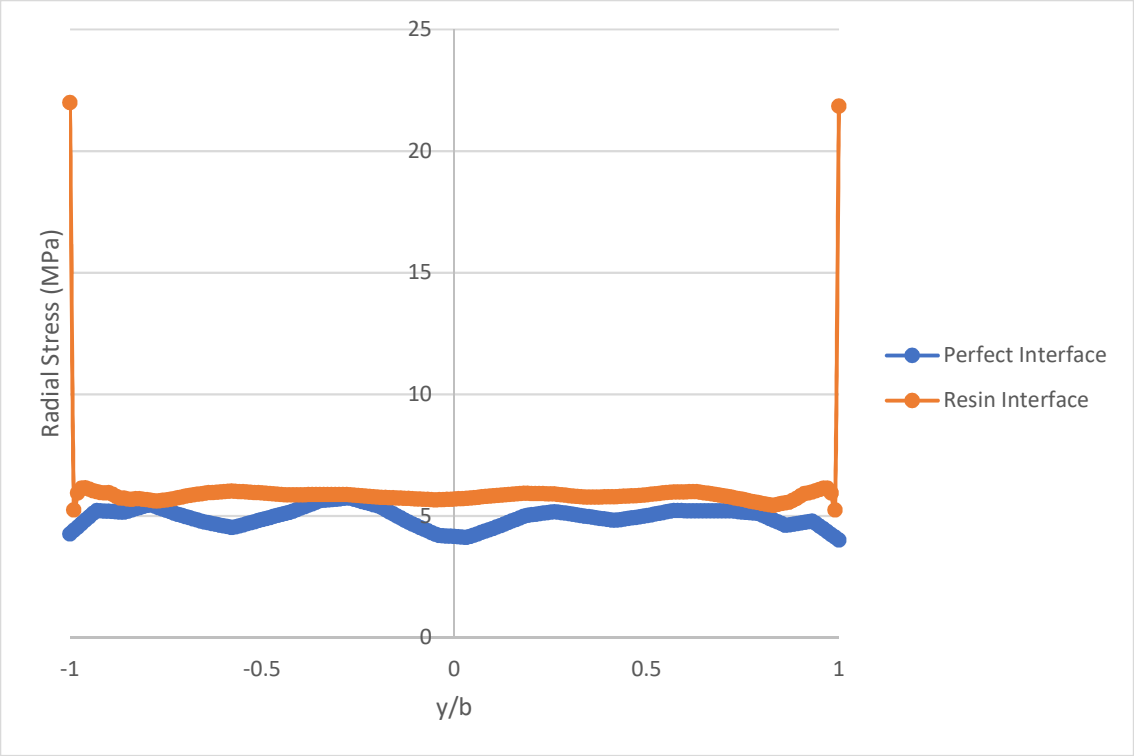

Figure 38: Radial stress distribution across the laminate width for the perfect and resin interface modeling approaches at the transition between the vertical arm and the curve of the curved coupon.

It has been shown that resin interface modeling is required for predicting finite values of the interlaminar stress at the free edge of a curved laminate. Perfect interface models should only be used for looking at in-plane stresses through the thickness of laminates.

4.1.3 Summary – Verifying Modeling Method

It has been shown that a 3-D model is required to predict the interlaminar stress distribution across the width of a curved composite coupon because the interlaminar stress is not constant. In addition, to determine the localized stress gradients at the free edge of the curved composite component a resin interface model is required. There may be combinations of lay-ups, loading, and geometry that do not require 3-D or resin interface modeling as the maximum interlaminar stresses may occur in the mid-plane and can be predicted by 2-D models, but it is difficult to know what these combinations are. While Gozluku *et al*'s 2-D model was able to predict the location of the delamination initiation, it was not reported whether or not the magnitude of loading that caused failure was predicted accurately. As a result a 3-D resin interface model must be employed to get the entire picture of interlaminar stresses acting in a curved composite component. As such, it is recommended to use a 3-D resin interface model in

all laminates with angled plies and this was the modeling approach used for all remaining models in this thesis.

4.2 Determining the Main Contributor to Delamination Initiation

The purpose of this study was to determine how curvature in a laminate affects the contributions of each component of interlaminar stress to delamination initiation. The effects of curvature were determined by comparing the maximum value of σ_{33} between straight and curved coupons that had the same value of σ_{11}. Five lay-ups were considered as shown in Table 7. These five lay-ups were loaded to the same σ_{11} (along the length of the coupon). The maximum compressive value of σ_{11} in the top ply of the curve was made equal to σ_{11} in the top ply of the straight laminate by adjusting the displacements applied to each model. Referring to Table 7 the axial stresses (σ_{11}) applied in order to maintain an equivalent loading case can be seen. The Hoyt failure criterion from reference [25], seen in Equation (5) in Section 2.1.5.2 was used to compare the contributions of σ_{33} and τ_{13} to failure initiation between a straight and curved geometry. The Hoyt failure criterion used the material allowables for σ_{33} and τ_{13} as defined in Table 2.

Table 7: Loading conditions applied to the straight and curved laminates in order to model equivalent loading.

Lay-Up	Min σ_{11} – Curve (MPa)	Top Lamina σ_{11} – Straight (MPa)
$[0/10]_s$	-1851	-1848
$[0/20]_s$	-1888	-1871
$[0/45]_s$	-1901	-1897
$[0/70]_s$	-1878	-1874
$[0/90]_s$	-1864	-1861

When comparing the contribution of the three interlaminar stresses to delamination initiation it is expected that σ_{33} is the largest contributor. This was stated by Yarrington *et al.* in reference [23] and is evident in the failure criterion proposed by Adams and Wake in reference [24] where the only interlaminar stress considered is σ_{33}. In order to confirm that this is in fact, the case, a study was performed in order to determine the main contributor to delamination initiation.

The model of the curved composite component was run using the same method as described in Section 3.0. Additionally, a 100 mm straight coupon with a width of 30 mm and a thickness of 3.36 mm was used with a displacement applied at one end and fixed in all directions at the other end. It was a 3-D resin interface model and the interlaminar stresses were extracted

across the width of the laminate. The model was meshed with 75 elements within t/2 from the free edge, four elements through each lamina and eight through each resin interface. The meshing, loading, and constraints can be seen in Figure 39.

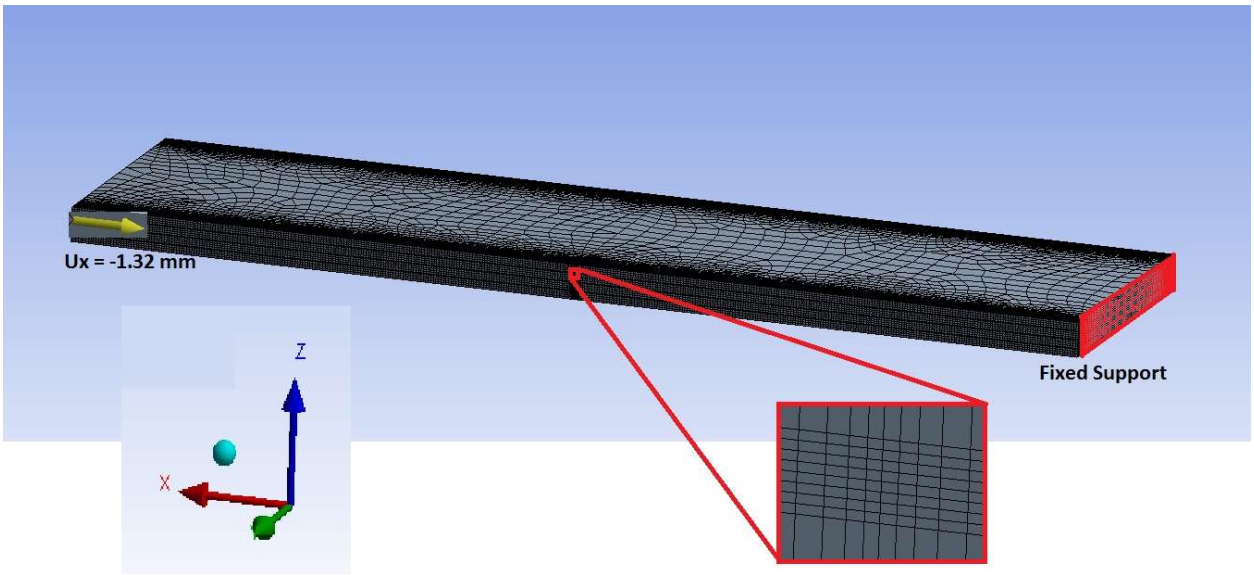

Figure 39: Straight laminate fixed in all directions in one end and compressed by 1.32 mm along the x-axis on the other end.

The maximum values of σ_{33} and τ_{13} were determined across the width of the laminates; at the midspan for the straight coupon and at the transition between the vertical arm and the curve for the curved coupon. The Hoyt criterion was calculated for each lay-up for both geometric configurations. Referring to Figure 40, the Hoyt criterion is broken down into contributions by the interlaminar normal stress and the interlaminar shear stress. The overall Hoyt failure criterion is represented by the sum of these two contributions. In this study the individual contributing factors were investigated in order to determine which interlaminar stress played a greater role in delamination initiation.

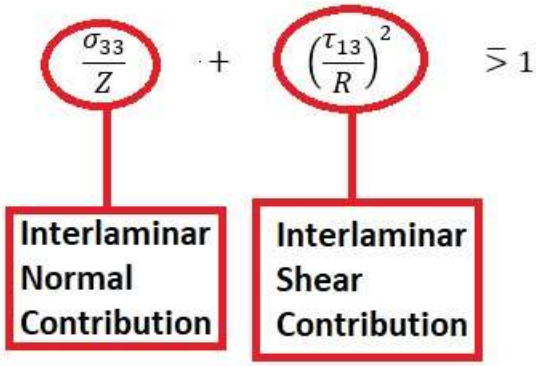

Figure 40: Hoyt failure criterion broken down by contribution of σ_{33} and τ_{13}.

4.2.1 Results and Observations – Determining the Main Contributor to Delamination Initiation

The Hoyt failure criterion for five lay-ups of the form $[0/\theta]_s$ and the two geometric configurations can be seen in Figure 41. The contribution of σ_{33} to the Hoyt criterion for the curved and straight laminates can be seen in Figure 42 while the contribution of τ_{13} to the Hoyt criterion can be seen in Figure 43. In practical applications, a Hoyt failure criterion value greater than one would represent failure of the component via delamination. However, since an arbitrary displacement was used and there is a linear relationship between the displacement and the stresses, the results are discussed in terms of relative comparisons.

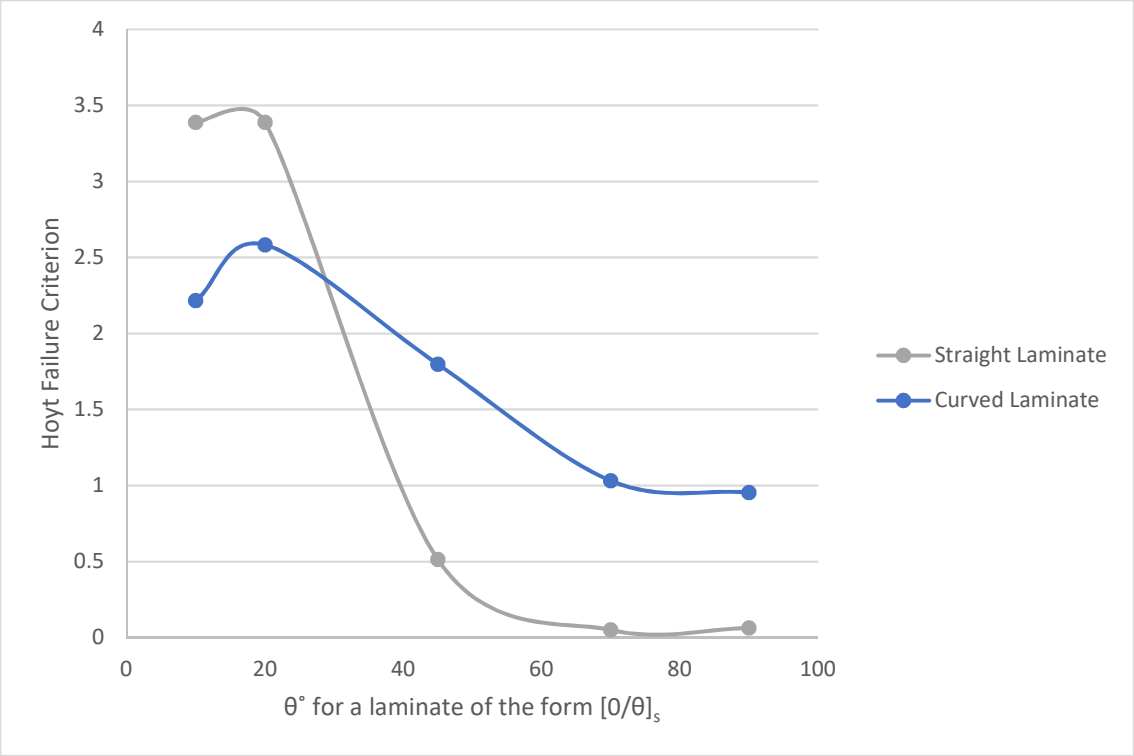

Figure 41: Hoyt failure criterion by lay-up for the curved and straight laminates using maximum σ_{33} and τ_{13} values at the transition between the vertical arm and the curve of the curved coupon.

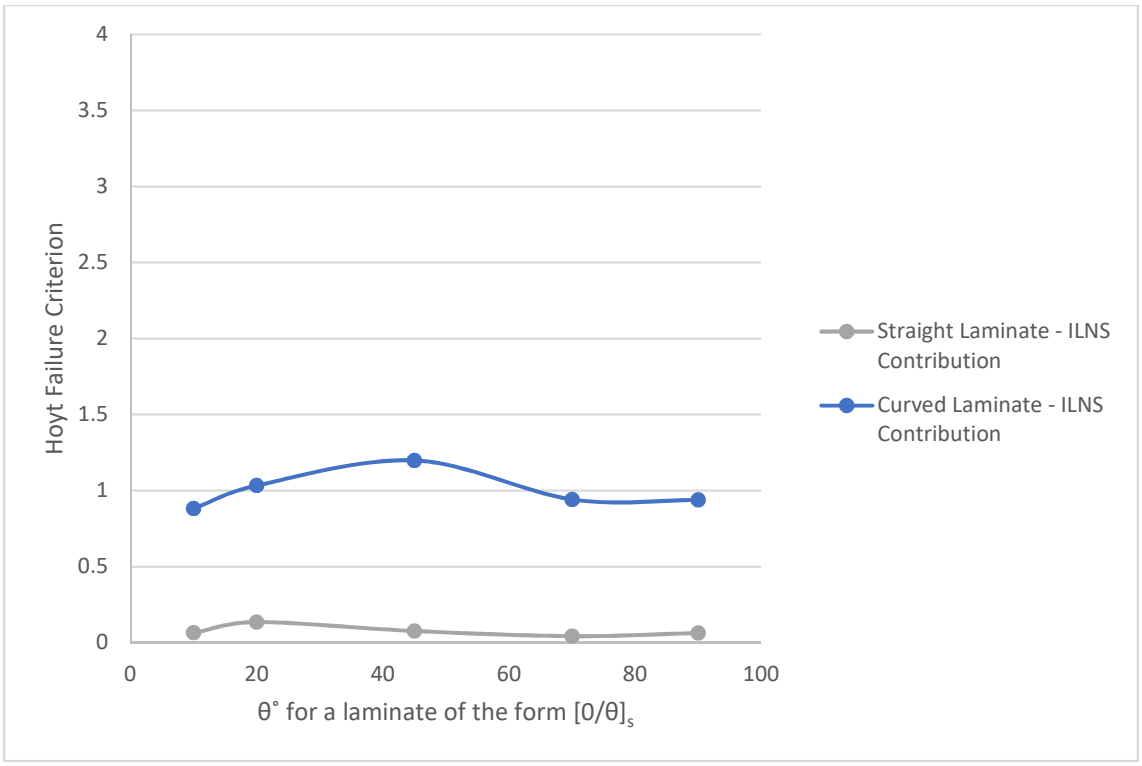

Figure 42: Interlaminar normal stress contribution of Hoyt failure criterion by lay-up for the curved and straight laminates using maximum σ_{33} value at the transition between the vertical arm and the curve of the curved coupon.

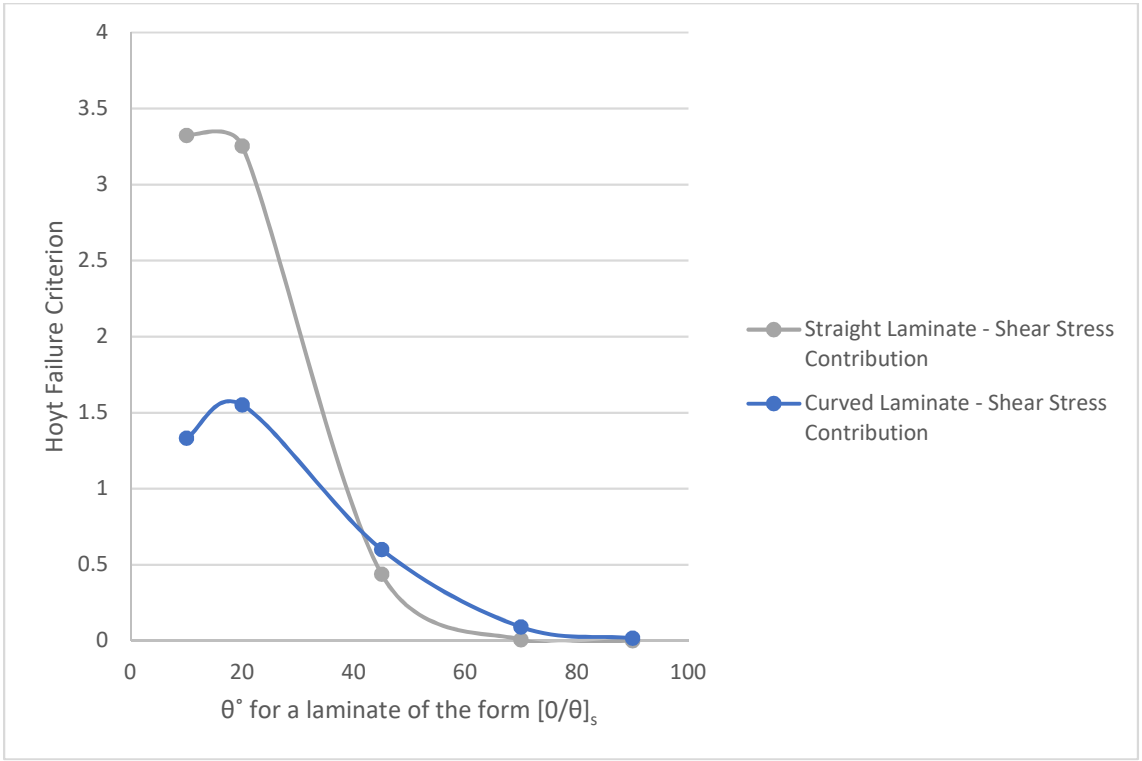

Figure 43: Interlaminar shear stress contribution of Hoyt failure criterion by lay-up for the curved and straight laminates using maximum τ_{13} value at the transition between the vertical arm and the curve of the curved coupon.

Referring to Figure 41 it is evident that the $[0/10]_s$ and $[0/20]_s$ lay-ups have a higher Hoyt failure criterion in the straight coupon as compared to the curved coupon by an increase of 53% and 31% respectively. However, for the lay-ups of $[0/45]_s$, $[0/70]_s$, and $[0/90]_s$ the curved laminates have a higher Hoyt failure criterion by an increase of 252%, 1960%, and 1483% respectively. The difference in which configuration has the greater Hoyt failure criterion can be further explained by the contribution that each interlaminar stress plays in delamination initiation.

Table 8 and Table 9 show the percentage contribution of each interlaminar stress to the overall Hoyt failure criterion by percentage contribution for a straight and curved laminate respectively. Figure 42 and Figure 43 show visual depictions of the contribution of each interlaminar stress to the overall failure criterion. For the $[0/10]_s$, $[0/20]_s$, and $[0/45]_s$ straight laminates, the interlaminar normal stress plays a small role (2% - 14%). Whereas they play a larger role in the $[0/70]_s$ and $[0/90]_s$ laminates (86% and 100%) where the overall Hoyt value is almost negligible for this loading. For a curved laminate the interlaminar normal stress contribution is smallest in the $[0/10]_s$ and $[0/20]_s$ laminates with contributions of 40% to the overall failure criterion. Whereas the interlaminar normal stress is the dominating factor for failure for the $[0/45]_s$, $[0/70]_s$, and $[0/90]_s$ laminates with contributions of 67%, 91%, and 99% respectively.

Table 8: Interlaminar stress contribution to overall Hoyt failure criterion by % contribution – straight.

Lay-Up	σ_{33} – Contribution to Failure	τ_{13} – Contribution to Failure
$[0/10]_s$	2 %	98 %
$[0/20]_s$	4 %	96 %
$[0/45]_s$	14 %	86 %
$[0/70]_s$	86 %	14 %
$[0/90]_s$	100 %	0 %

Table 9: Interlaminar stress contribution to overall Hoyt failure criterion by % contribution – curved.

Lay-Up	σ_{33} – Contribution to Failure	τ_{13} – Contribution to Failure
$[0/10]_s$	40 %	60 %
$[0/20]_s$	40 %	60 %
$[0/45]_s$	67 %	33 %
$[0/70]_s$	91 %	9 %
$[0/90]_s$	99 %	1 %

The results presented above are dependent on the material allowable Z and R that were assumed, and not merely on the level of stress. Lower values of Z would mean that σ_{33}

contributes more to the Hoyt criterion and lower R values would mean that τ_{13} would contribute more to the Hoyt criterion.

4.2.2 Conclusion – Determining Main Contributor to Delamination Initiation

In conclusion, the above study illustrated that a curved coupon will always have higher radial stress contributions than a straight coupon showing that the curvature creates the σ_{33}. Additionally, in curved coupons the σ_{33} is always present and always contributes at least 40% to the Hoyt criterion while τ_{13} can have a contribution of as low as 1%. This shows that σ_{33} always needs to be considered in curved coupons. Finally, in a straight coupon both the σ_{33} and the τ_{13} can vary from 0% to 100% and is dependent on the lay-up. Both stresses need be considered for failure analysis in straight coupons. As a result of these conclusions, the remainder of the study performed focused on interlaminar normal stresses in curved components.

4.3 Geometry Effect on Radial Stress - Radius of the Curve

A parametric study was performed on an isotropic homogeneous curved component in order to determine the effect of the radius of the curve on the value of the maximum radial stress (σ_{33}). An isotropic homogenous model was used in place of an orthotropic model in order to isolate the effects of geometry. The inner radius of the component was varied between 2.5 mm and 15 mm. The maximum value of σ_{11} was made constant (780 MPa) for each testing case by altering the applied displacement. The model used to perform this study was constructed from the baseline model that was described in Section 3.0. Visual representations of the smallest radius (2.5 mm) and the largest radius (15 mm) can be seen in Figure 44 and Figure 45 respectively. The horizontal and vertical arm lengths of the curve remain the same as the baseline model, while the inner radius of the curve was varied. A Young's modulus of 200 GPa and a Poisson's ratio of 0.3 were used to represent a generic steel [57]. A coarse mesh was used for the analysis and the results were extracted at the mid-plane as free edge effects need not be considered in an isotropic material.

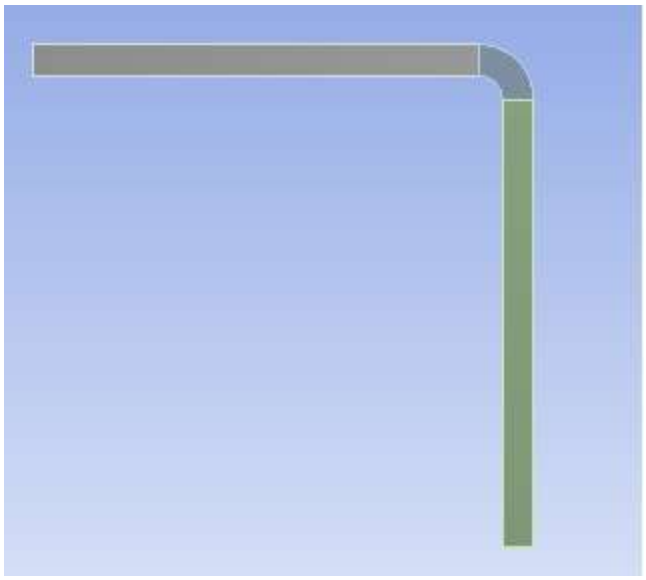

Figure 44: Visual representation of the curved component with an inner radius of 2.5 mm.

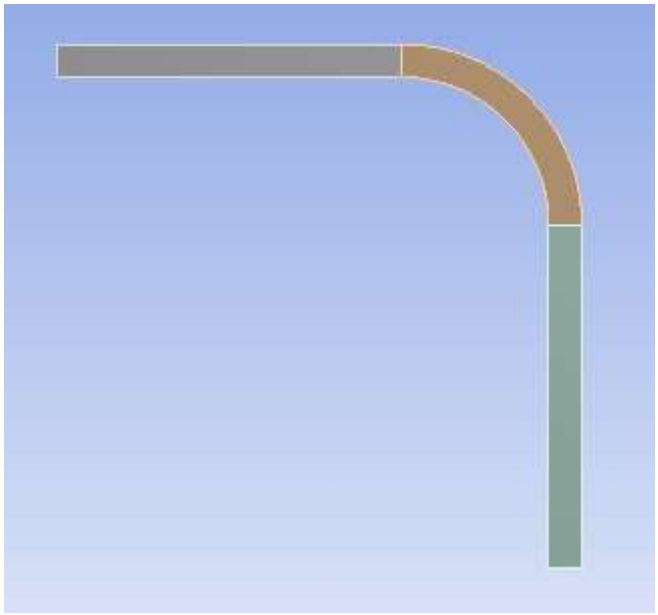

Figure 45: Visual representation of the curved component with an inner radius of 15 mm.

4.3.1 Observations and Results – Radius of the Curve

Figure 46 shows that as the radius of the curve increases the maximum radial stress (σ_{33}) decreases. If the inner radius were to be extended to infinity, the laminate would

become straight and there would be no radial stress. On the contrary, if the component's inner radius were made to be 0 mm, which would represent a 90˚ angled component, there would be a stress singularity where the radial stress would approach infinity.

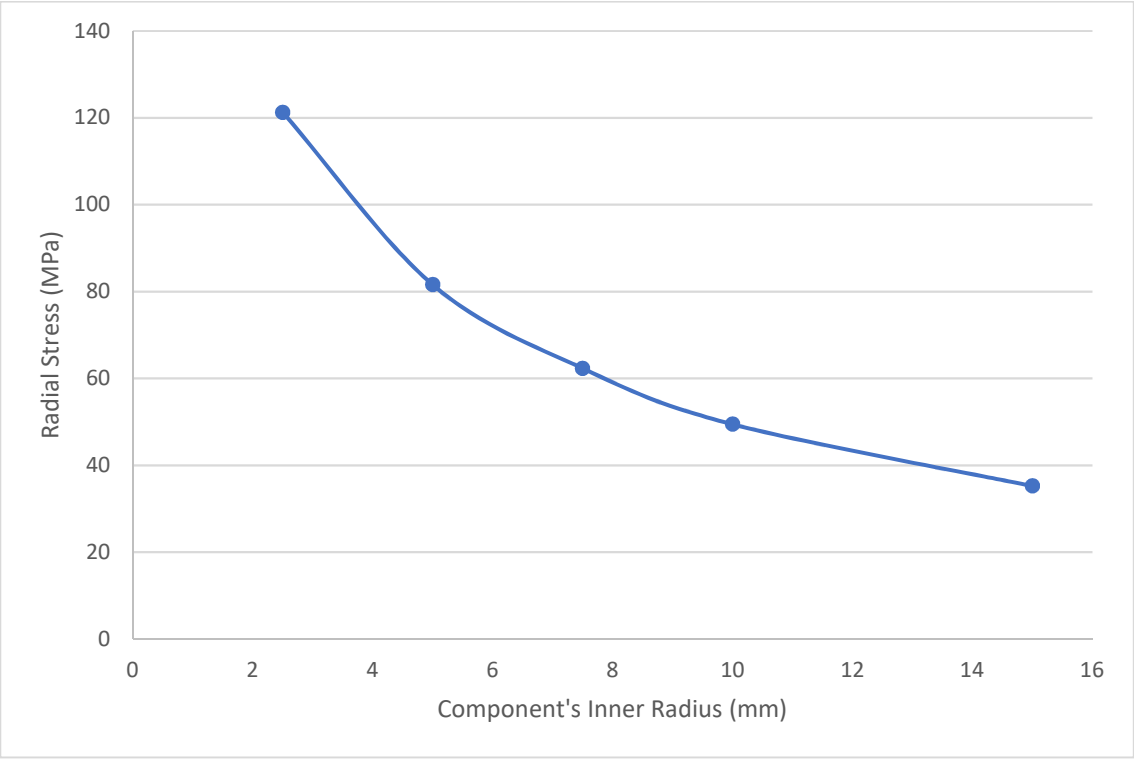

Figure 46: Maximum radial stress by curved component's inner radius for the parametric study varying the radius of the curved component.

The observations made here for the isotropic material are expected to hold true for laminates with angled plies as well. In terms of expected results, it is confirmed by the basic design principle that sharp changes in geometry can result in stress concentrations [58].The more gradual the change, the lower the stress that will be experienced.

4.3.2 Conclusions – Radius of the Curve

In conclusion, as the radius of a curve is decreased, the maximum radial stress experienced in the curve increases. When comparing a curved laminate coupon to a straight laminate coupon of the same lay-up and subjected to the same overall σ_{11}, the curved laminate coupon would fail earlier. This is strictly because of the geometry and the σ_{33} generated by the curvature. Additionally, the σ_{33} generated by geometry could be compounded with the addition

of free edge effects expected to be generated as a result of the material mismatch between the plies of the laminate. This is investigated in Section 4.4.

Out of plane stresses, such as the radial stresses in the curved coupon, are of particular interest when comparing components made of isotropic materials such as steel to those made of composite materials due to the potential modes of failure. In composites, the strength in the out of plane direction is significantly less than that of the axial direction, whereas in isotropic materials the strength is the same in all directions. In many components, the stress in the in-plane direction will be larger than that of the out of plane direction therefore the radial stresses can be ignored in isotropic materials. In composites the out of plane stress, however small it is, could exceed the material allowable thus leading to failure via delamination. Therefore, the radial stress that is generated in a curved composite component is of critical importance and must be considered in component design and failure prediction.

4.4 Determining the Location of Maximum Interlaminar Normal Stress

The distribution of σ_{33} within a component can depend on such things as material properties, geometry (curved or straight) and the ply lay-up. These are investigated in the following section to determine where the maximum σ_{33} is expected to occur. Special emphasis is placed at the region t/2 from the free edge. The location of the maximum σ_{33} was investigated for a curved laminate component. Firstly, the effects of the Young's modulus (E) and the Poisson's ratio (υ) on the σ_{33} distribution across the width of a curved component was investigated. Isotropic and unidirectional laminates were considered so that the free edge effects caused by material mismatch were not present. Secondly, the effects of the curve on the σ_{33} distribution across the width of the curved laminate were determined through comparison to a straight laminate for five different ply lay-ups. Free edge effects due to material mismatch between the angled plies were expected to be seen in this study for both the straight and curved coupons. Finally, the overall free edge effects were isolated in the curved coupon by subtracting the baseline radial stress across the width of the curved laminate. The free edge effects of the curved coupon were then compared to the free edge effects of the straight coupon with the same lay-up.

4.4.1 Effect of Young's Modulus and Poisson's Ration on σ_{33} for a Curved Component

Two different Young's moduli, two Poisson's ratios, an isotropic and an orthotropic material were all considered and their σ_{33} distributions across the width of a curved composite component were compared to one another. The purpose of this study was to determine which

mechanical properties play a role in the σ_{33} distribution of a curved component, and what effect they have.

The model that was used for this study had the same geometry and boundary conditions as the model mentioned in Section 3.0. The models were constructed using the ANSYS solid modeler and all models were created as homogenous with no resin layer. The material properties varied by model and can be seen in Table 10. The applied displacement was adjusted for each model to obtain a maximum circumferential stress of 780 (+/- 10) MPa. A coarse mesh was sufficient because the free edge effects due to material mismatch were not present. The path that was used for this study is across the maximum radial stress value in the curve, determined at the midplane of the coupon. It is located at a similar location to where Gozluku *et al*. determined maximum radial stress in their study [46].

Table 10: Material properties by model number for interlaminar normal stress of a unidirectional curved component study.

Model	E_{11} (GPa)	ν_{12}, ν_{13}	E_{22}, E_{33} (GPa)	ν_{23}
1	200	0.3	N/A	N/A
2	200	0.15	N/A	N/A
3	45	0.3	N/A	N/A
4	142	0.2	9.81	0.4

4.4.1.1 Observations and Results - Effect of Young's Modulus and Poisson's Ration on σ_{33} for a Curved Component

Figure 47 shows that all four models had the same radial stress of 50 +/- 1 MPa at the mid-plane of the laminate regardless of material properties. The maximum value is expected to occur at the mid-plane of the curved components as the mid-plane has the highest lateral constraint, which occurred for all except Model 4 where the maximum σ_{33} occurred near the free edge. The mid-plane is where plane strain is assumed to occur and why 2-D plane strain analyses are often used [47]. This constraint and resulting stress gradually reduce towards the edge of the curved component.

The Young's Modulus appears to play little to no effect on the σ_{33} distribution of the curved components as seen by comparing Model 1 (E = 200GPa) to Model 3 (E = 45 GPa). Referring to Figure 47, Models 1 and 3 have the identical radial stress distribution. Even though the stiffness differs between the two models, the applied displacement had been adjusted in order to produce the same maximum σ_{11} values, resulting in the same distribution of σ_{33}.

As the Poisson's ratio was decreased from 0.3 (Model 1) to 0.15 (Model 2) while keeping the Young's Modulus the same, the difference between the radial stress at the free edge of the component increased from 40 MPa to 47 MPa. This is expected as Model 2, with the smaller ν has less lateral contraction, meaning there is more constraint and therefore a higher stress.

Additionally, the overall interlaminar normal stress distribution has less variation between the maximum value at the mid-plane and the value at the free edge. The isotropic components all appear to have slight increases in radial stress near the free edge of the coupon. These increases vary depending on the location on the curved coupon where the stress results are taken. It is not currently known, what causes these slight increases.

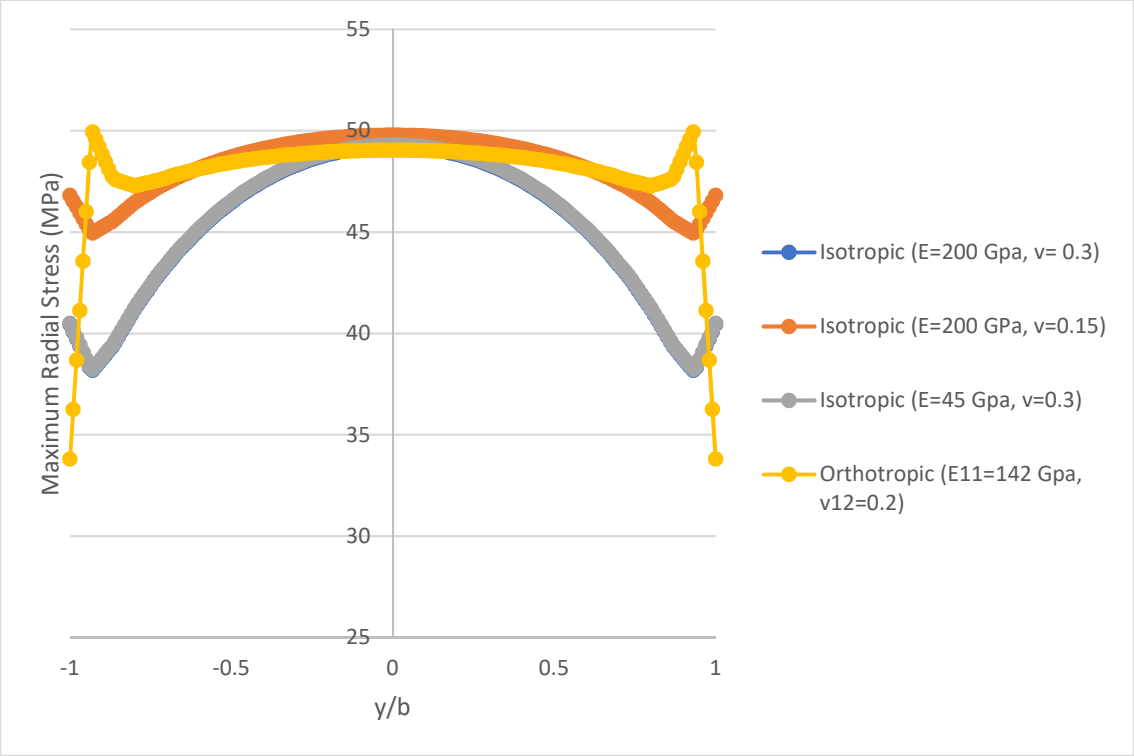

Figure 47: Radial stress distribution across the curved component's width for varying mechanical properties at the location of maximum radial stress.

The main difference that can be seen between the isotropic and the orthotropic models in Figure 47 is that there is an extra tail in Model 4, which does not exist in the isotropic materials. As this is a unidirectional laminate, the variation across the width is not due to the material mismatch as is the case in laminates with angled plies. The reasoning for these additional tails are investigated further below.

Another investigation was completed to determine the effects of the lateral and transverse values of E and ν. Two additional models were constructed, one with the E remaining constant in all directions, while the Poisson's ratio varied and the other one varied the E, while the Poisson's ratio varied. The properties of these models can be seen in Table 11.

Table 11: Material properties by model number for interlaminar normal stress of a unidirectional curve study – orthotropic.

Model	E_{11} (GPa)	ν_{12}, ν_{13}	E_{22}, E_{33} (GPa)	ν_{23}
4	142	0.2	9.81	0.4
5	142	0.2	9.81	0.2
6	142	0.2	142	0.4

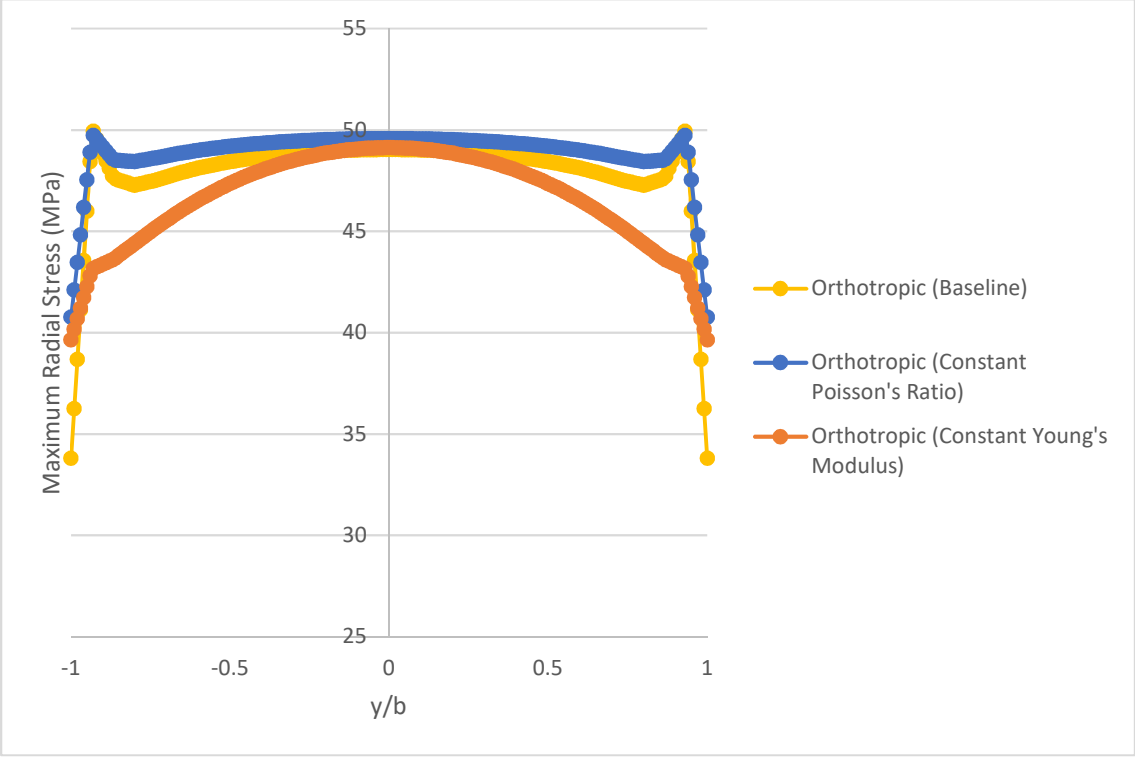

Figure 48: Radial stress distribution across the curved component's width for orthotropic materials with differing mechanical properties at the location of maximum radial stress.

Referring to Figure 48, it is evident that when comparing models 4 and 5, ν_{23} does not have a significant contribution to the overall distribution. Comparing models 4 and 6 shows that changing the value of E_{22} and E_{33} affects both the local stresses at the free edge as well as the shape of the overall distribution

4.4.1.2 Conclusion – Interlaminar Normal Stress Distribution of a Curved Component of Varying Material Properties

In conclusion, the maximum σ_{33} value in a curved component without differing plies whether an isotropic component or a unidirectional orthotropic composite component, is

expected to occur at the mid-plane of the curved coupon. Once differing plies are stacked on top of one another, free edge effects may play a role in moving the maximum location of σ_{33}, which will be investigated in Section 4.4.2.

Additionally, the variation across the width in an isotropic component is controlled by the Poisson's ratio. The larger the Poisson's ratio, the larger the decrease that will be seen towards the free edge of the curved component. In isotropic materials, the Young's modulus only drives the stiffness of the component but does not change the shape of the distribution.

Orthotropic materials differentiate from isotropic materials in terms of σ_{33} distribution at the free edge of the component. In orthotropic materials, these effects are more pronounced. It was determined that the variation of these edge effects relies on the E_{22} value of the orthotropic material.

Finally, free edge effects in curved components were observed which differ from the free edge effects in composite materials due to material mismatch. In the curved isotropic components, there is a slight increase at y/b = 0.93 regardless of material properties, whereas in the unidirectional orthotropic material there appears to be a decrease at y/b = 0.93. When keeping the Young's Modulus constant in the orthotropic material, the free edge effect decreasing the σ_{33} still exists at y/b=0.93, but on a much smaller scale. As the above models are modeled without a resin interface and are either isotropic or unidirectional, there is no material mismatch. These free edge effects are due to other factors. They are not expected to play a role in the further models of this thesis where resin interface modeling is used and material mismatch is expected to be the driving factor of free edge effects.

4.4.2 Effects of Geometry and Lay-Up on σ_{33}

The purpose of the following study was to determine the effects of the component geometry by comparing curved and straight coupons of differing lay-ups. Using the same models as Section 4.2 the maximum value of σ_{33} in the straight and curved laminates across the width of the component are compared. Additionally, the σ_{33} distributions are compared to one another across the width of the straight coupon and the curved coupon (results taken at the bottom of the curve.) Additionally, the effect of the lay-up on the free edge stresses in the curved laminate coupon is investigated. The applied displacement was adjusted so that all models had the same σ_{11}.

4.4.2.1 Effect of Geometry on σ_{33}

The maximum values of σ_{33} are plotted for six different lay-ups for both the curved and the straight geometry in Figure 49. The results are taken at the top resin interface for both components. They are taken at the mid-length of the straight laminate and at the bottom of the curve for the curved laminate. This further illustrates that in all modeled laminates the σ_{33} is larger for a curved component when compared to a straight component of the same lay-up.

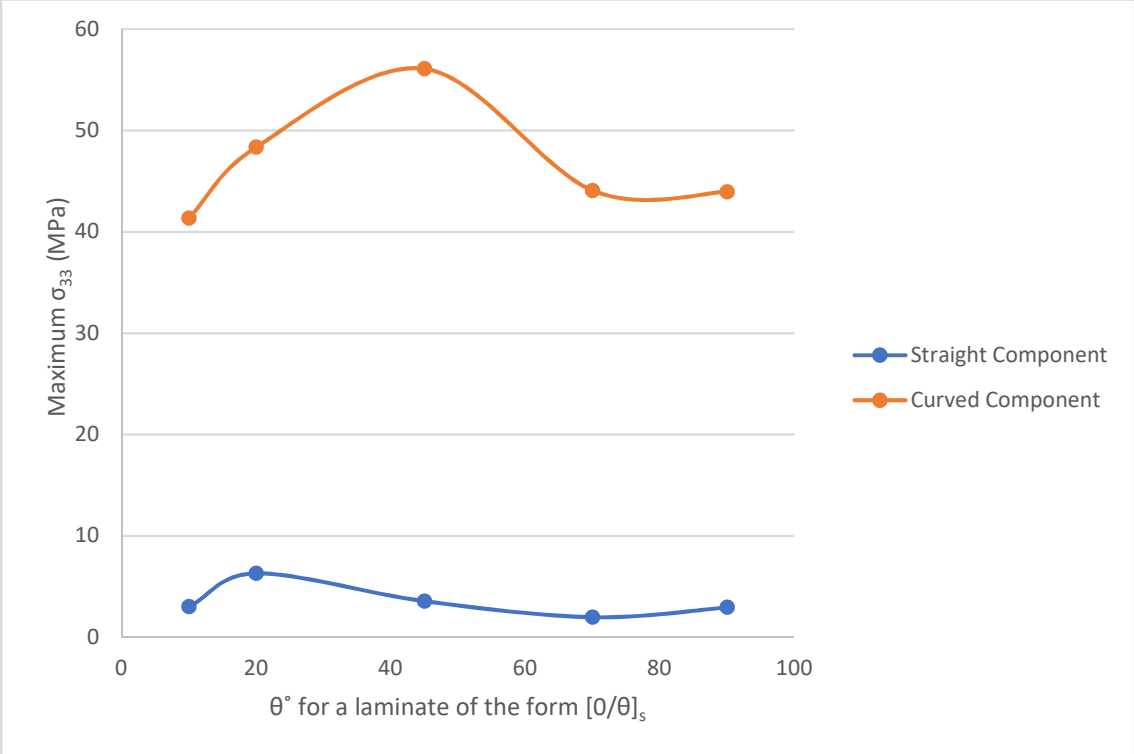

Figure 49: Maximum σ_{33} by laminate lay-up for straight and curved geometries (taken at bottom of curve) at the top resin interface between the top two plies.

A ratio between the maximum values of σ_{33} for the curved coupon and the straight coupon for each lay-up is presented in Table 12 as the σ_{33} Factor of Increase. A value greater than one in all cases re-affirms that the maximum σ_{33} value in all modeled laminates is greater in the curved component when compared to the straight component.

Table 12: Calculated σ_{33} Factor of Increase by lay-up of laminate.

Lay-Up	σ_{33} Factor of Increase
Unidirectional	∞
$[0/10]_s$	13.7
$[0/20]_s$	7.7
$[0/45]_s$	15.7
$[0/70]_s$	22.2
$[0/90]_s$	14.9

The σ_{33} distributions across the width of the curved and straight laminates at the bottom of the curve can be seen in Figure 50, Figure 51 and Figure 52 for unidirectional, $[0/45]_s$ and $[0/90]_s$ laminates respectively. Refer to Appendix A for the results for $[0/10]_s$, $[0/20]_s$, and $[0/70]_s$.

All of the curved laminate lay-ups, have a constant value of $\sigma_{33} = 40$ MPa across the bulk of the width to within y/b values less than t/2 from the free edge, while the straight laminate lay-ups all have a constant σ_{33} of 0 MPa. It is not until just prior to y/b = t/2 from the free edge that the σ_{33} distribution differs for the different layups. The distribution of σ_{33} across the width of the component can be separated into two regions, identified in Figure 53 as Segment 1 (constant value) and Segment 2 (free edge effects). Segment 1 appears to be influenced entirely by the radial stress induced by the curve in the component. The fact that the straight laminate of the same lay-up has a σ_{33} of 0 MPa across Segment 1 and the curved laminate has a σ_{33} of 40 MPa further substantiates this claim.

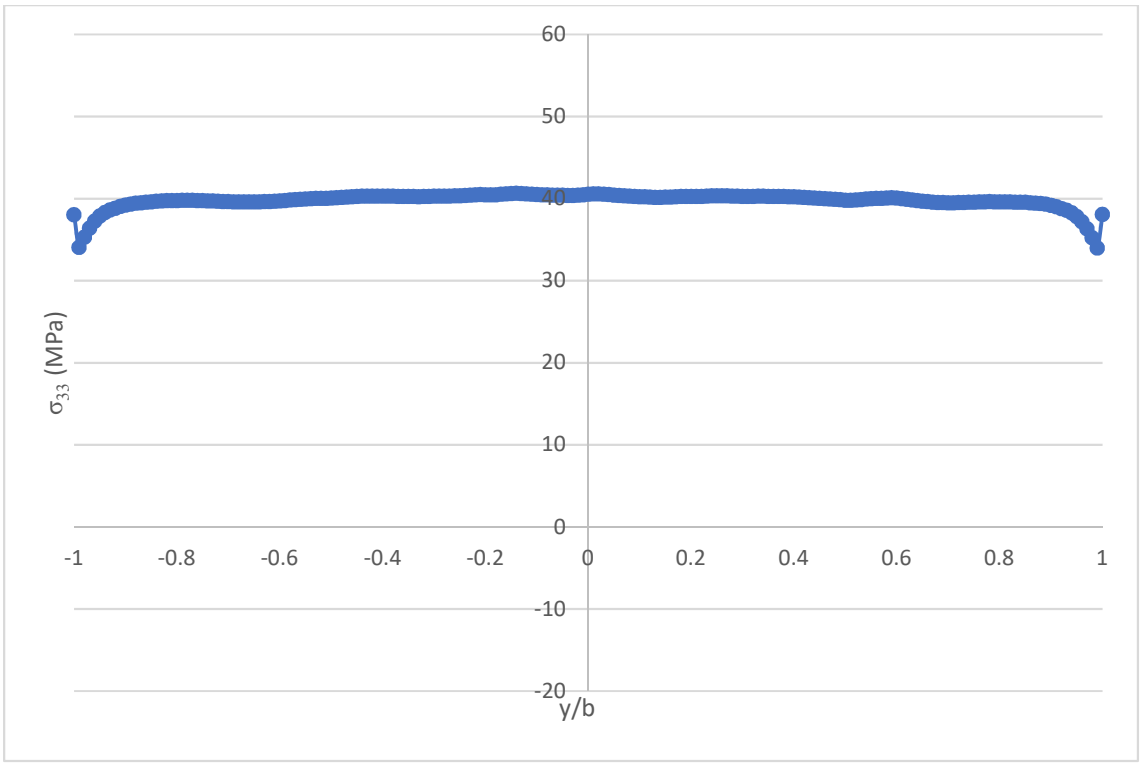

Figure 50: Radial stress distribution across a unidirectional laminate width for the resin interface modeling approach at the transition between the vertical arm and the curve of the curved coupon.

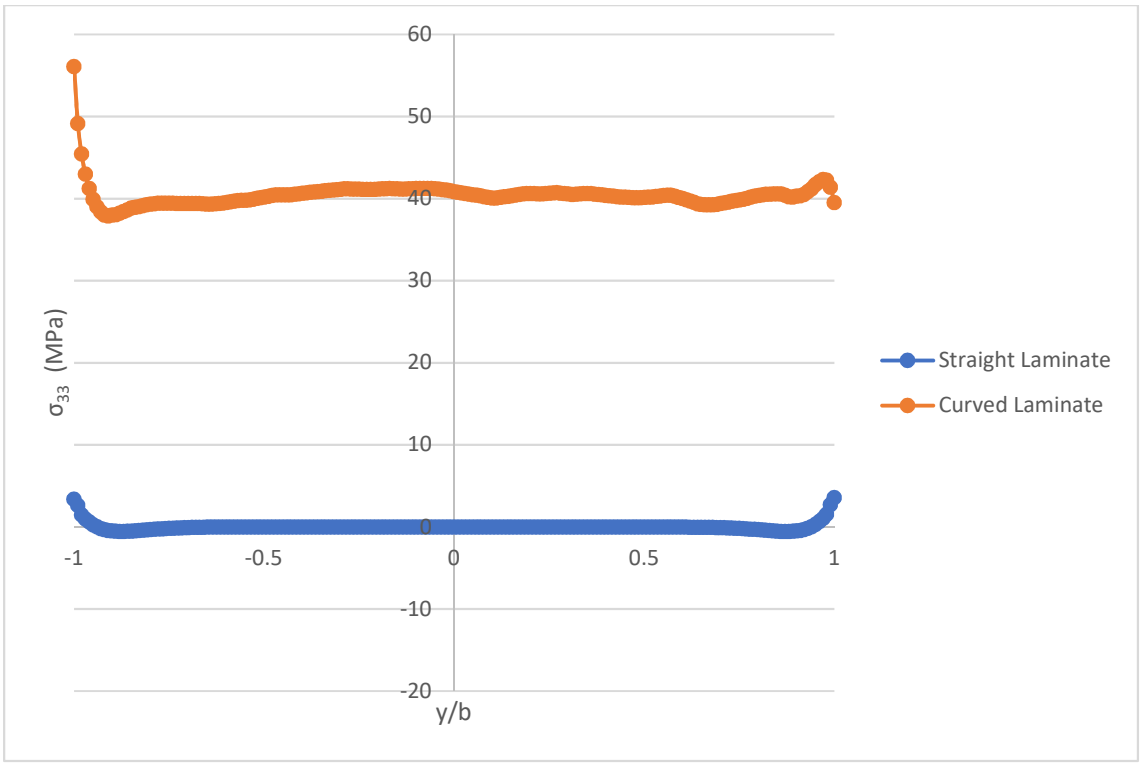

Figure 51: σ_{33} distribution across the laminate width for straight and curved laminates of a $[0/45]_s$ lay-up at the transition between the vertical arm and the curve of the curved coupon.

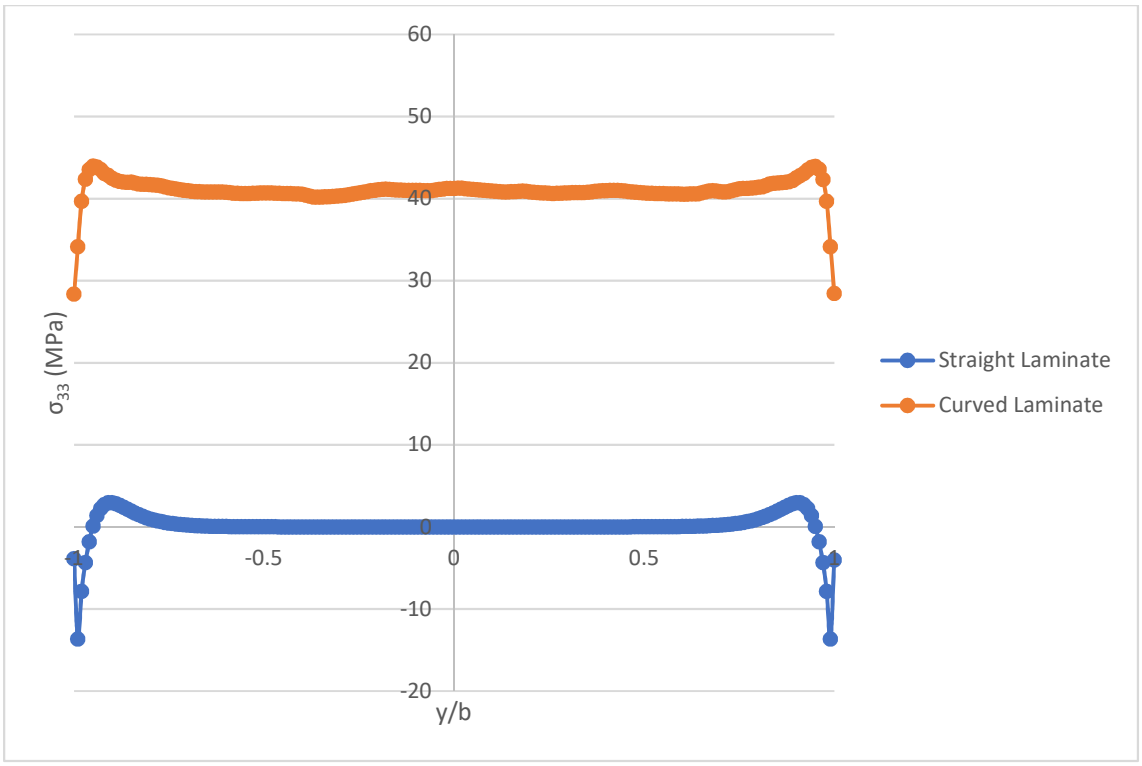

Figure 52: σ_{33} distribution across the laminate width for straight and curved laminates of a $[0/90]_s$ lay-up at the transition between the vertical arm and the curve of the curved coupon.

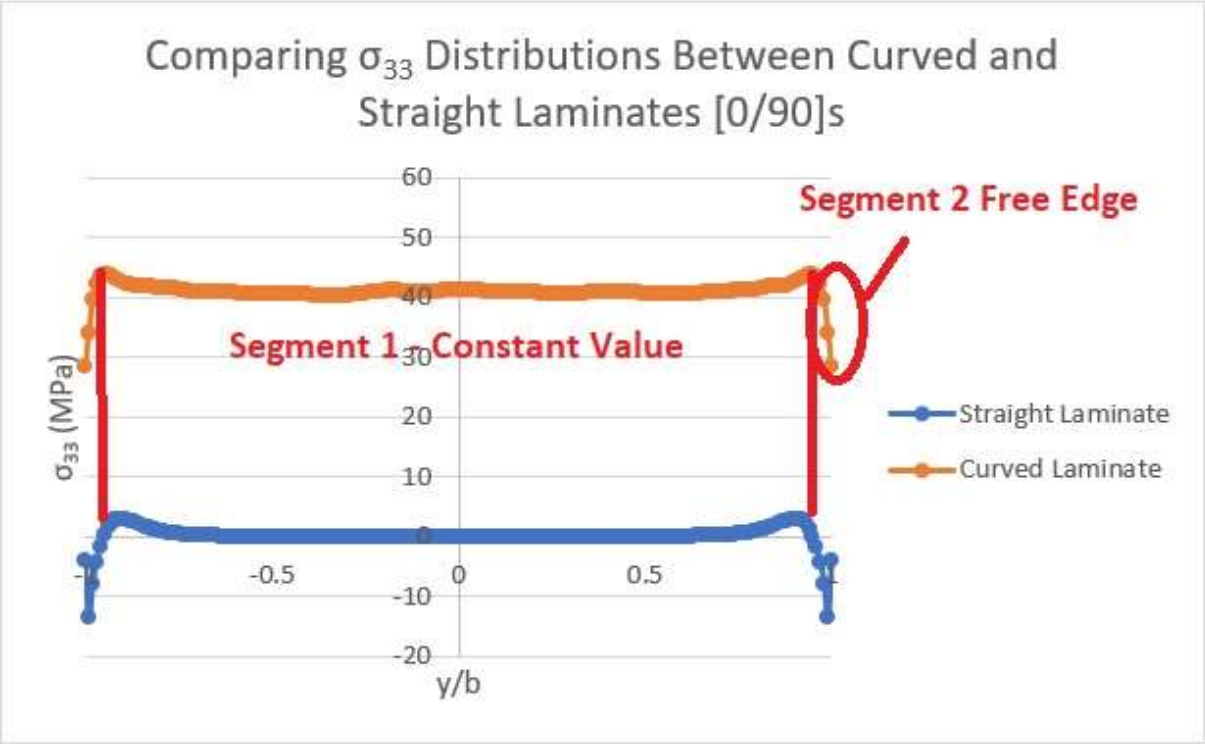

Figure 53: σ_{33} distribution across the laminate width for straight and curved laminates of a $[0/90]_s$ lay-up at the transition between the vertical arm and the curve of the curved coupon – separated by segment.

In both the curved and straight laminates, the free edge effect due to material mismatch is recognized and is identified in Figure 53 as Segment 2. The free edge effects are different for each lay-up and different for the straight and the curved laminates as shown in Figure 50 to Figure 52. The normal interlaminar stresses in the edge region will be examined further in Section 4.4.2.3.

Referring to the σ_{33} distributions of the $[0/45]_s$ curved laminate in Figure 51, it can be seen that the free edge effects are not symmetric. The maximum σ_{33} value on one side is 56 MPa and 39 MPa on the other side. Curved laminates with angle plies do not have the same symmetrical distribution that the straight coupons have. Some lay-ups of laminates will want to twist when a bending moment is applied. The lack of symmetry in the σ_{33} distribution is due to the boundary conditions in the straight laminates allowing for the component to twist freely as compared to the curved laminate where the geometry and boundary conditions can restrict the natural twisting of the laminate and thus induce additional stresses into the laminate. In addition to the boundary conditions, the lay-up also affects whether or not the distribution will be symmetrical. Lay-ups that are not prone to twisting such as the $[0/90]_s$ and the $[0/0]_s$ have symmetrical distributions while the $[0/45]_s$ that is prone to twisting has an unsymmetrical distribution. The relative twisting of the curved laminates will be investigated in Section 4.5 as well as the impact the induced torsion has on the σ_{33} distribution.

4.4.2.3 Effect of Lay-Up on σ_{33} in the Edge Region

The σ_{33} results from Section 4.4.2.2 showed that although all curved laminates had a value of $\sigma_{33} = 40$ MPa across the bulk of the coupon (Segment 1), the stresses in the edge regions within t/2 from the free edge (Segment 2) differed by lay-up. In this sub-section, the free edge effects seen in the curved laminate for different lay-ups are compared to the corresponding straight laminate in order to separate the effects of component geometry from the effects of the layup.

In order to isolate the effect that the lay-up has on the free edge region (Segment 2) for the angled ply lay-ups, the baseline $\sigma_{33} = 40$ MPa caused by the curve in the coupon (the radial stress seen in Figure 50) is subtracted from the curved component's σ_{33} distribution. This has the effect of normalising the stress, allowing the edge effects to be compared more easily to the those of the straight laminate.

σ_{33} across the width of the curved and straight components can be seen in Figure 54 and Figure 55 for the $[0/45]_s$ and the $[0/90]_s$ lay-ups respectively. The results for the additional lay-ups can be seen in Appendix B. Normalising the curve in both cases allows the effect of lay-up to be isolated from the geometric effects in the free edge region (Segment 2).

Looking at the $[0/45]_s$ laminate in Figure 54, it is evident that the same overall σ_{33} distribution exists in segment 1, but not in segment 2. Since the free edge distribution is different between the two edges, this indicates unsymmetric loading that would be typical of induced torsion. This was not seen in the $[0/90]_s$ laminate as cross-ply laminates do not twist when they are subjected to a bending load.

Looking at the $[0/90]_s$ laminate in Figure 55 it can be seen that both the straight and curved laminates have the same overall distribution once the σ_{33}=40 MPa caused by the curvature was removed. This means that the overall distribution is completely governed by the lay-up of the laminate. Even the stress distribution in the free edge region is the same whether it is a straight or curved coupon. The presence of the curve does increase the magnitude of σ_{33}, but does not change the distribution.

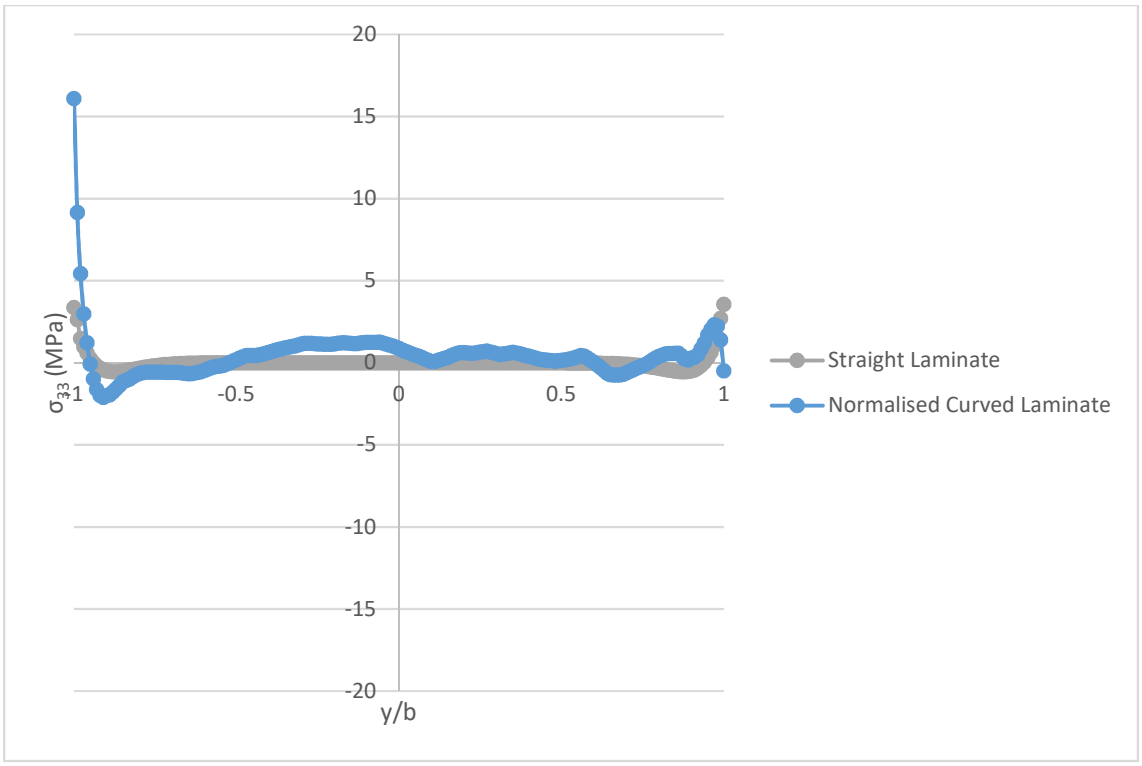

Figure 54: σ_{33} distribution across the laminate width for straight and curved laminate with isolated edge effects of a $[0/45]_s$ lay-up at the transition between the vertical arm and the curve of the curved coupon.

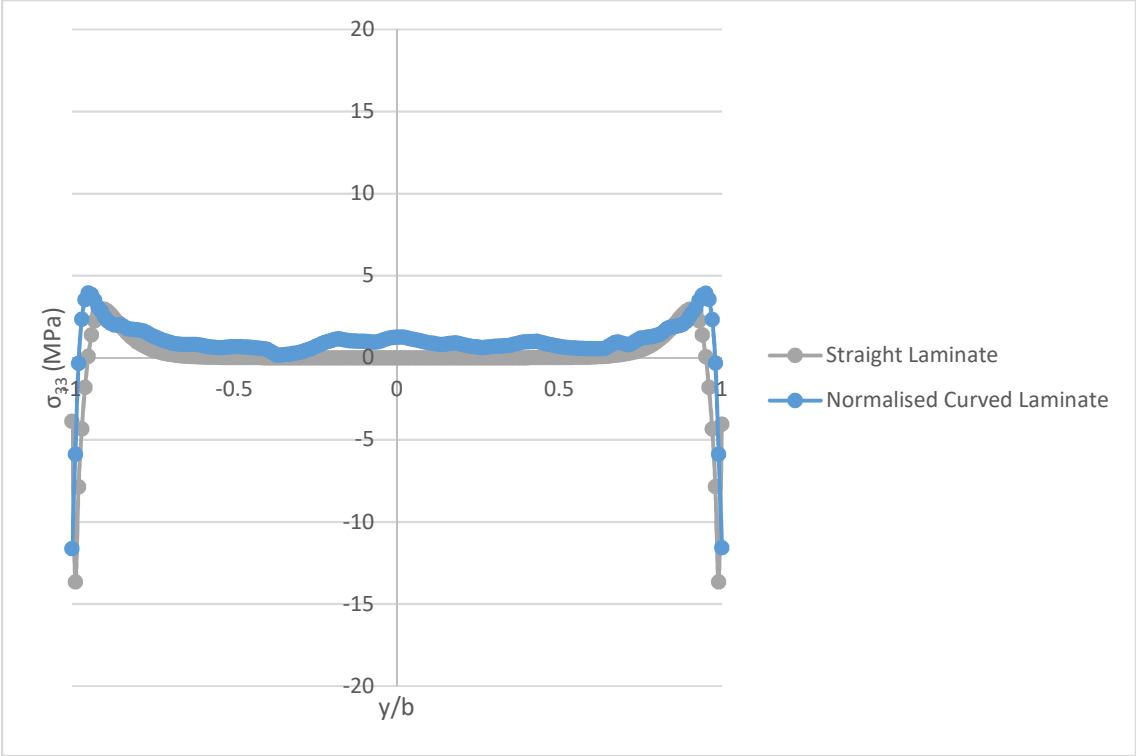

Figure 55: σ_{33} distribution across the laminate width for straight and curved laminate with isolated edge effects of a $[0/90]_s$ lay-up at the transition between the vertical arm and the curve of the curved coupon.

4.4.2.4 Conclusion – Comparing Straight and Curved Laminates

When comparing curved laminates and straight laminates with the same σ_{11}, the σ_{33} is always higher in the curved component due to the radial stress induced around the curve. This means that failure information gathered from tests on straight laminates may not be directly transferrable on curved laminates.

There are two distinct segments when looking at σ_{33} across the width of the curved laminate. Segment 1 is a constant value that occurs across the middle of the laminate between $y/b < t/2$ from the free edge on both sides. The magnitude of σ_{33} for segment 1 is controlled by the geometry of the curve as well as where around the curve the results are taken. Segment 2 occurs at $y/b > t/2$ from the free edge and contains the local edge effects that are driven by lay-up. When comparing the isolated free edge effects in a curved composite with a straight composite of the same lay-up, the coupons considered here only differ by a constant magnitude that is due to the presence of the curve. The local free edge effects and the shape of the distribution in segment 1 are the same. Any differences are due to the fact that if a coupon twists when bending is applied, the internal state of loading is different between the curved and straight coupons. This results in an unsymmetric distribution across the width of the curved coupon that

was not present in the straight coupon that was free to deform with no induced stresses. The effects of induced torsion on σ_{33} distribution will be further investigated in Section 4.5.

4.5 Determining How Induced Torsion Affects σ_{33} Distribution in a Curved Laminate

It is evident that beyond the radial stress induced by geometry (curved versus straight) and the free edge effects due to material mismatch, there is another factor affecting the σ_{33} distribution across the width of a curved laminate. Referring to Section 4.4.2.3, the unsymmetrical distribution of σ_{33} was indicative of an internal torsional load. In order to aid in understanding this effect, two locations around the curve that are expected to experience different magnitudes of induced torsion were considered. The top of the curve is expected to have more induced torsion than the bottom of the curve due to the boundary conditions placed on the model and therefore the distribution of σ_{33} across with width should be more asymmetric.

4.5.1 Determining Contributing Factors to Induced Torsion in a Curved Laminate

As stated in Section 3.0, two locations were probed one at the top of the curve and one at the bottom of the curve. So far, only the location at the bottom of the curve has been investigated. It is expected that the value of the radial stress will change depending on the location around the curve where the results are probed [59]. It is expected that at the top of the curve there should be less twisting than at the bottom. This is due to the boundary conditions that were placed on the model shown in Figure 56. Because the lower end of the vertical arm is free to move in the X and Y directions, it is also free to twist about the Z axis. There will be minimal stress generated from the induced torsion at the bottom of the curve due to this freedom. The end of the coupon that is displaced by 25mm in the Z direction applied the prescribed displacement over an edge. This means that the horizontal arm is not able to twist about its X axis. This restriction of twisting induces torsional stresses at the top of the curve.

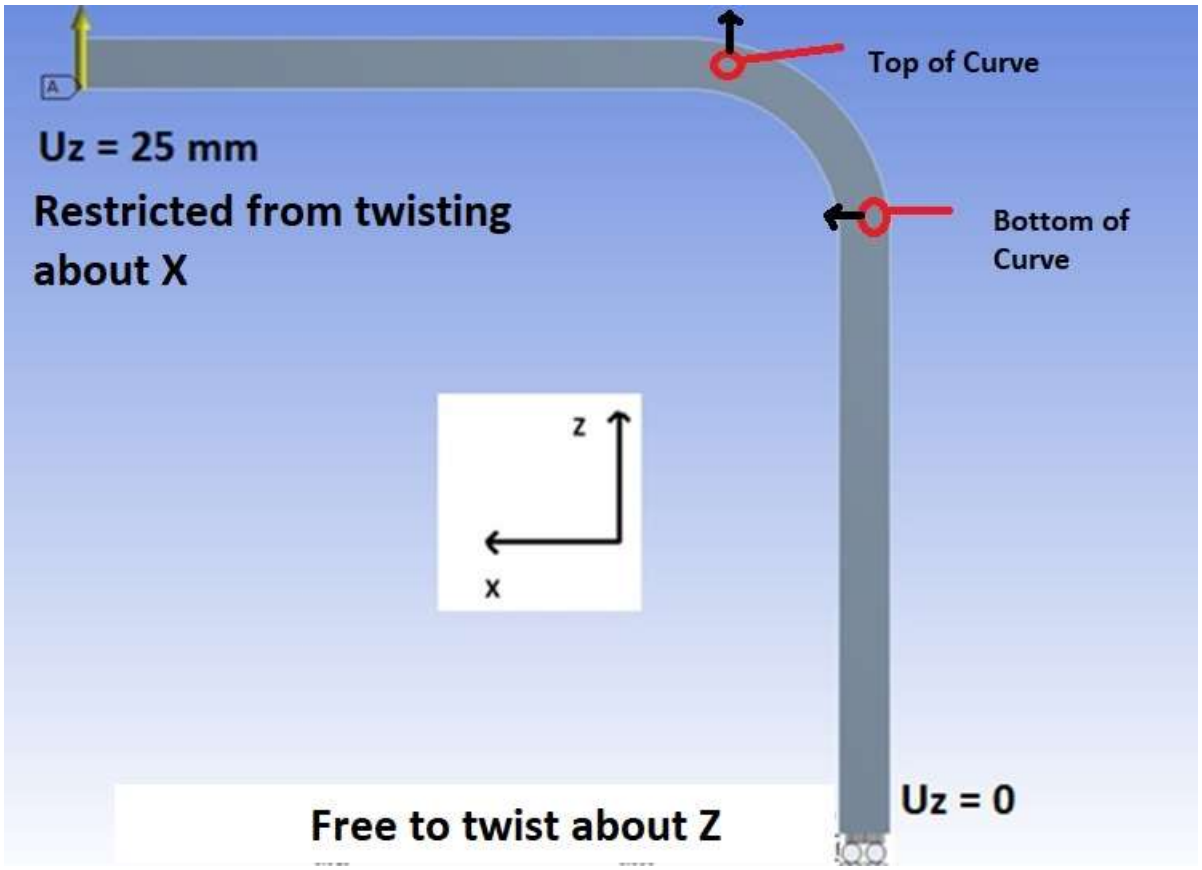

Figure 56: Influence of boundary conditions on twisting in the curved component .

The model set up is as per Section 3.0 Materials and Methodology. The same five $[0/\theta]_s$ lay-ups and the unidirectional laminate are looked at as per Section 4.4, however results along both the top and bottom of the curve are extracted in order to observe the effect of induced torsion.

4.5.1.1 Results and Observations - Determining Contributing Factors to Induced Torsion in a Curved Laminate

Sample σ_{33} distributions along the top and bottom locations of the curve can be seen for the $[0/0]_s$, $[0/20]_s$ and the $[0/90]_s$ curved coupons in Figure 57, Figure 58, and Figure 59 respectively. The comparison between the σ_{33} distribution at the top of the curve and at the bottom of the curve for the remaining lay-ups not displayed here can be seen in Appendix C. The $[0/0]_s$ and $[0/90]_s$ lay-ups have a symmetric distribution about the mid-plane of the laminate for both probed locations, which indicates that no torsional stresses are induced. The σ_{33} distributions for the $[0/20]_s$ lay-up are not symmetric, with the top of the curve showing more

asymmetry. This indicates that the top of the curve is more constrained and more torsional loads are induced due to this imposed constraint as compared to the bottom of the curve.

Figure 60 and Figure 61 show the vertical arm and the horizontal arm respectively and the contours represent their out of plane displacement (displacement in the twisting direction – X direction for the vertical arm and Z direction for the horizontal arm). The curved contours on the vertical arm in Figure 60 illustrate that twisting is occurring, as the out of plane displacement varies across the width of the curved coupon. The straight contours on the horizontal arm in Figure 61 illustrate a lack of twisting as the out of plane displacement is constant across the width of the curved coupon. The magnitude of the induced torsion will be dependent on the amount of constraint but also the tendency of the laminate to twist when loaded in bending. The effect of the laminate's lay-up on induced torsion will be investigated in Section 4.5.2.

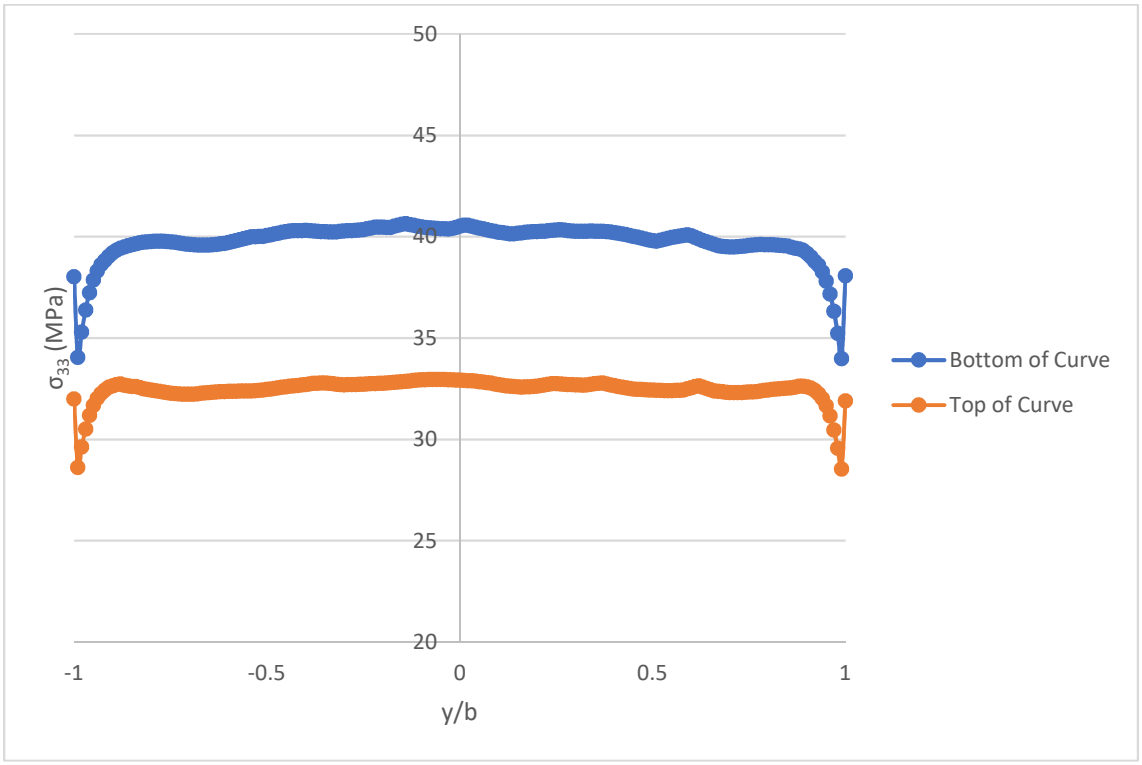

Figure 57: σ_{33} distribution across the laminate width for curved laminate of a unidirectional lay-up at the bottom of the curve and the top of the curve where they transition to the vertical and horizontal arms respectively.

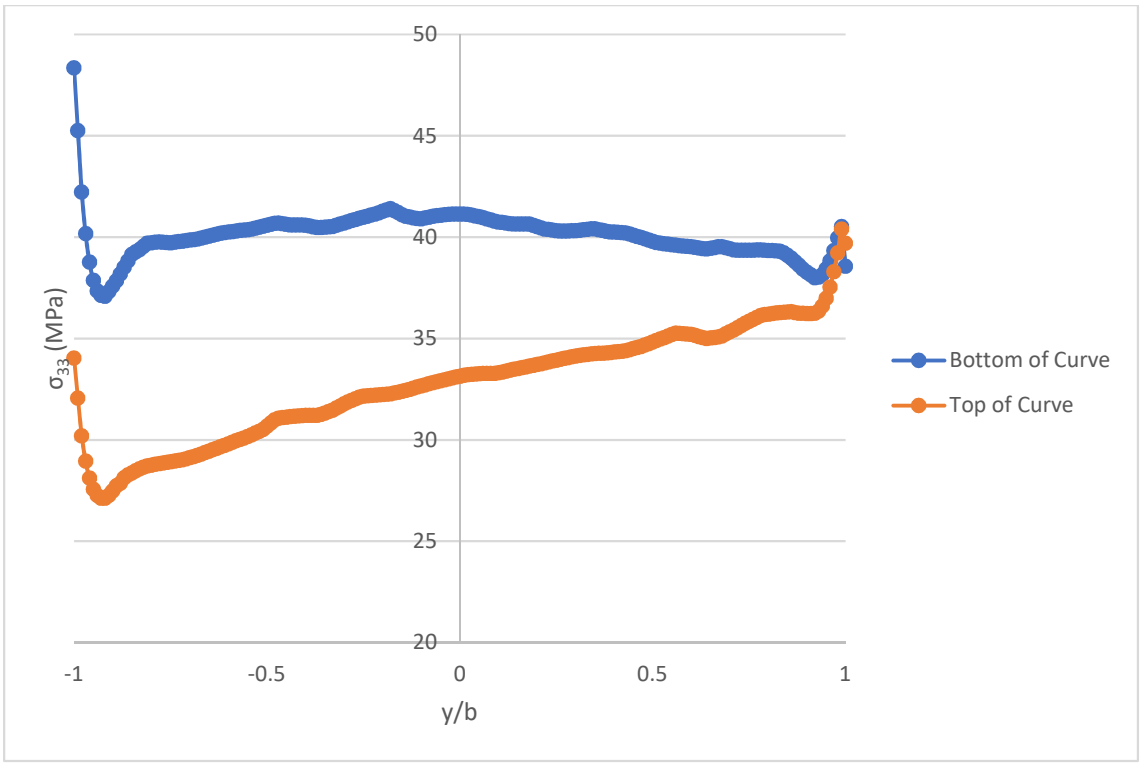

Figure 58: σ_{33} distribution across the laminate width for curved laminate of a $[0/20]_s$ lay-up at the bottom of the curve and the top of the curve where they transition to the vertical and horizontal arms respectively.

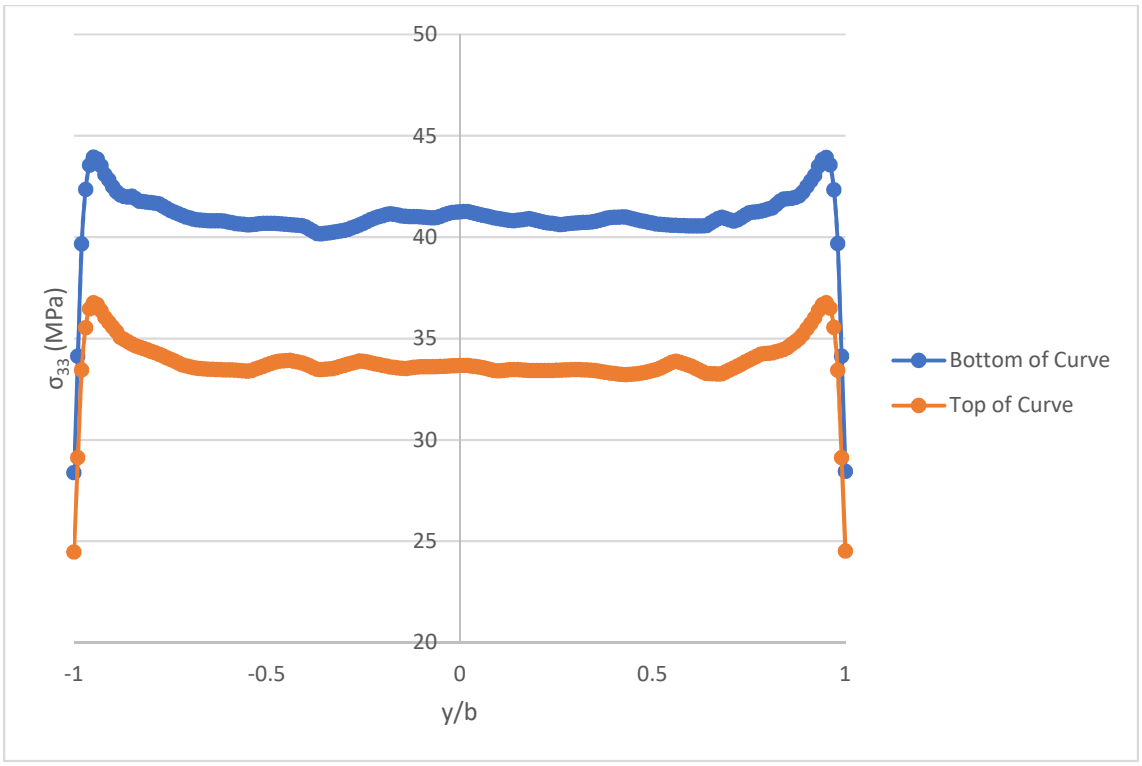

Figure 59: σ_{33} distribution across the laminate width for curved laminate of a $[0/90]_s$ lay-up at the bottom of the curve and the top of the curve where they transition to the vertical and horizontal arms respectively.

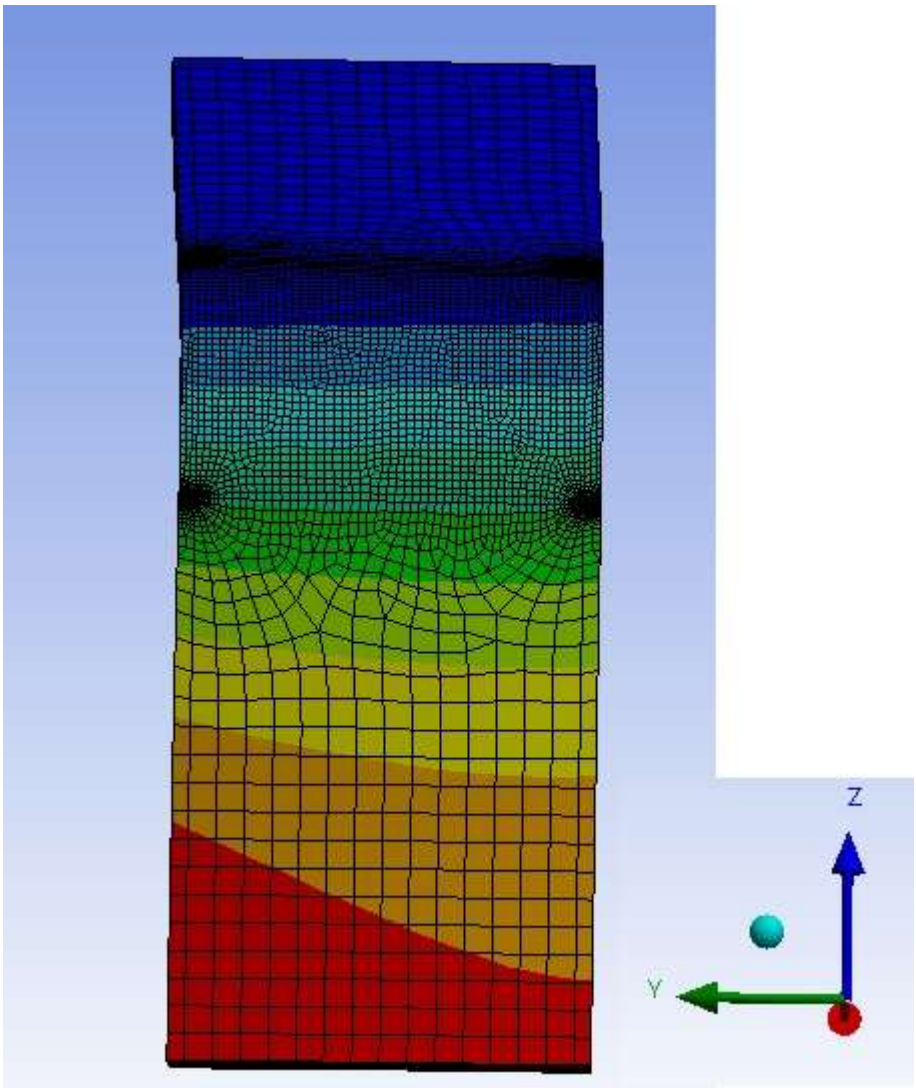

Figure 60: $[0/20]_s$ vertical arm of curved laminate with contours illustrating non-linear out of plane (X direction) displacement.

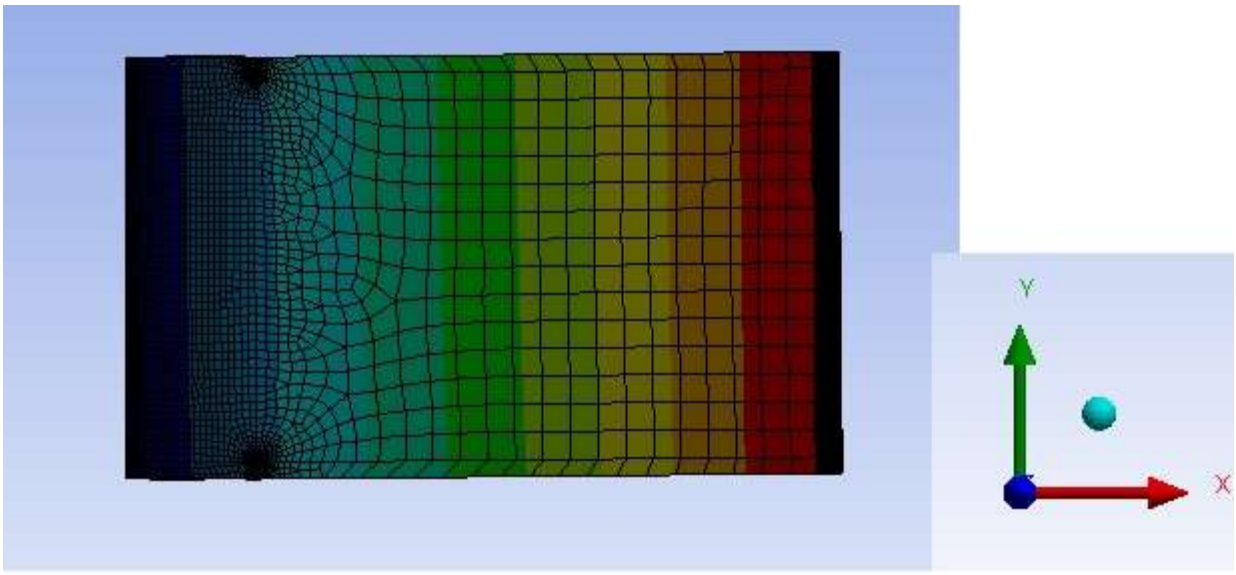

Figure 61: $[0/20]_s$ horizontal arm of curved laminate with contours illustrating uniform out of plane (Z direction) displacement.

Figure 57 - Figure 59 showed that the bottom of the curve had consistently higher σ_{33} values than the top of the curve. This is summarized in Figure 62 for each of the six curved coupon lay-ups. Also evident is that the $[0/45]_s$ and $[0/20]_s$ laminates have the two maximum values of σ_{33} at both the bottom and top of the curve, while the $[0/70]_s$ and $[0/90]_s$ have a magnitude only 2-3 MPa greater than the unidirectional and $[0/10]_s$ laminates at both locations. The difference between the maximum value of σ_{33} in the top and bottom of the curve for each lay-up are summarized in Table 13.

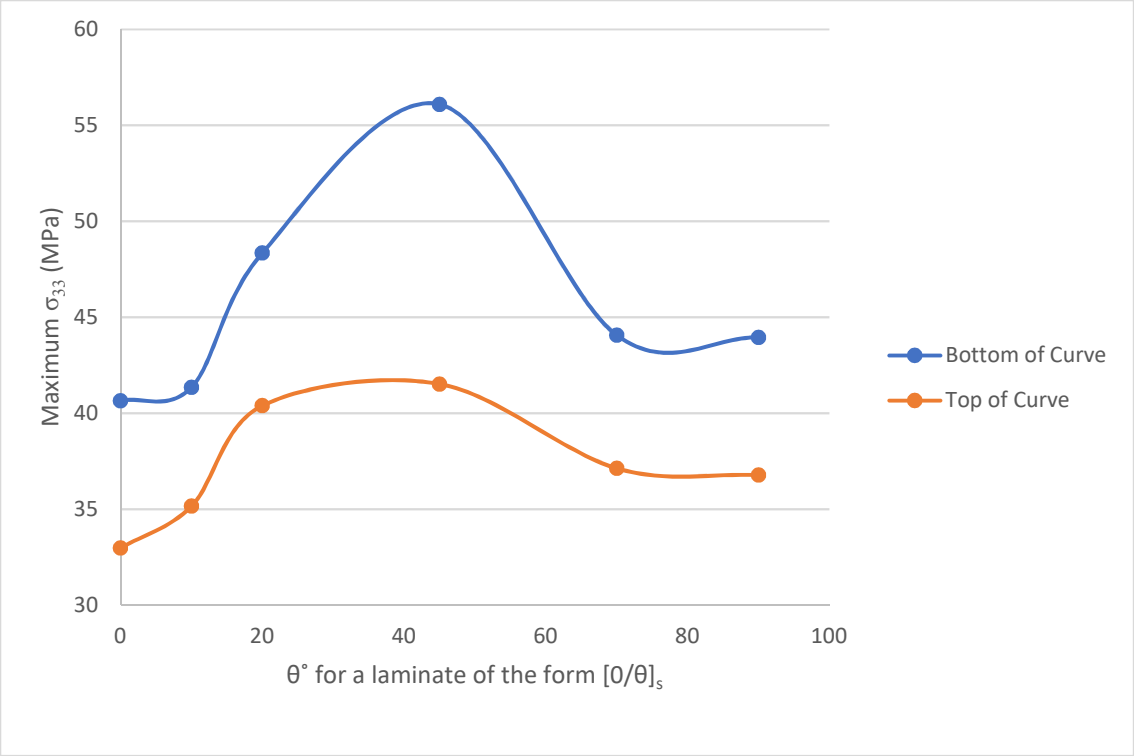

Figure 62: Maximum σ_{33} value by laminate lay-up at the bottom of the curve and the top of the curve where they transition to the vertical and horizontal arms respectively.

Table 13: Comparing the difference in maximum σ_{33} between probed locations by lay-up.

Lay-Up	**Difference in Maximum σ_{33} Between the Bottom and Top of the Curve (MPa)**
Unidirectional	7.7
$[0/10]_s$	6.2
$[0/20]_s$	8.0
$[0/45]_s$	14.6
$[0/70]_s$	6.9
$[0/90]_s$	7.2

Figure 62 and Table 13 show that the maximum σ_{33} value is consistently higher for the bottom of the curve than for the top of the curve. The unidirectional and $[0/90]_s$ lay-ups show maximum σ_{33} values that are 7-8 MPa higher for the bottom of the curve as compared to the top. Based on their stiffness matrices, these lay-ups do not twist when a bending moment is applied. This means that the higher stresses are at the bottom of the curve due to bending. The distance between the load and the top of the curve is 40 mm and is 50 mm to the bottom. This 25% increase in moment arm leads to a 25% increase in σ_{33}. However, the $[0/45]_s$ laminate has a difference of 14.6 MPa, which indicates that the increase due to the moment arm couples with

another factor which is dictated by the lay-up of the laminate. This is thought to be the laminate's proneness to twisting which will be verified in Section 4.5.2.

The locations of the maximum σ_{33} across the width did not occur at the same location for each lay-up. For example, the maximum occurred at the mid-plane for the unidirectional laminate, but occurred just prior to the free edge for the $[0/70]_s$ and $[0/90]_s$ laminates. Because of this inconsistency, the values at the free edge were also extracted and are shown in Figure 63. The differences between the bottom of the curve and the top of the curve can be seen in Table 14. Looking at just the free edge illustrates that there is now a difference between the laminates that are supposed to twist and those that are not supposed to. The $[0/10]_s$, $[0/20]_s$, $[0/45]_s$, and $[0/70]_s$ laminates all have larger differences than the cross-ply and the unidirectional laminate. This shows that the lay-up of the laminates also plays a role in how much torsion is induced. This will be investigated in Section 4.5.2.

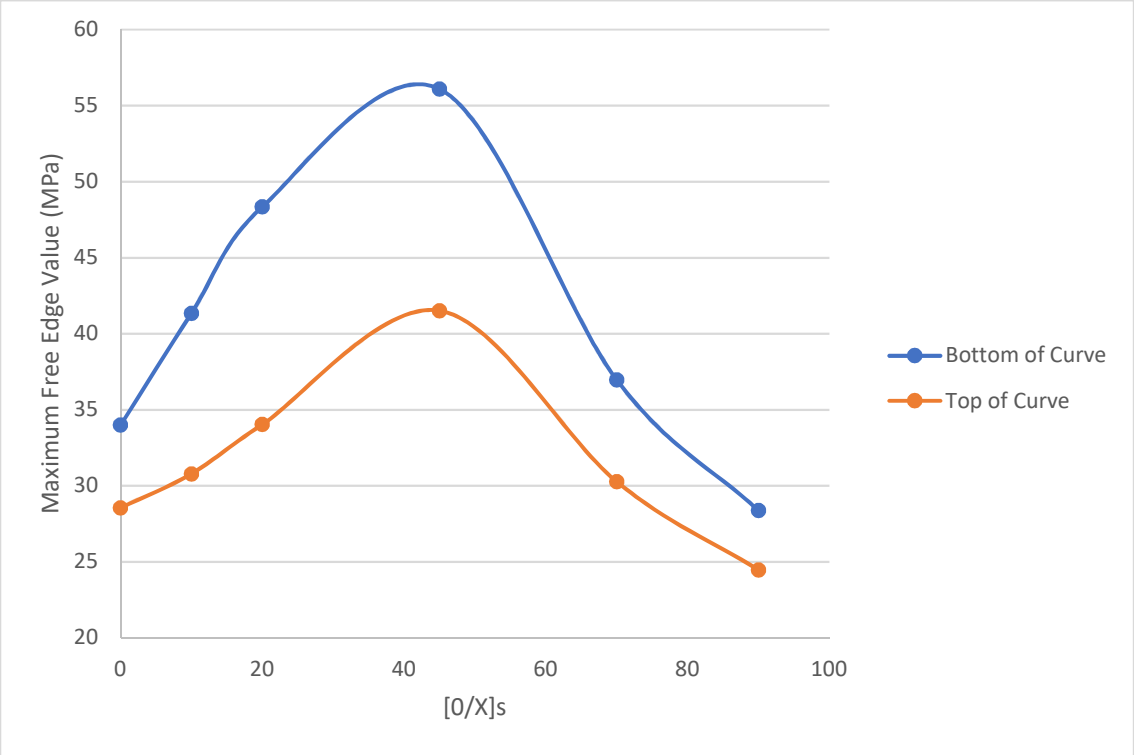

Figure 63: σ_{33} values at the free edge by laminate lay-up at the bottom of the curve and the top of the curve where they transition to the vertical and horizontal arms respectively.

Table 14: Comparing the difference in maximum σ_{33} at the free edge between probed locations by lay-up.

Lay-Up	Difference in Maximum σ_{33} (MPa) at Free Edge
Unidirectional	5.4
$[0/10]_s$	10.6
$[0/20]_s$	14.3
$[0/45]_s$	14.6
$[0/70]_s$	6.7
$[0/90]_s$	3.9

4.5.1.2 Conclusion - Determining Contributing Factors to Induced Torsion in a Curved Laminate

In conclusion, the σ_{33} results are affected by the magnitude of the moment and the torque induced in the laminate. This was shown by extracting results at two different locations that have different internal moments and torques. The internal moment increases with an increasing moment arm resulting in higher stresses at the bottom of the curve.

4.5.2 Determining How the Lay-Up Affects σ_{33} Distribution Due to Induced Torsion

In Classical Laminate Theory (CLT), the stiffness matrix is unique for each laminate lay-up analysed. Each stiffness matrix has a value termed "D_{16}" which couples the moment applied and the resulting twisting purely based on the lay-up of the laminate [56] as described in Section 2.1.2.3. The greater the value of D_{16}, the more prone the laminate is to twisting when subjected to a bending moment as in the current case of the curved coupon. The D_{16} values were calculated using CLT for the lay-ups analysed in this thesis. These results can be seen in Table 15.

Table 15: D16 value for each lay-up.

Lay-Up	D16 (kN*mm)
$[0/0]_s$	0
$[0/10]_s$	8.4
$[0/20]_s$	14.4
$[0/45]_s$	13.1
$[0/70]_s$	2.5
$[0/90]_s$	0

4.5.2.1 Results and Observations - Determining How the Lay-Up Affects σ_{33} Distribution Due to Induced Torsion

To verify that D_{16} could be a predictor for σ_{33} from the induced torque rather than the twisting directly, an index was created called the "σ_{33} Distribution Asymmetry Factor" of the model. This index is defined as the value of σ_{33} at y/b = 0.9 minus the value of σ_{33} at y/b = -0.9 and quantifies the asymmetry in the stress distribution across with width of the component. This removes the effects of the free edge and focuses on the lack of symmetry in Segment 1 of the distribution. All results for this study were extracted at the top of the curve as the effects of induced torsion are clearer due to their larger magnitude.

Refer to Figure 64 to see a plot of the σ_{33} Distribution Asymmetry Factor in relation to the D_{16} value for the six lay-ups. A trendline was added to determine the linearity of the relationship and the R^2 value of 0.9744 illustrates a linear relationship. Furthermore, the linear relationship illustrates that D16 is an effective parameter for determining which layup is expected to have more induced torsion.

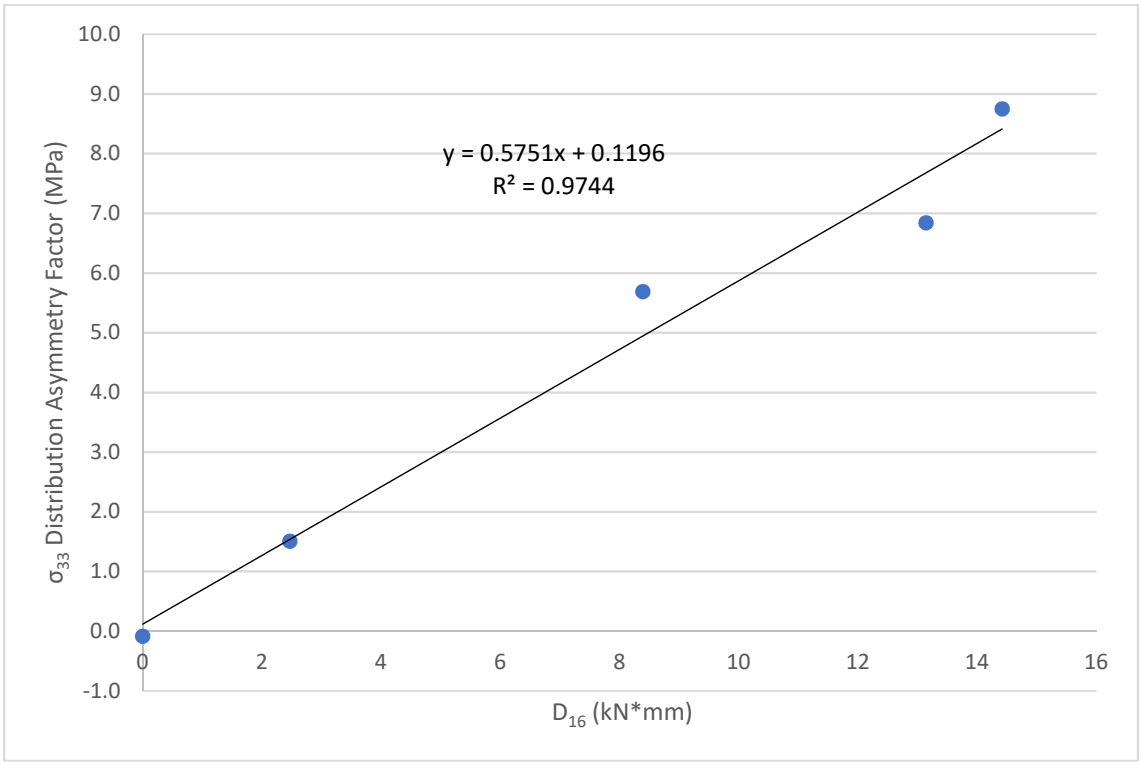

Figure 64: σ_{33} Distribution Asymmetry Factor of a layup measured across the top of the curve compared to its D16 value

Figure 64 shows that although a higher value of D_{16} predicts more asymmetry and in turn more induced torsion, Figure 65 shows it is not necessarily a predictor of higher values of σ_{33}. The maximum σ_{33} does not show a clear correlation with D_{16} because in some lay-ups the torsional effects can be additive, but in some cases subtractive depending on the specific shape of the distribution in the free edge region.

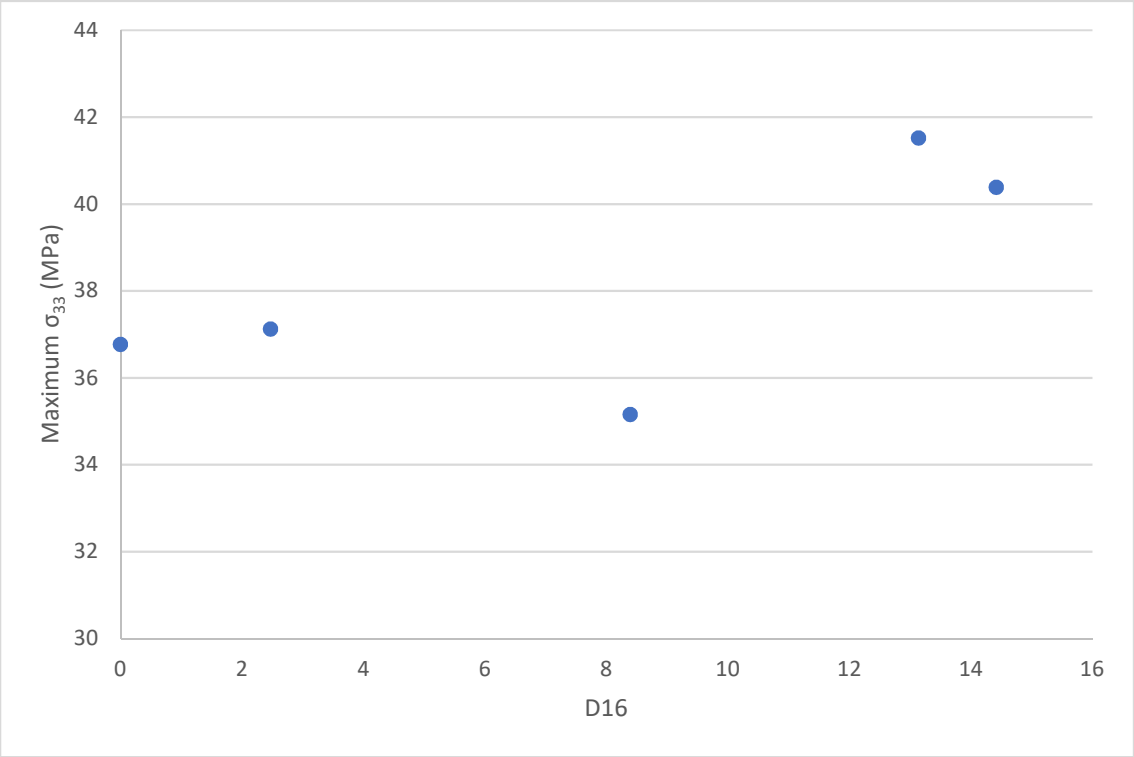

Figure 65: Maximum σ_{33} value of a curved laminate at the top of the curve where it meets the horizontal arm compared to the D16 value of a laminate with the same lay-up.

4.5.2.1 Conclusion - Determining How the Lay-Up Affects σ_{33} Distribution Due to Induced Torsion

In conclusion, a laminate that has a higher tendency to twist when subjected to bending (high D_{16}) results in more asymmetry in the σ_{33} distribution across the width of the coupon. Asymmetry is an indication of more induced torsion and more induced torsion will occur when a component that wants to twist cannot, due to the constraints imposed by the boundary conditions. A high D_{16} does not necessarily result in higher σ_{33} for the lay-ups considered. What this illustrates is that a rigorous analysis for each specific laminate is needed in order to predict delamination initiation as the effects of the coupon's constraints are difficult to predict. There are effects caused by moments, induced torsion and local edge effects that contribute to asymmetry,

increasing or decreasing σ_{33} that without taking every factor into account, an accurate failure analysis cannot be completed.

5.0 Discussion

5.1 The Necessity of Using a 3-D Resin Interface Model to Analyse Interlaminar Stress Distribution

It is necessary to use a 3-D model to analyse interlaminar stresses across the width of a curved laminate. When analysing a 2-D model as has been done in literature, only a single value for σ_{33} across the width of the laminate is observed. For the laminates modeled in this thesis, the maximum value only occurred in the mid-plane for the unidirectional laminate. All other laminates with angled plies had the maximum value of σ_{33} occur away from the mid-plane. In addition for the six laminates, the difference between the maximum interlaminar normal stress and the value of interlaminar normal stress at the mid-plane could differ by up to 37% as can be seen in Table 16. In addition, referring to Figure 66, three locations are denoted as 1, 2, and 3 where maximum σ_{33} values occurred in this study. The red line down the centre of the curve represents the mid-plane of the laminate. Only point 1 appears on the mid-plane of the laminate and would be identified in a 2-D analysis. Point 2 is just prior to the free edge at y/b = 0.95 and represents the maximum value of σ_{33} of the $[0/70]_s$ and $[0/90]_s$ laminates. Point 3 is directly at the free edge and represents the maximum value of σ_{33} for the $[0/10]_s$, $[0/20]_s$ and $[0/45]_s$ laminates. Maximum stresses occurring at Points 2 and 3 could only be identified from a 3-D analysis.

Table 16: Comparing mid-plane values to free edge values using values taken from where the bottom of the curve meets the vertical arm.

Lay-Up	Mid-Plane Value (MPa)	Maximum Value (MPa)	% Difference
Unidirectional	40.5	40.6	0.2
$[0/10]_s$	40.8	41.4	1.5
$[0/20]_s$	41.1	48.4	18
$[0/45]_s$	40.9	56.1	37
$[0/70]_s$	41.3	44.1	6.8
$[0/90]_s$	41.3	44.0	6.5

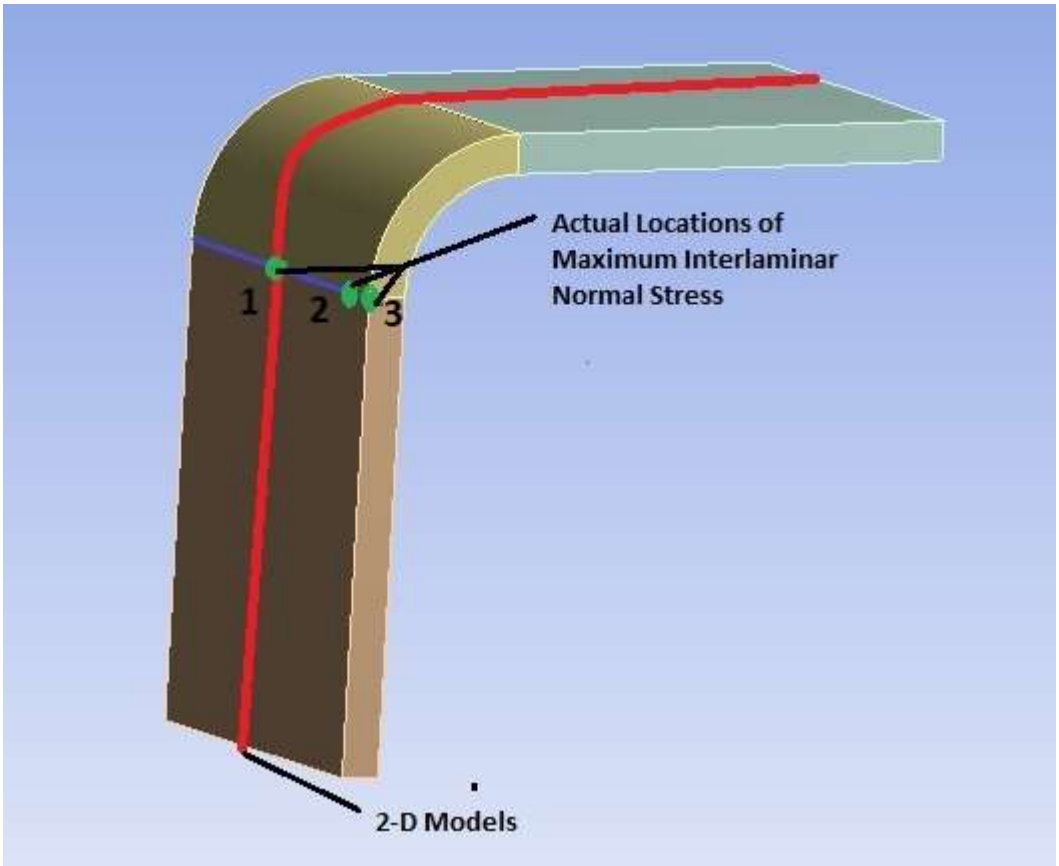

Figure 66: Location of maximum interlaminar normal stress across the bottom of the curve where it meets the vertical arm.

There are two main issues when analysing a laminate that requires the use of a 3-D model. Namely, in Section 4.4.2, it was shown that free edge effects are present in laminates. As has been shown in Section 4.0, there are various aspects that could potentially increase the interlaminar normal stress relative to the mid-plane value at the free edge of the laminate. These free edge effects are dependent on the σ_{11} which is applied to the laminate as well as the lay-up of the laminate. In literature, most laminates that are looked at are cross-ply or unidirectional where there is a smaller stress variance across the width of the laminate. Although the impact of the free edges is minimized by looking at these types of lay-ups, the impact of the stress variance is not negligible. Furthermore, the stress variance is definitely not negligible for laminates with angled plies where it was observed that there was a local increase of up to 37% at the free edge. A 3-D model allows the stress variance to be observed anywhere on the curve (including across the width), as opposed to the mid-plane only, when compared to a 2-D model. In most laminates, a 2-D model is irrelevant and should be used for failure prediction or detailed stress analysis.

The second conclusion that was made as to why a 2-D model cannot be used to model most curved laminates is the torsion which is induced in the laminates due to lay-up, loading, and boundary conditions. Looking at the interlaminar normal stress distribution for the $[0/20]_s$

laminate in Figure 58, one can see that there is an asymmetry in the σ_{33} distribution across the width due to the induced torsion. This increase at one edge is in addition to the free edge effects that were seen in Section 4.4.2. A 2-D model would not capture this increase due to the induced torsion and would once again assume that the maximum value is at the mid-plane of the laminate.

Overall, because the interlaminar normal stress (σ_{33}) is not constant across the width of a laminate, a 2-D model is not sufficient when performing failure analyses. The free edge effects due to lay-up, and the induced torsion due to lay-up, loading, and boundary conditions result in overall variations as well as local variations around the curve and across the width. A 3-D model must be used to get a complete picture of the interlaminar stress distribution across the width of the coupon.

5.2 Failure in a Laminate Curved Component Compared to an Isotropic Curved Component

As was briefly discussed in Section 4.3, there is a stark contrast in the difference between failure of curved composite components and curved isotropic components such as steel brackets. The failure mode and failure strength are two aspects that are different for laminate components. Failure mode is the means by which the component fails, such as yielding, fracture and delamination. Failure strength is defined as the loading that can be applied to the component prior to the failure mode occurring.

When analysing the failure of an isotropic component, for example steel, the failure mode is often assumed to be yielding. Von Mises criterion is typically the failure criterion used to perform the stress analysis which considers the multi-axial stress state. However, for an isotropic component in bending all other stress components are significantly small when compared to σ_{11}, so for the purposes of this discussion point it is assumed that only the σ_{11} stress would be significant. The simplified stress criteria which will be used simply states that if the circumferential stress (σ_{11}) exceeds the yield stress, yielding occurs (Equation (9)).

$$\frac{\sigma_{11}}{\sigma_y} \geq 1 \qquad (9)$$

When analysing the failure in composite components, failure modes that are not present in isotropic materials such as delamination, must be considered. As stated previously, delamination initiation can be predicted based on exceeding the failure criteria which often involves the ratio of $\frac{\sigma_{33}}{Z} \geq 1$.

For either isotropic or laminate components in bending, the maximum stress is typically the circumferential stress (σ_{11}). However, failure is predicted using different assumed failure modes therefore different stresses and different material allowables. For curved coupons, a radial stress is present that depends on the radius of curvature and exists for both isotropic components and composite components. The σ_{33} induced around the curve is not considered when analysing failure in an isotropic component as σ_{11} is significantly greater and σ_{33} becomes negligible. For laminates, σ_{33} may become the only stress considered as σ_{11} plays no role in delamination initiation. As a result of the above points, composite components require a completely different stress analysis than an isotropic component as σ_{33} is not easily determined.

For isotropic materials, such as generic steel, the yield strength is the critical strength when looking at failure of the component which is on the order of 350 MPa [57]. For laminate coupons the critical strength is the out-of-plane tensile strength (Z), which in a graphite epoxy composite is 47 MPa [51]. Laminates often fail due to delamination based on σ_{33} rather than in fibre failure based on σ_{11} because the Z is significantly lower than that of the fibre failure allowable.

Overall, when looking at curved components, the method by which it fails will be determined by the nature of the material it is composed of. An isotropic component will often fail via yielding, where a composite component will often fail by delamination. As the critical failure value (Z) in a laminate is substantially smaller than the yield strength in a steel, the radial stress around the curve is substantially more important. The radial stress, which can often be ignored in designing steel components, must be considered as the primary source of failure in a curved composite component.

5.3 The Challenge of Creating 3-D Resin Interface

It was stated by Martin in 1991 that the free edge effects in curved composite components cannot be ignored when conducting stress analyses [48]. However, researchers still conduct 2-D analyses assuming that the coupon is in a state of plane strain and that the maximum σ_{33} value occurs at the mid-plane of the laminate. Thurnerr *et al.* stated that the 3-D FEA models can be time intensive and often too difficult to construct [54], and coupling their reasoning with the smaller variation of σ_{33} expected in the often studied unidirectional and cross-ply laminates, plane strain is often a valid assumption [47].

When looking at Thurnerr *et al.*'s claim that 3-D FEA model of curved composite components can be too time intensive, it does warrant some merit. The model described in Section 3.0 took approximately five minutes to run on an Intel (R) Xeon (R) CPU E7-4870 v2 @ 2.30 GHz 2.29 GHz (2 Processors) with 32 GB of RAM and if non-linearities were coupled with the resin interface 3-D model, the time to perform each analysis would increase to one hour. In

comparison a linear perfect interface model took about one minute to run. The perfect interface model, however, cannot determine the values of the σ_{33} between two plies of differing angles due to the stress singularity introduced at the free edge.

The mesh creation can also be time intensive when creating a 3-D curved laminate model. This is due to the amount of small elements required at the free edge of the laminate in order to reach mesh convergence. Mesh creation tools are now available which allow different plies to be automatically created from a baseline surface mesh, but significant manual input is still required in the free edge region of the curved laminate to ensure there are enough elements at the free edge to reach a converged finite value of σ_{33}. The model created as per Section 3.0 required 50 elements in a region of 1.68 mm from the free edge (t/2). In addition, resin interface models require more elements through the thickness of the laminate. For the model created as per Section 3.0, four elements were required through each lamina ply and eight elements were required through each resin interface for a total of 40 elements through the thickness of the 3.36 mm thickness. The perfect interface model, required 16 elements through the thickness of the laminate. This lead to 57% more nodes in the resin interface model (281752) when compared to a perfect interface model (160125).

As per Section 3.0, the method by which results were extracted in this thesis was along the top and bottom of the curve where the curve transitions to the horizontal and vertical arm respectively. The location of the maximum σ_{33} around the curve was unknown and the mesh was simpler to refine in this region than if it were to be refined elsewhere on the curve. In addition, the refinement could not take place along the entire edge of the curve as the model would not run efficiently. The effect of refining only four locations around the edge of the curve is that the maximum result of σ_{33} could not be located with certainty. As a result of this the exact location of delamination initiation could not be determined for the laminates analysed in the study. However, the meshing method used was able to determine the effects that changing the lay-up and the induced torsion have on the σ_{33} distribution across the width of the laminate.

Martin's conclusions [48] were confirmed throughout this thesis, as free edge effects and varying σ_{33} distributions due to induced torsion have been realized in curved composite components and can cause the maximum σ_{33} value to occur away from the mid-plane of the laminate, thus leading to delamination initiation in other locations. This is especially true in laminates with angled plies, however it was also found to be true in cross-ply laminates. Therefore, as was confirmed in Section 5.1, despite the difficulties in using a 3-D mesh to model composite curved components, it is required in order to obtain an accurate picture of the interlaminar stress distribution.

5.4 Effect of Disregarding Interlaminar Shear Stress Distribution

The study performed in this thesis focused on the σ_{33} distribution across the width of the laminate and disregarded the effects of τ_{13}, for reasons mentioned in Section 4.2, and τ_{23} as its small magnitude was negligible. As was shown in Section 4.2, the interlaminar shear does play a role in delamination initiation for some lay-ups. An entire failure analyses on these lay-ups, would require that the effects of interlaminar shear be included. As it appeared that changing the geometry of the composite from a straight coupon to a curved coupon affected mostly interlaminar normal stress, it became the focus of this thesis. Adding a curve to the geometry had a minor effect on the τ_{13} distribution but it increased the values of σ_{33} by up to 1960%. As the τ_{13} is relatively geometry independent when compared to the σ_{33} for straight and curved components, the study of its effect on delamination initiation in a curved composite component was disregarded. However, a potential area of research exists to study interlaminar shear distribution in a future study.

6.0 Conclusions and Recommendations

6.1 Conclusions

Five major conclusions were determined over the course of this research as follows:

- Three-dimensional resin interface models are required to model curved composite composites as two-dimensional models could underpredict the maximum value of σ_{33} by up to 37% in the laminates considered in this thesis.

- Interlaminar normal stress becomes a main contributor in delamination of a curved laminate due to radial stress induced in the curve. In the $[0/90]_s$ lay-up, σ_{33} contributed 99% of the Hoyt failure criterion, while the τ_{13} contributed 1% of the Hoyt failure criterion.

- Maximum radial stress increases as the radius of curvature is decreased and approaches zero in a straight coupon without any curvature.

- The maximum interlaminar normal stress can occur in the free edge region or mid-plane depending on the lay-up, implying that three-dimensional models should be used for failure analysis or detailed stress analysis.

- Constraining the coupon induces an internal torsion which can increase the interlaminar normal stress by up to 41% for the laminates considered in this thesis.

6.2 Recommendations

Five recommendations for future areas of study and further research include:

- Performing a failure analysis of a curved composite component using the modeling method proposed in this thesis. Once the failure location was predicted, experimental verification could be performed. The finite element model would be large as the entire curve would need to be modeled using small elements to ensure that the exact location of failure could be converged. One experiment that could be re-created was already performed by Capt Rod Short in 2010 [60].

- Investigations of more common lay-ups such as angle-ply $[\theta/-\theta]_s$, and quasi-isotropic lay-ups could be performed. These lay-ups have practical applications and the location of maximum σ_{33} would be of interest in determining where delamination initiation would be expected.

- Varying other geometric parameters of the curve, such as the thickness could lead to other variations of σ_{33} throughout the curved component. Varying these parameters would give a better understanding of how to design in order to minimize $\sigma_{33,}$ and reduce delamination risk.

- Modeling of interlaminar shear (τ_{13}) in the same manner in which the interlaminar normal stress (σ_{33}) was modeled. As was shown, the interlaminar shear does play a role in delamination initiation. What should be studied is how the behaviour of the interlaminar shear changes by changing the same parameters as was done throughout this thesis (lay-up, geometry, induced torsion, probed location).

- A parametric study optimizing the design of a curved component by increasing the load a curved component can be subjected to prior to failure. There is benefit to using composites to create the curved component by decreasing the weight while maintaining the high stiffness.

References

[1] D. S. Cairns and L. A. Wood, *Composite Materials for Aircraft Structures,* Bozeman: Montana State University, 2009.

[2] K. Marcel, T. Vopat, V. Simna and M. Necpal, "Influence of Unltrasonic Assistance on Delamination During Machining of Different Composite Materials," in *Proceedings of the 28th International DAAAM Symposium*, Bratislava, 2017.

[3] H. Ghiasi, K. Fayazbakhsh, D. Pasini and L. Lessard, "Optimum stacking sequence design of composite materials Part II: Variable stiffness design," *Composite Structures,* vol. 92, pp. 1-13, 2010.

[4] W. L. Geleta, "Delamination Behaviour of L-Shaped Laminated Composites," *International Journal of Aeronautical and Space Sciences ,* 2018.

[5] D. Cao, D. Qingfeng, H. Hu, Y. Xhong and S. Li, "Computational investigation of both intra-laminar matrix cracking and inter-laminar delamination of curved composite components with cohesive elements," *Composite Structures,* vol. 192, pp. 300-309, 2018.

[6] P. E. Labossiere, *ME 354 Course Notes - Chapter 4 - Beams: Curved, Composite, Unsymmetrical,* Washington: University of Washington, 2007.

[7] C. T. Herakovich, Mechanics of Fibrous Composites, New York: Wiley, 1998, pp. 112-136.

[8] NDT Resource Centre, "Anisotropy and Isotropy," NDT Resource Centre, [Online]. Available: https://www.nde-ed.org/EducationResources/CommunityCollege/Materials/Structure/anisotropy.htm. [Accessed 23 November 2018].

[9] T. Abbey, "Composites in FE Analysis," NAFEMS, [Online]. Available: https://www.nafems.org/about/regional/americas/events/newsletter/april2017/. [Accessed 2018 November 23].

[10] S.-Y. Lee and J.-H. Roh, "Two-dimensional strain-based interactive failure theory for multidirectional composite laminates," *Composites Part B: Engineering,* vol. 69, pp. 69-75, 2015.

[11] A. Chehouri, "Stress and Failure Analysis of Multidirectional Laminates," MathWorks, 03 Dec 2014. [Online]. Available: https://nl.mathworks.com/matlabcentral/fileexchange/44717-stress-and-failure-analysis-of-multidirectional-laminates--fpf---tsai-wu-. [Accessed 15 June 2018].

[12] U. S. Koruche and S. F. Patil, "Application of Classical Lamination Theory and Analytical Modeling of Laminates," *International Research Journal of Engineering and Technology,* vol. 2, no. 2, pp. 958-965, 2015.

[13] Mohite, "Module 5: Laminate Theory, Lecture 17 Laminate Constitutive Relations," 18 August 2014. [Online]. Available: https://nptel.ac.in/courses/101104010/downloads/Lecture17.pdf. [Accessed 19 March 2019].

[14] CAE, "Using Composites Analysis to Predict Interlaminar Stresses," CAE , [Online]. Available: https://caeai.com/resources/using-composites-analysis-predict-interlaminar-stresses. [Accessed 22 November 2018].

[15] C. Kassapoglou and P. A. Lagace, "An efficient method for the calculation of interlaminar stresses in composite materials," *J. Appl. Mech.,* vol. 53, pp. 744-750, 1986.

[16] C. A. Rose and C. T. Herakovich, "An Approximate Analytical Solution for Interlaminar Stresses in Angle-Ply Laminates," *Composites: Design, Manufacture, and Application,* pp. 28-W-1-28-W-13, 1991.

[17] C. A. Rose and C. T. Herakovich, "An Approximate Solution for Interlaminar Stresses in Laminated Composite Subjected to Bending and Extension," in *Proceedings, American Society of Composites Seventh Technical Conference* , Stamford CT, 1992.

[18] C. A. Rose and C. T. Herakovich, "An Approximate Solution for Interlaminar Stresses in Composite Laminates," *Compos. Eng.,* vol. 3, no. 3, pp. 271-285, 1993.

[19] J. Ekh, "Multi-Fastener Single-lap Joints in Composite Structures," Royal Institute of Technology, Stockholm, 2006.

[20] J. Pilling, "Toughness in Composites - Part 2," [Online]. Available: http://www.mse.mtu.edu/~drjohn/my4150/class9/class9a.html. [Accessed 19 March 2019].

[21] SlideShare, "Delamination in Composites," [Online]. Available: https://www.slideshare.net/soorajndt22/delamination-in-composites. [Accessed 19 March 2019].

[22] A. Puck and H. Schurmann, "Failure Analysis of FRP Laminates by Means of Physically Based Phenomenonological Models," *Composites Science and Technology,* vol. 58, pp. 1045-1067, 1998.

[23] P. Yarrington, J. Zhang, C. Collier and B. A. Bednarcyk, "Failure Analysis of Adhesively Bonded Composite Joints," American Institute of Aeronautics and Astronautics Inc., Hampton VA, 2005.

[24] R. D. Adams and W. C. Wake, "Structural Adhesive Joints in Engineering," Applied Science Publishers, London, 1984.

[25] D. M. Hoyt, S. H. Ward and P. J. Minguet, "Strength and Fatigue Life Modleing of Bonded Joints in Composite Structure," in *Proc. American Society for Composites (ASC) 15th Technical Conference* , 2000.

[26] R. S. Long, "Static Strength of Adhesively Bonded ARALL-1 Joints," *Journal of Composite Materials,* vol. 25, pp. 391-415, 1991.

[27] L. Tong, "An Assessment of Failure Criteria to Predict the Strength of adhesively Bonded Composite Doubler Lap Joints," *Journal of Reinforced Plastics and Composites,* vol. 16, no. 18, pp. 698-713, 1997.

[28] P. P. Camanho and F. L. Matthews, "Delamination Onset Prediction in Mechanically Fastened Joints in Composite Laminates," *Journal of Composite Materials,* vol. 33, no. 10, pp. 906-927, 1999.

[29] E. Velazquez and J. B. Kosmatka, "Stresses in Half-Elliptic Curved Beam Subjected to Transverse Tip Forces," in *50th AIAA/ASME/ASCE/AHS/ASC Structures, Structural Dynamics, and Materials Conference*, Palm Springs, CA, 2009.

[30] C. K. Cheung and H. C. Sorenson, "Effect of Axial Loads on Radial Stress in Curved Beams," *Wood and Fiber Science,* vol. 15, no. 3, pp. 263-275, 1983.

[31] S. Timoshenko and J. N. Goodier, Theory of elasticity, 2nd ed., New York: McGraw-Hill, 1951.

[32] M. Tauhiduzzaman and L. A. Carlsson, "Influence of constraints on the effective inplane extensional properties of honeycomb core," *Composite Structures,* vol. 209, pp. 616-624, 2019.

[33] R. B. Pipes and N. J. Pagano, "Interlaminar stresses in composite laminates under uniform axial extension," *J. Compos. Mater.,* vol. 4, pp. 538-548, 1970.

[34] E. F. Rybicki, "Approximate three-dimensional solutions for symmetric laminates under inplane loading," *J. Compos. Mater,* vol. 5, pp. 354-360, 1971.

[35] I. Raju and J. Crews, "Interlaminar stress singluarities at a straight free edge in composite laminates," *Comput. Struct,* vol. 14, no. 1-2, pp. 21-28, 1981.

[36] A. S. Wang and F. W. Crossman, "Some new results on edge effect in symmetric composite laminates," *J. Compos. Mater.,* vol. 11, pp. 92-106, 1977.

[37] R. Y. Kim and S. R. Soni, "Experimental and analytical studies on the onset of delamination in laminated composites," *J. Compos. Mater.,* vol. 18, pp. 70-80, 1984.

[38] J. C. Brewer and P. A. Lagace, "Quadratic stress criterion for initiation of delamination," *J. Compos. Mater.,* vol. 22, pp. 1141-1155, 1988.

[39] G. Isakson and A. Levy, "Finite-element analysis of interlaminar shear in fibrous composites," *J. Compos. Mater.,* vol. 5, pp. 273-276, 1971.

[40] P. Murthy and C. Chamis, "A study of interply layer effects on the free edge stress field of angle ply laminates," *Comput. Struct.,* vol. 20, no. 1-3, pp. 431-441, 1985.

[41] M. Haboussi, H. Dumontet and J. Billoet, "On the modelling of interficial transition behaviour in composite materials," *Comp. Mater. Sci,* vol. 20, pp. 251-266, 2001.

[42] M. Haboussi, H. Dumontet and J. Billoet, "Proposal of refined interface models and their application for free-edge effect," *Compos. Interface,* vol. 8, no. 1, pp. 93-107, 2001.

[43] H. Kim, J. Lee and M. Cho, "Free-edge interlaminar stress analysis of composite laminates using interface modeling," *J.Eng. Mech.,* vol. 138, pp. 973-983, 2012.

[44] G. Wimmer, C. Schuecker and H. E. Pettermann, "Numerical simulation of delamination onset and growth in laminated composites," in *Austrian Aeronautics Research/Netwoek for Materials and engineering at the Institute of Lightweight Design and Structural Biomechanics, Vienna University of Technology*, Vienna, Austria, 2006.

[45] C. T. Sun and S. R. Kelly, "Failure in composite angle atructures Part I: initial failure," *J Reinforced Plast Compos,* vol. 7, pp. 220-232, 1988.

[46] B. Gozluku, I. Uyar and D. Coker, "Intersonic delamination in cirved thick composite laminates under quasi-static loading," *Mechanics of Materials,* vol. 80, pp. 163-182, 2015.

[47] J. P. Lucas, "Delamination fracture: Effect of fibre orientation on fracture of a continuous fibre composite laminate," *Eng. Fract. Mech.,* vol. 42, pp. 553-561, 1992.

[48] R. H. Martin and W. C. Jackson, "Damage Prediction in Cross-Plied Curved Composite Laminates," NASA, Hampton VA, 1991.

[49] M. Biernacki, "Microcracking of Thin Cross-Ply Carbon-Epoxy Laminates in Flexural Fatigue," RMC, Kingston, 2012.

[50] N. V. Bhat and P. A. Lagace, "An Analytical method for the evaluation of interlaminar stresses due to material discontinuities," *J. Compos. Mater,* vol. 28, no. 3, pp. 190-210, 1994.

[51] Cytec Industries Inc., "Cytec Engineered Materials," Cytec Industries Inc., 2008.

[52] Structure Point Concrete Software Solutions, "Finite Element Aspect Ratio Influence in Concrete Foundation Models," Structure Point, Skokie IL.

[53] A. Javidinejad, "FEA Practical Illustration of Mesh-Quality-Results Differences between Structured Mesh and Unstructured Mesh," *ISRN Mechanical Engineering ,* 2012.

[54] C. Thurnherr, R. Groh, P. Ermanni and P. Weaver, "Investigation of failure initiation in curved composite laminates using a higher-order beam model," *Composite Structures,* vol. 168, pp. 143-152, 2017.

[55] H. Y. Sarvestani, "Free-edge stresses in general cross-ply laminates," *Scientia Iranica,* vol. 21, no. 2, pp. 387-402, 2014.

[56] C. T. Herakovich, "Lamination Theory," in *Mechanics of Fibrous Composites*, Wiley, 1998, pp. 112-136.

[57] ANSYS Inc., "ANSYS Material Database," Canonsburg PA.

[58] R. Hibbler, Mechanics of Materials 8 ed., Boston: Prentice Hall, 2011.

[59] A. Yu and G. Nie, "Explicit solutions for shearing and radial stresses in curved beams," *Mechanics Research Communications,* vol. 32, pp. 323-331, 2005.

[60] C. R. Short, "Analysis of Carbon BMI Laminates Using Classical Plate Theory, First Order Shear Deformation Theory and Testing," RMC, Kingston ON, 2010.

Appendices

Appendix A Results of Comparison Between Straight and Curved Laminates – Interlaminar Normal Stress

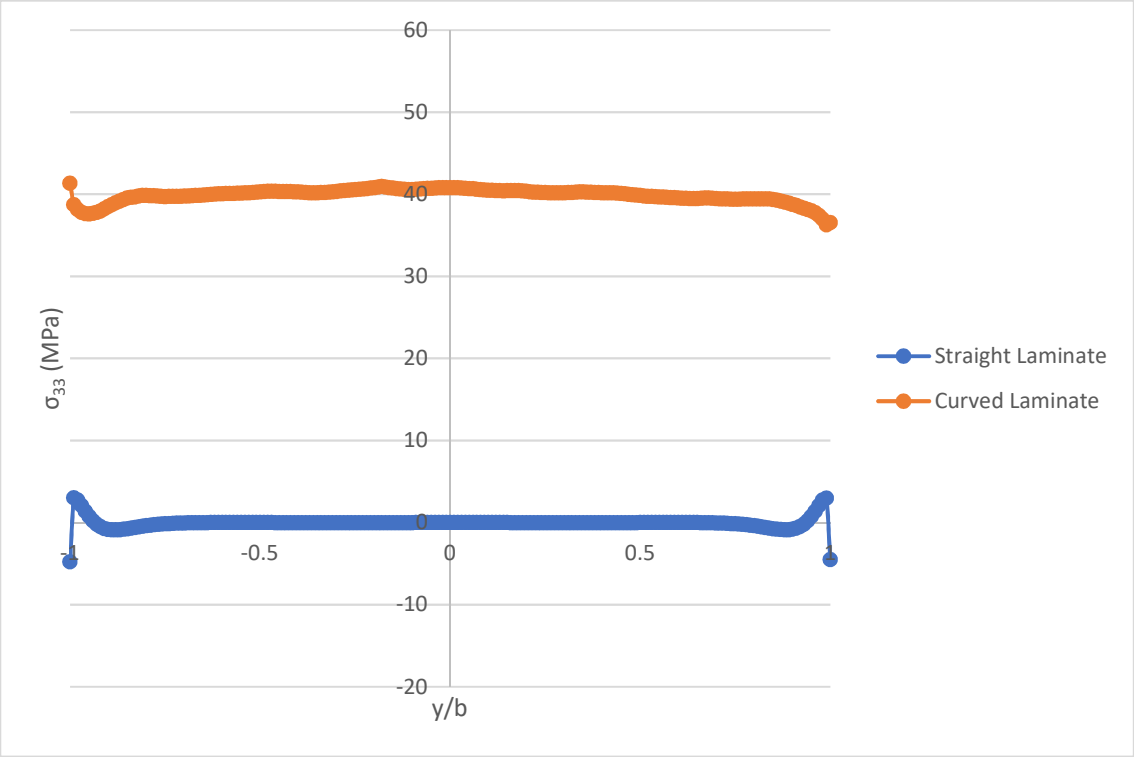

Figure A- 1: σ_{33} distribution across the laminate width for straight and curved laminates of a $[0/10]_s$ lay-up at the transition between the vertical arm and the curve of the curved coupon

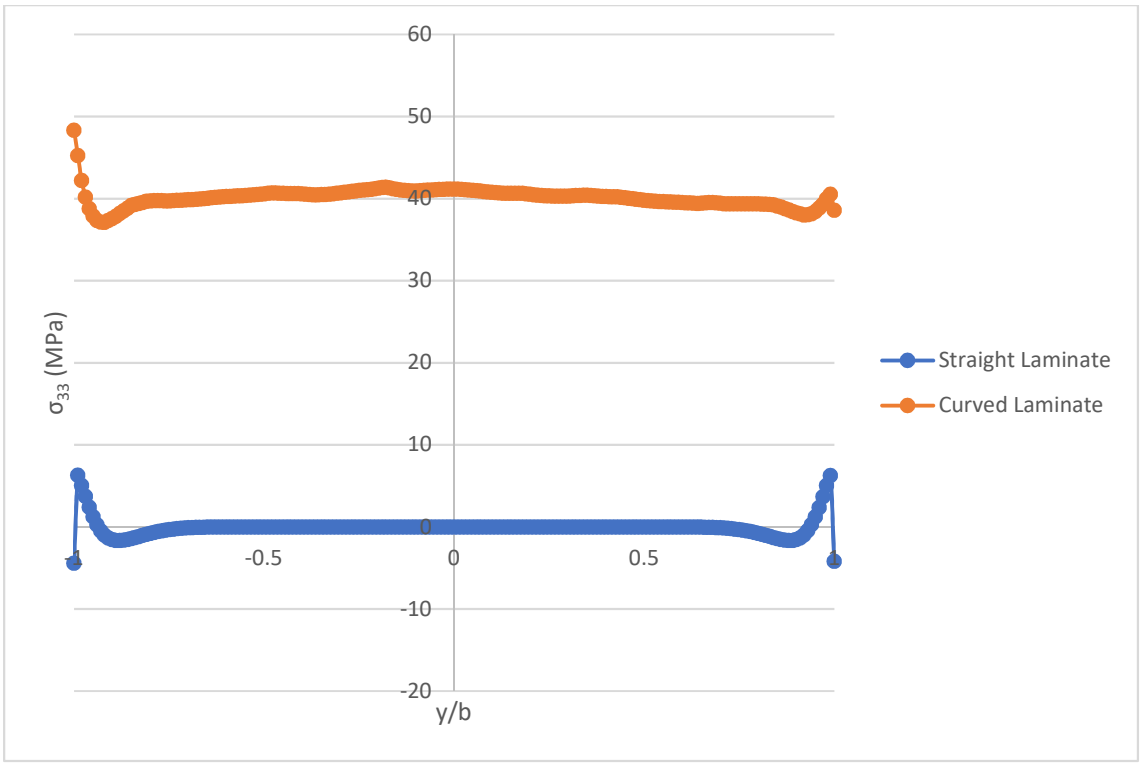

Figure A- 2: σ_{33} distribution across the laminate width for straight and curved laminates of a $[0/20]_s$ lay-up at the transition between the vertical arm and the curve of the curved coupon

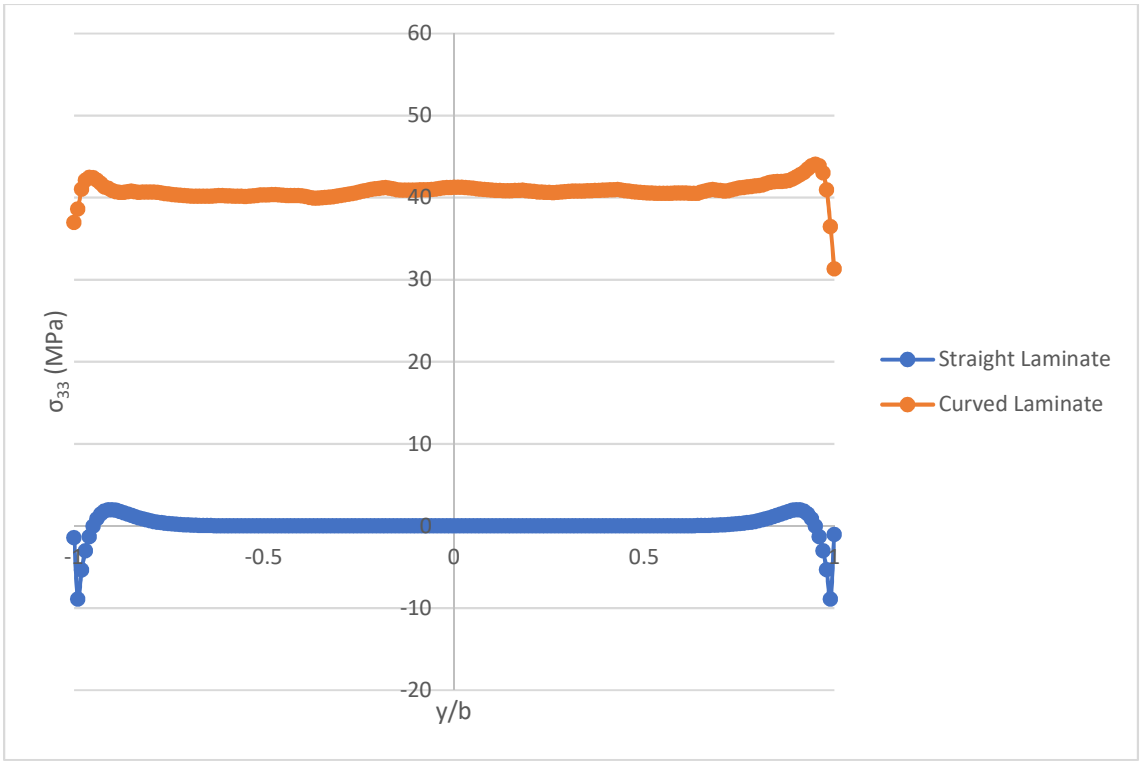

Figure A- 3: σ_{33} distribution across the laminate width for straight and curved laminates of a $[0/70]_s$ lay-up at the transition between the vertical arm and the curve of the curved coupon

Appendix B Results of Comparison Between Free Edge Effects of Straight and Curved Laminates

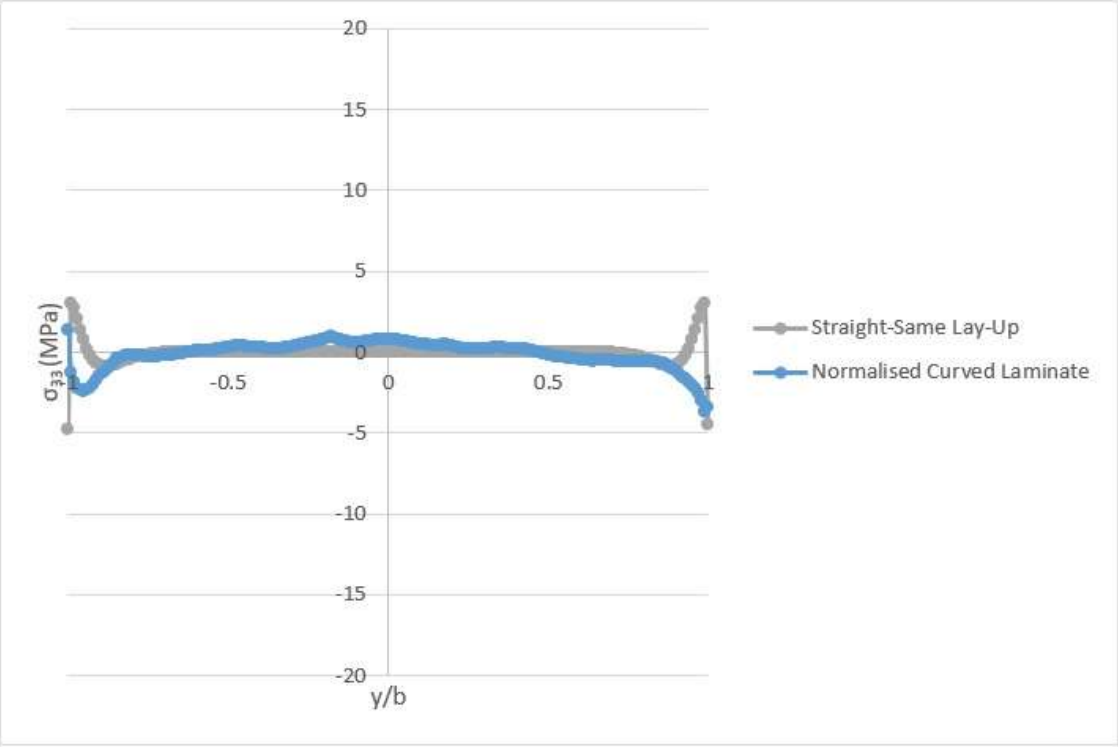

Figure B- 1: σ_{33} distribution across the laminate width for straight and curved laminate with isolated edge effects of a $[0/10]_s$ lay-up at the transition between the vertical arm and the curve of the curved coupon

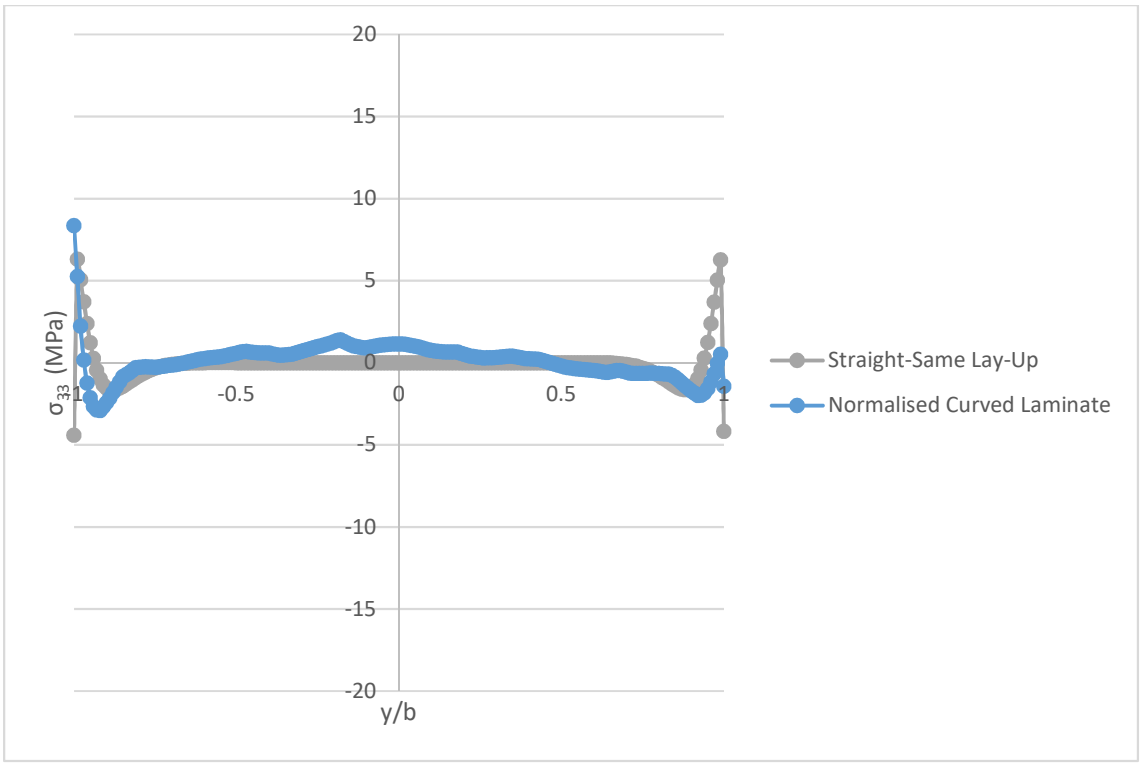

Figure B- 2: σ_{33} distribution across the laminate width for straight and curved laminate with isolated edge effects of a $[0/20]_s$ lay-up at the transition between the vertical arm and the curve of the curved coupon

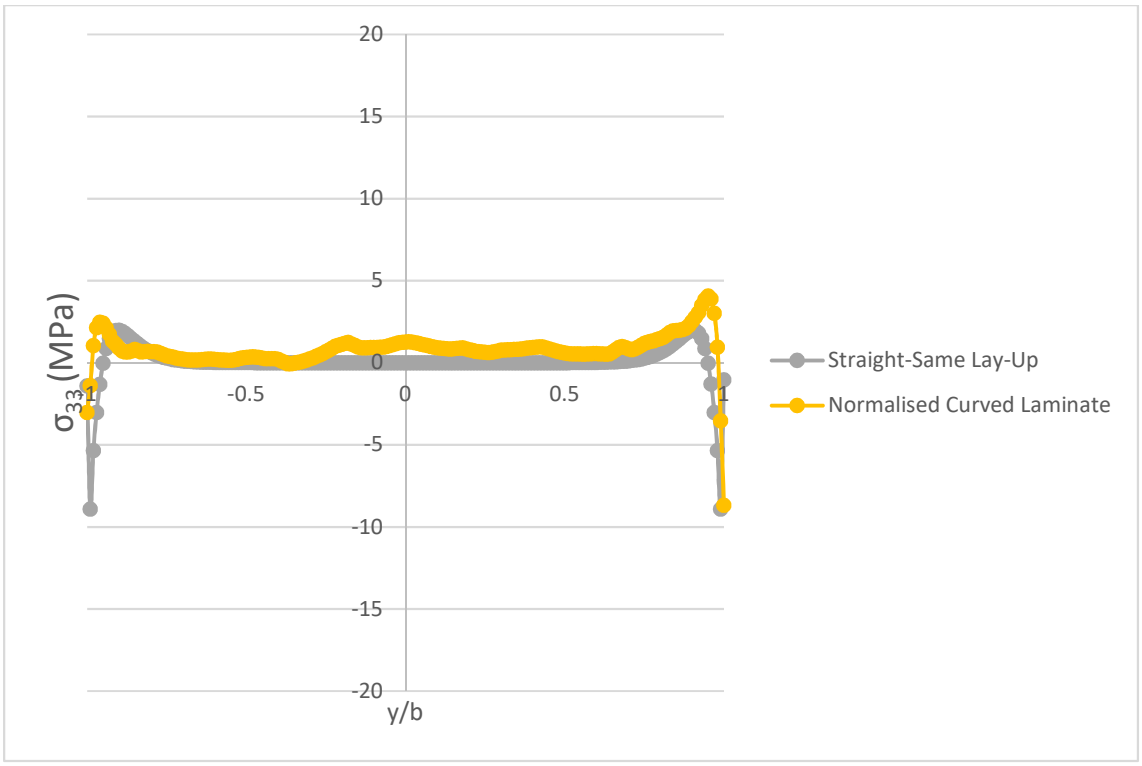

Figure B- 3: σ_{33} distribution across the laminate width for straight and curved laminate with isolated edge effects of a $[0/70]_s$ lay-up at the transition between the vertical arm and the curve of the curved coupon

Appendix C Results of Stress Distribution Comparison Between Top of Curve and Bottom of Curve

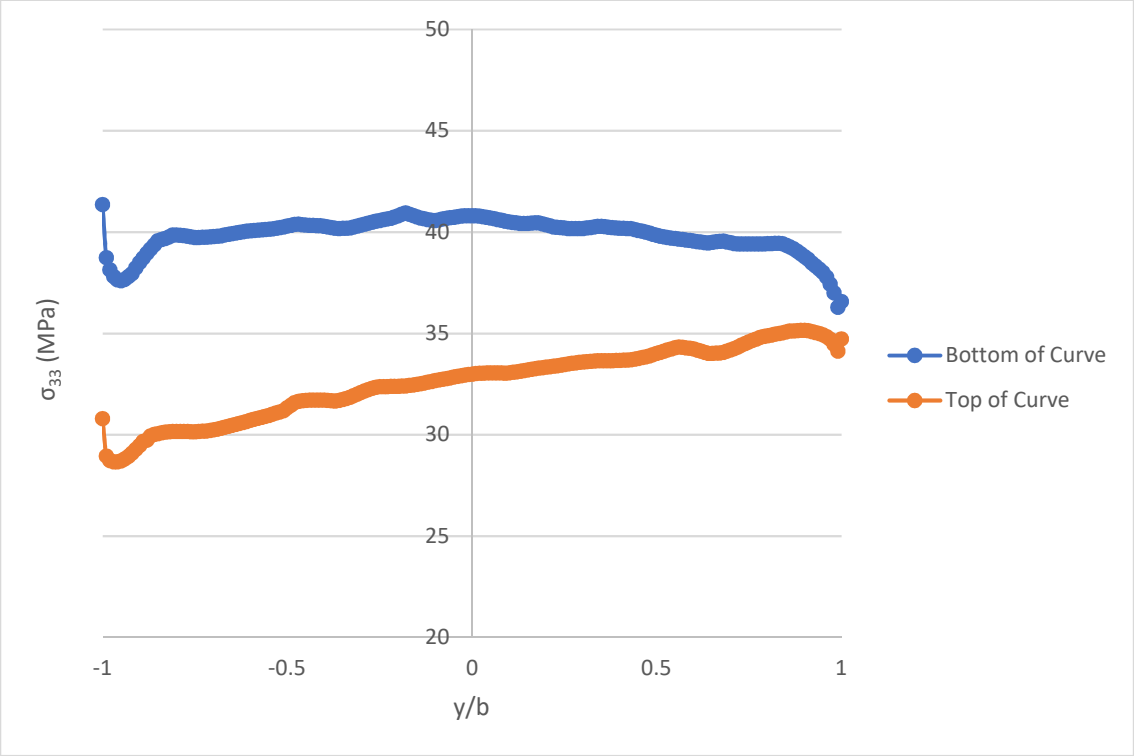

Figure C- 1: σ_{33} distribution across the laminate width for curved laminate of a $[0/10]_s$ lay-up at the bottom of the curve and the top of the curve where they transition to the vertical and horizontal arms respectively

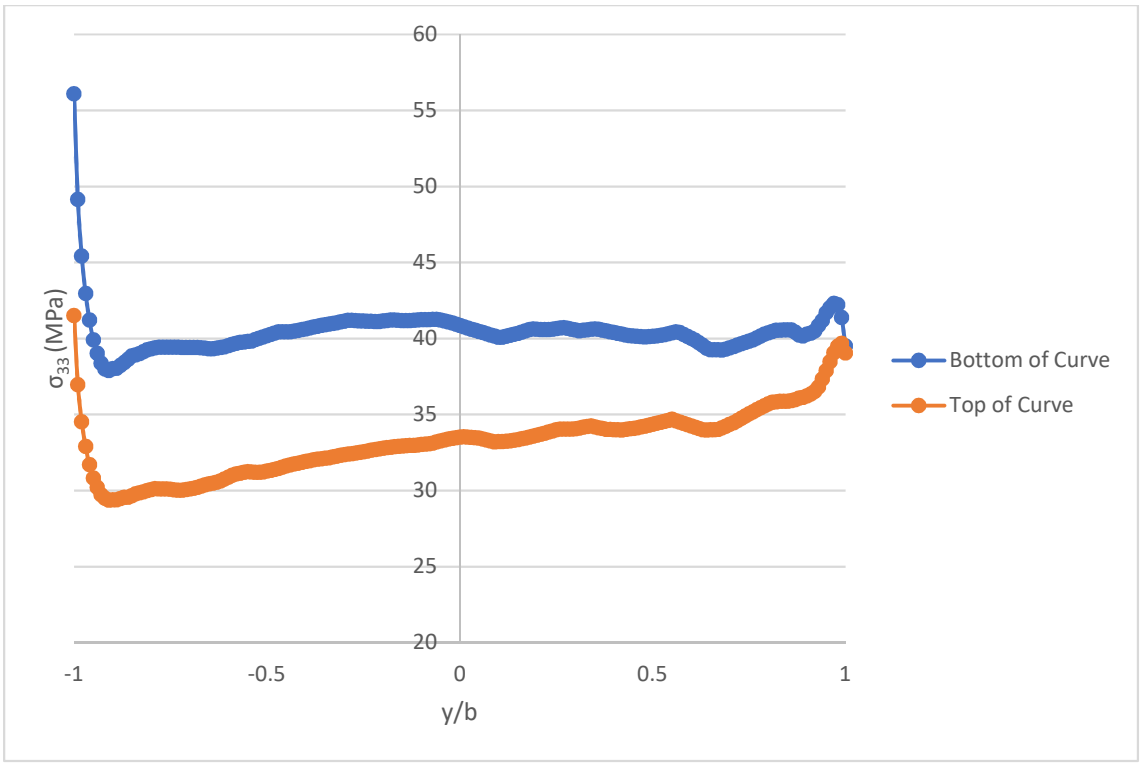

Figure C- 2: σ_{33} distribution across the laminate width for curved laminate of a $[0/45]_s$ lay-up at the bottom of the curve and the top of the curve where they transition to the vertical and horizontal arms respectively

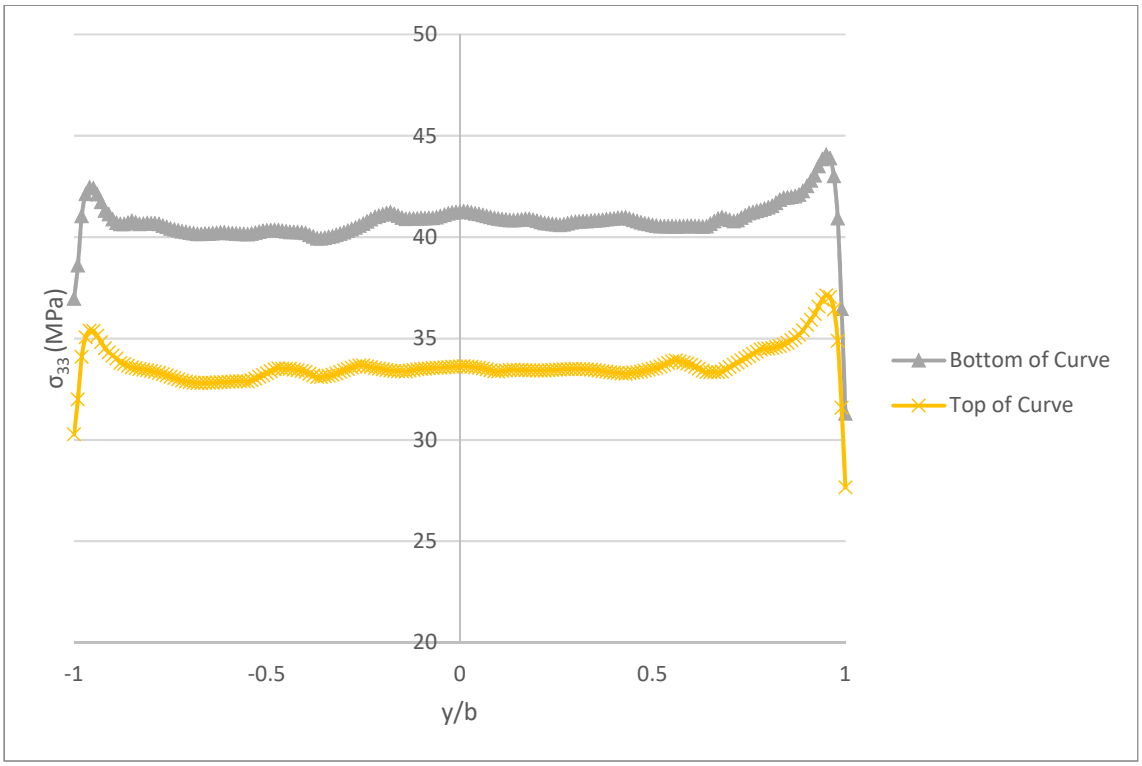

Figure C- 3: σ_{33} distribution across the laminate width for curved laminate of a $[0/70]_s$ lay-up at the bottom of the curve and the top of the curve where they transition to the vertical and horizontal arms respectively